ISBN 9985-9058-5-7
ISSN 1406-023X

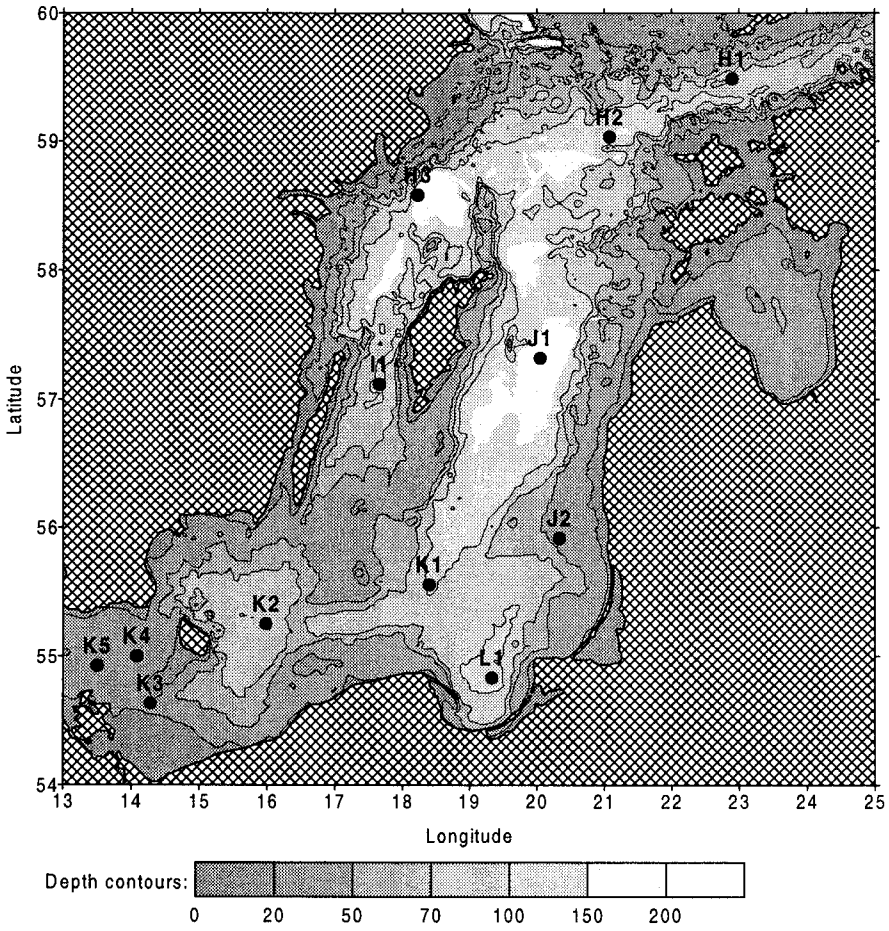


# DEEP WATER OVERFLOW, CIRCULATION AND VERTICAL EXCHANGE IN THE BALTIC PROPER

Edited by Jüri Elken

ESTONIAN MARINE INSTITUTE
Report Series, No. 6

TALLINN, 1996

ESTONIAN MARINE INSTITUTE
Report Series, No. 6

ISBN 9985-9058-5-7
ISSN 1406-023X

# DEEP WATER OVERFLOW, CIRCULATION AND VERTICAL EXCHANGE IN THE BALTIC PROPER

Edited by Jüri Elken

TALLINN, 1996

DOCUMENT DATA SHEET

| *EDITOR* | *E-MAIL* | *PUBLICATION* |
|---|---|---|
| Jüri Elken, Ph.D | elken@phys.sea.ee | *DATE* Detsember, 1996 |

*TITLE*

Deep water overflow, circulation and vertical exchange in the Baltic Proper

*REFERENCE*

Estonian Marine Institute, Report Series No. 6, 91 pp.

*ABSTRACT*

Analysis of the data from hydrographic monitoring and process-oriented polygon observations, made in the period 1979-1995, is presented. Lateral and vertical transport as well as diffusive fluxes in the intermediate layer are quantified by a diagnostic box model. Mesoscale and turbulence observations from that period are analysed in relation to the water exchange between the sub-basins and the wind forcing. Problems of turbulence modelling are considered within the RAT theory. Transport mechanisms are investigated with the use of 3D circulation model.

| *ISSUING ORGANISATION* | *TELEPHONE* |
|---|---|
| Estonian Marine Institute<br>Paldiski str.1<br>EE0031 Tallinn<br>ESTONIA<br>Director Ahto Järvik | 372 2 453598 |
| | *TELEFAX* |
| | 372 6 311069 |

| *KEYWORDS* | *CONTRACT* |
|---|---|
| BALTIC SEA<br>HYDROGRAPHIC CHANGES<br>DEEP WATER OVERFLOW<br>VERTICAL MIXING<br>BOX MODELS<br>CIRCULATION MODELS | *PROJECT*<br>ETF Grants<br>No. 907/92/231<br>*ORDER PRICE*<br>30 DEM |

Copies of this report can be ordered from the library of the Estonian Marine Institute

**Available in the EMI Report Series:**

1. **Hydrographic studies within the Gulf of Riga Project, 1993-1994.**

   Ed. by A. Toompuu and J. Elken (1995)

2. **IRBEX - 95 Data Report.**

   Ed. by U. Lips and M.-J. Lilover (1995)

3. **Studies on measuring and modelling the water and nutrient exchange of the Gulf of Riga.**

   Ed. by Ü. Suursaar and V. Astok (1996)

4. **Harmful substances in the ecosystem of the Gulf of Finland . Part I. Trace metals.**

   Ed. by H. Jankovski (1996)

5. **Coupled 3D hydrodynamic and ecosystem model FinEst.**

   Ed. by R. Tammsalu (1996)

6. **Deep water overflow, circulation and vertical exchange in the Baltic Proper.**

   Ed. by J. Elken (1996)

**CONTENTS**

## Abstract

Data from the hydrographic monitoring and process-oriented polygon observations, made in the period 1979-1995, are analysed with respect to deep water overflow, circulation and vertical exchange in the Baltic Proper. Stratification changes observed in the Gotland Basin - overall decrease of salinity and vertical stability during the stagnation period, warming-up of the intermediate layers at the end of eighties and deep water renewal after the major saline water inflow in 1993, are described. Lateral and vertical transport as well as diffusive fluxes in the intermediate layer are quantitatively analysed by a diagnostic box model. Compared with the earlier calculations, smaller flow rates have been estimated in the Gotland Basin. Mesoscale observations from that period are analysed in relation to the water exchange between the sub-basins and the wind forcing. With the use of circulation model it was found, that baroclinic eddies which modify the deep circulation are generated in the deep channels by intruding dense water. The circulation model also gave, that dense water transport in the deep channels may be approximated by a sum of the density- and wind-driven components, with the maximum overflow occurring in the Stolpe Channel at north-easterly winds and in the Hoburg Channel at northerly winds. Overflowing water is preferably spreading anti-clockwise along the right-hand slopes of the downstream basins. Warming-up of the intermediate layers was governed by the enhanced wintertime advection along the eastern slope of the Gotland Basin and subsequent detachment of warm-core deep lenses spreading the warmer slope water over the basin interior. Important role of the Northern Basin as a sink for the intermediate water is pointed out. Problems of turbulence modelling are considered within the RAT theory. Turbulence observations have revealed minor vertical salt fluxes in the halocline during the normal conditions. Therefore, stronger cross-isopycnal mixing is expected to take place during the storms by generation of inertial waves which lead to shear instability. Surface layers are effectively supplied with salt during the winter storms by entrainment of the halocline top layers. Signs of intensified mixing have been found near the slopes.

# 1. INTRODUCTION

The Baltic Sea is one of the largest brackishwater bodies in the world. Annual freshwater supply amounts to 439 $km^3$ for the period 1951-1970 (HELCOM, 1990) which comprises 2 % of the volume of the sea, known as 21 600 $km^3$. Water exchange with the North Sea, combined with the freshwater supply, feeds a strong saline stratification in deeper parts of the sea and maintains a decrease of salinity from the entrance area towards the regions of strong river influence. Therefore the Baltic Sea may be considered as a **huge estuary** (*e.g.* Stigebrandt, 1983). Estuarine dynamics is essentially driven by fluctuating water exchange with the North Sea (Matthäus and Lass, 1995), and the subsequent, mainly density-driven transport of saline and diluted waters in a cascade of sub-basins (Omstedt, 1990) which together with vertical mixing causes long-term changes in hydrographic conditions (Matthäus, 1990). Wind forcing over the Baltic Sea induces variable circulation, with compensating flows due to the semi-enclosed boundaries (Krauss and Brügge, 1992), and activates also Kelvin waves and upwelling (Fennel and Sturm, 1992). In this respect the Baltic Sea may be regarded as a **large lake**. Meso- and small-scale dynamics of the Baltic Sea is essentially governed by fronts (Pavelson, 1988), baroclinic eddies (Elken *et al.,* 1994) and thermohaline effects (*e.g.* intrusive finestructure, Aitsam *et al.,* 1984, Lips and Laanemets, 1994), which trigger the transport and mixing. For these motions the Baltic Sea is like a **small ocean**.

Marked hydrographic and ecological changes occurred in the Baltic Proper during the last stagnation period. Absence of intense North Sea water inflows since 1977 until 1993 led to overall decrease of salinity and vertical stability. Anoxic conditions prevailed in the deep waters due to lacking of effective aeration, making conditions for the cod spawning and the bottom life unfavourable in large areas. The stagnation period was terminated in 1993 by the major inflow of highly saline and oxygenated water (Matthäus and Lass, 1995). Altering of the events of large saline water inflows followed by much longer stagnation periods is, by no doubt, greatly affecting how the environmental key issues - eutrophication due to high nutrient loads, harmful algae blooms, accumulation of toxic substances in the food web *etc.* appear in the marine environment. Therefore understanding and proper modelling of the salt cycle in the Baltic is a prerequisite for appropriate dealing with ecological and environmental management problems. Since both the hydrographic and ecological conditions vary considerably from one sub-region to another, having sometimes even opposite trends, need for the sub-regional consideration is obvious.

The aim of the present study is to investigate mutual relationships of deep water overflow, circulation and vertical exchange in the deep basins of the Baltic Proper, with a focus on the Eastern Gotland Basin. While general features of the large-scale water exchange have been derived from the steady state budget calculations (*e.g.* Kõuts and Omstedt, 1993), the channel flow models (e.g. Pedersen, 1977, Lundberg, 1983) and from the horizontally integrated non-steady 'filling box' models (*e.g.* Stigebrandt, 1983, 1987, Omstedt, 1990), then little is known how the observed particular changes in the saline water sphere may be quantified in terms of the exchange components, both on the inter- and intra-basin scale. Our study is based on the data from hydrographic monitoring and process-oriented polygon observations made in the period 1979-1995. Several models are used for the analysis. The items of interest include the effects of

wind- and density-driven circulation, mesoscale motions, slope dynamics and intermittent mixing. In other words, we attempt to combine the approaches of huge estuary, large lake and small ocean for the explanation of the salt cycle.

The present report is composed from 9 Chapters. The Gotland Basin as the largest region of the Baltic Proper is the main area of interest. Following this introduction, regional characteristics of the Baltic Proper and its sub-regions are outlined in Chapter 2. Chapter 3 presents a detailed description of the changes of salinity, vertical stability, temperature-salinity relation and oxygen, observed in the deep sub-regions of the Baltic Proper during 1979-1995. The observed changes are used to quantify the transports and mixing by a diagnostic box model applied for the intermediate layers of the Gotland Basin as given in Chapter 4. Mesoscale observations are summarised in Chapter 5, with the focus on hydrodynamic structures in the up- and downstream basins, along and between the basins, mesoscale eddies in the connecting channels, and seasonally appearing slope effects. Attention is paid to the deep wintertime warm jets and lenses contributing to the observed warming-up of intermediate layers. Chapter 6 presents estimates of vertical mixing in terms of Richardson number statistics and turbulent kinetic energy dissipation rate. Possible energy sources for turbulence generation are discussed. Problems of turbulence modelling are considered within the RAT theory in Chapter 7. 3D circulation model is used to study the mesoscale eddies, spreading of deep water and dense water transport in the connecting channels as given in Chapter 8. Finally, Chapter 9 provides discussion of the results and gives the conclusions regarding the salt cycle on the Baltic Proper.

A number of scientists took part in the preparation of this report. Separate Sub-Chapters were written as follows: 5.3 - Juss Pavelson, 5.5 - Urmas Lips and Jüri Elken, 5.6 - Madis-Jaak Lilover and Jüri Elken, 6.1 - Madis-Jaak Lilover, 6.2 - Jaan Laanemets and Urmas Lips, 6.3 - Mikk Otsmann and Tiit Kullas, 7.1, 7.2, 7.3, 7.4 - Jaak Heinloo and Üllar Võsumaa. Other parts of the report were written by Jüri Elken.

# 2. REGIONAL CHARACTERISTICS

*Jüri Elken*

## 2.1. Topographic sub-division

The Baltic Sea consists of a number of sub-basins connected by straits and deep channels. Division of the Baltic Sea into regional subunits is commonly accepted from the hydrographic point of view (*e.g.* Fonselius, 1969; HELCOM, 1990; Omstedt, 1990), however the sub-division itself is subject to different approaches and definitions. In the present study the sub-division presented in Fig. 2.1 is used. Besides topographic features, the lines between the sub-regions which are important for quantitative modelling have taken into account also typical positions of hydrographic fronts in the surface layer (Elken *et al.*, 1987; Pavelson, 1988; Elken, 1994; Lips *et al.*, 1995). Topographic calculations and graphs are based on the bathymetry digitised with 1-mile resolution by the Baltic Sea Research Institute, Warnemünde (Seifert and Kayser, 1995).

The western connection areas to the Baltic Proper are rather shallow. The Kattegat, southeast from the typical position of the Skagerrak Front, is often considered as a part of the Baltic Sea. Major part of the Kattegat has depths less than 40 m. The Kattegat is connected with the Baltic Proper by two pathways. The eastern route - Öresund - is very narrow (smallest width - about 2 km) and shallow (sill depth - 8 m) but this pathway is only about 55 km long. Another way through the Belt Sea is some 180 km long and 20 m deep. The narrowest places have the width of 8 km. In the east the pathway is terminated by the Fehmarn Belt (Darss Sill) which is 32 km wide and 18 m deep.

The Baltic Proper can be divided into a number of deep basins. Large bays (Gulf of Bothnia, Finland and Riga) with remarkable freshwater influence are connected to the Baltic Proper in the north-east. Arkona Basin is the first sub-region counted from the connection area. It has rather smooth topography, with maximum depths amounting to about 50 m. Following further the saline water spreading pathway, the Arkona Basin is connected to the Bornholm Basin in the north by the Bornholm channel which is about 30 km wide and 40 m deep. The connection south of the Bornholm Island is some 100 km wide but the depth amounts only to 25 m. The Bornholm Basin is for the saline water sphere of the quasi-circular shape, with a diameter of 80-100 km and maximum depth of 95 m. Saline water flows out through the 80-km long Stolpe Channel which has about 20 km width by the 60-m isobath. In the right side of the downstream direction, towards south-east lies the Gdansk Basin with depths amounting to 110 m. On the left side, about 50 km wide and more than 100 m deep Hoburg Channel as a part of the Eastern Gotland Basin extends towards the Gotland Deep. In the Gotland Deep region, the Eastern Gotland Basin is some 130 km wide from the Gotland to the Latvian coast and 80 km wide on the 70-80 m depth level. The maximum depth amounts to 250 m. Further to the north, the Faro Deep, with rough bottom topography on the eastern flanks and a 115 m sill depth, connects to the Northern Deep, the center of the Northern Basin. From the zone of maximum depths, about 200 m deep, the Northern Basin extends to the east towards the Gulf of Finland as a deep channel with decreasing width and depth. In the north the Northern Basin is bounded by the Åland/Archipelago Sea constituting the gateway to the Gulf of Bothnia. Since the northern sills are rather shallow, only water above the halocline is penetrating northwards. In the west the Northern Basin is connected to the Western

Gotland Basin through the 30-km wide (by the 70 m isobath) and 110-m deep passage. Further to the south-west, the Western Gotland Basin includes the deepest place in the Baltic - the Landsort Deep with a 459 m depth, and a continuation with more regular channel topography which ends by the shallow regions (with depths less than 40 m) at the connection with the Bornholm, Gdansk and Eastern Gotland Basins.

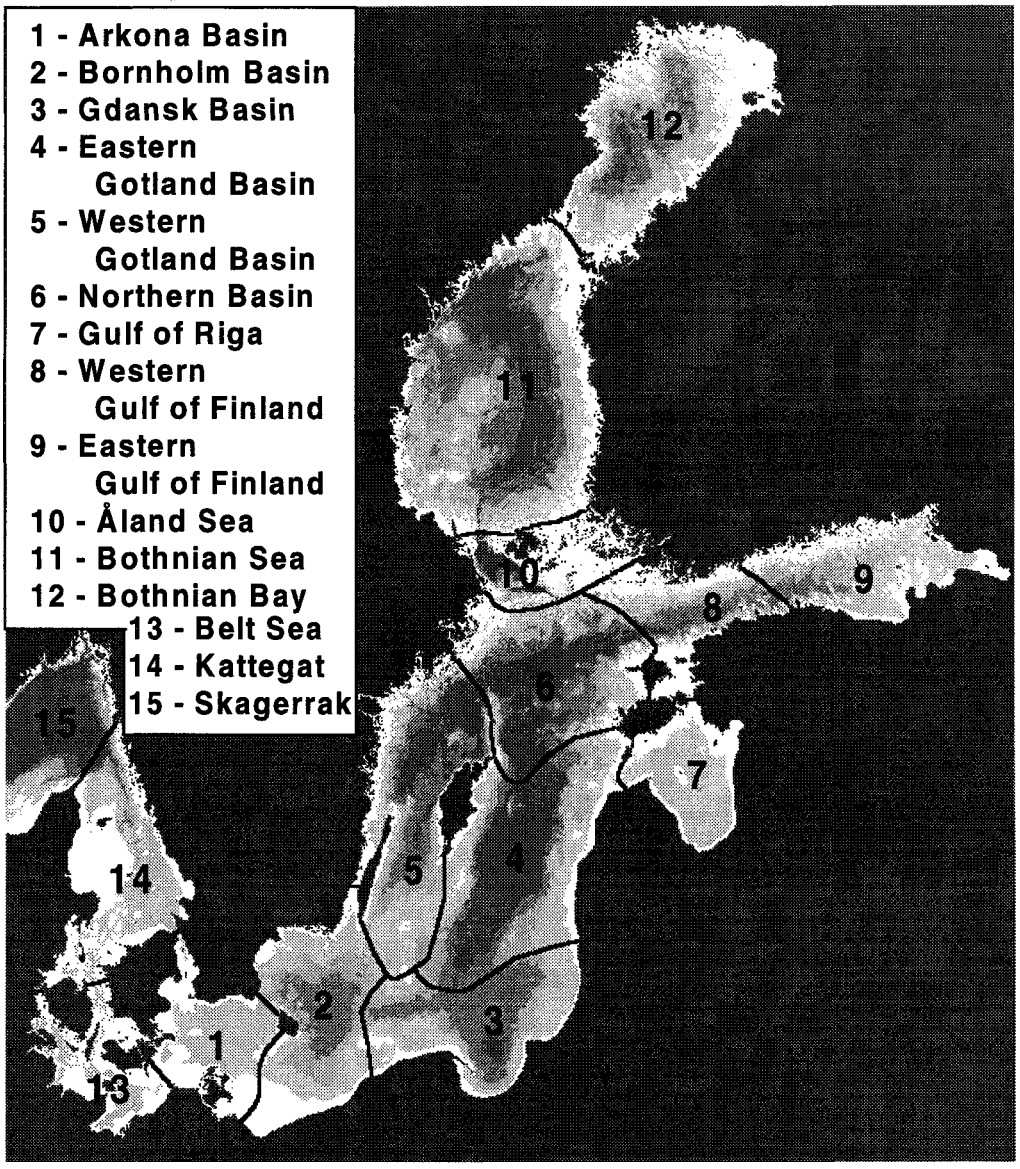


***Fig. 2.1.*** *Map of the Baltic Sea, with topographic sub-division used in the present study. The bottom topography is sketched by the grey colour, with dark shades corresponding to greater depths.*

Topography of the Baltic Proper is shown in more details in Fig. 2.1. Since the beginning of the century, regular hydrographic observations have been made in a number of stations. They have been also incorporated into the present HELCOM BMP monitoring programme

(HELCOM, 1988). These stations are further referenced at the regional hydrographic description.

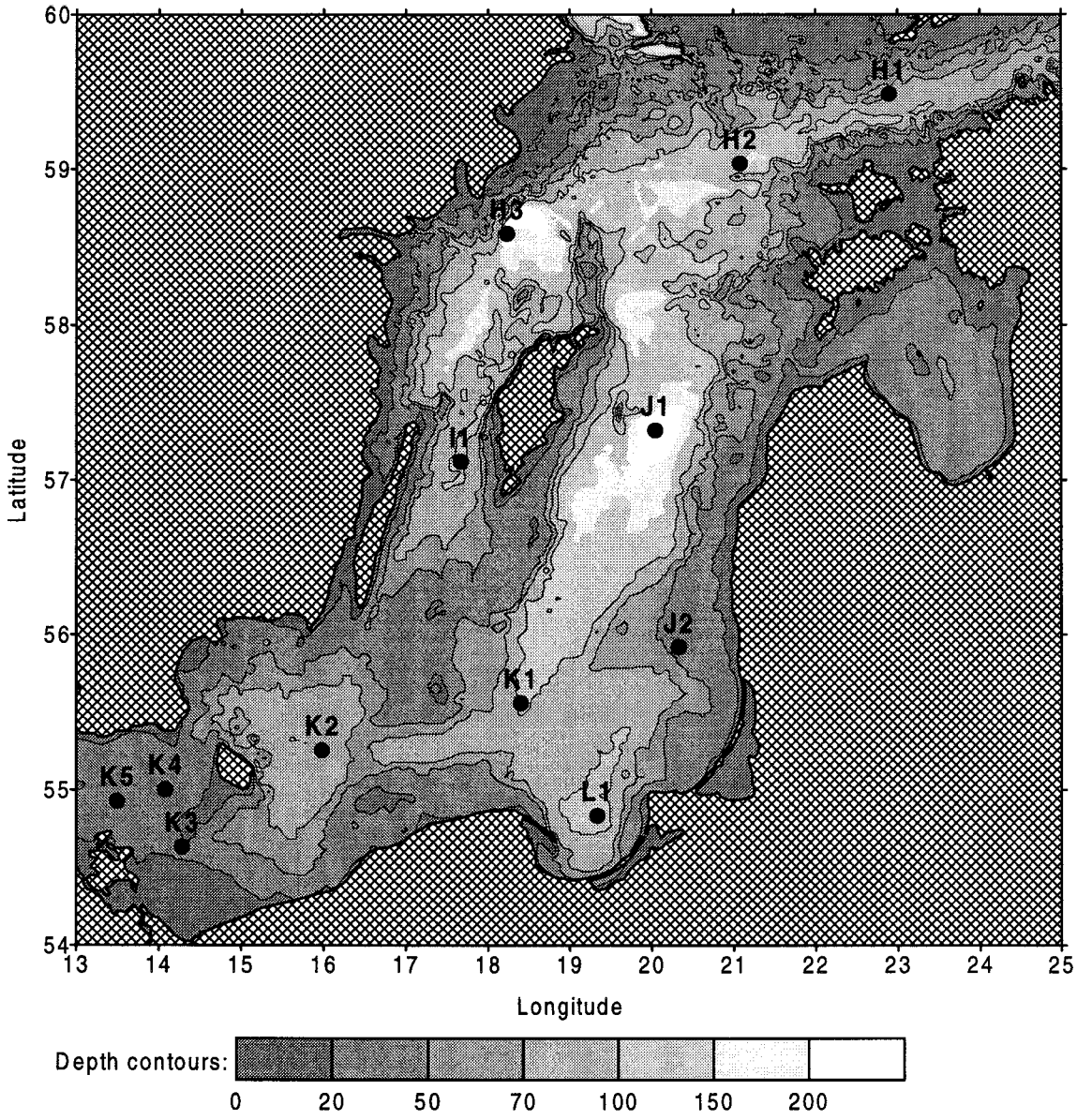


***Fig. 2.2.*** *Map of the Baltic Proper with the depth contours shown in the legend. Dots and labels represent the positions of the HELCOM BMP monitoring stations.*

## 2.2. Volumes and areas

The Baltic Proper is the largest part of the Baltic Sea. Its surface area (HELCOM, 1990) is 211,069 km$^2$ (51 % of the whole Baltic) and the volume is 13,045 km$^3$ (60 %). Topographic sub-division into the deep basins as presented in Fig. 2.1 allows calculation of hypsographic function - area of horizontal cross-section as a function of depth, $A(z)$ - for each basin. Integration of $A(z)$ from the bottom towards the sea surface gives the volume function $V(z)$ interpreted as the sub-area volume below the depth level $z$. Calculated $A(z)$ and $V(z)$ are given in Fig. 2.3.

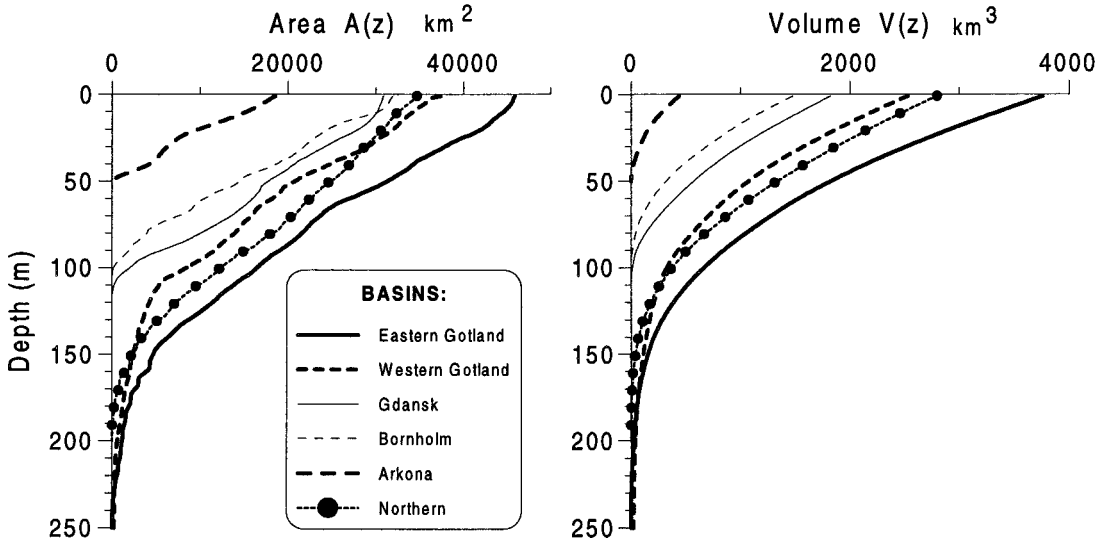


***Fig. 2.3.*** *Hypsographic functions, A(z) (area of horizontal cross-section at depth level z) and volume functions, V(z) (volume below depth level z) of the Baltic Proper basins. Digitized topography is taken from Seifert and Kayser (1995). Basin boundaries are defined as in Fig. 2.1.*

Numerical values of the surface areas and total volumes of the Baltic Proper sub-regions are presented in Table 2.1. In the context of the present deep water study, estimate of the saline water residence time (volume divided by the inflow rate) is of great importance. Adopting typical halocline depths for the basins, the Eastern Gotland Basin and the Northern Basin comprise about 60 % of the total saline water volume of the Baltic Proper. Monthly mean saline water inflow rates in different basins vary within the limits 10,000-60,000 $m^3/s$ (Stigebrandt, 1987a; Kõuts and Omstedt, 1993). Residence times were estimated at the assumed inflow rate of 20,000 $m^3/s$.

***Table 2.1.***
*Characteristics of the Baltic Proper sub-regions. Volumes and residence times of saline water are calculated at given halocline depths and inflow rate. Boundaries are specified as shown in Fig. 2.1.*

| **Basin** | **Surface area ($km^2$)** | **Total volume ($km^3$)** | **Typical halocline depth (m)** | **Volume of saline water ($km^3$)** | **Residence time of saline water at inflow rate 20,000 $m^3/s$** |
|---|---|---|---|---|---|
| Arkona | 18,505 | 440 | 35 | 47 | 0.9 months |
| Bornholm | 31,902 | 1,479 | 50 | 318 | 6 months |
| Gdansk | 30,824 | 1,822 | 60 | 402 | 8 months |
| Eastern Gotland | 45,904 | 3,763 | 70 | 1,278 | 24 months |
| Northern | 34,728 | 2,799 | 70 | 882 | 17 months |
| Western Gotland | 37,335 | 2,533 | 70 | 708 | 13 months |

## 2.3. Mean water balance

The Baltic Sea is a brackish-water sea, containing a mixture of riverborne freshwater and ocean saltwater. Rivers drain directly into the Baltic Proper 100 $km^3$ freshwater per year (HELCOM, 1990) comprising 21 % of the total runoff. Together with the Gulf of Finland and the Gulf of Riga, freshwater drainage amounts to 243 $km^3$/year. The Gulf of Bothnia adds 193 $km^3$/year. This makes the outflow-inflow difference at the sea entrance equal to 475 $km^3$/year. Annual precipitation exceeds evaporation by 39 $km^3$. Based on the salt conservation (Knudsen, 1900), deep-water inflow makes on the long-term average 475 $km^3$/year. The mean water balance is illustrated in Fig. 2.4.

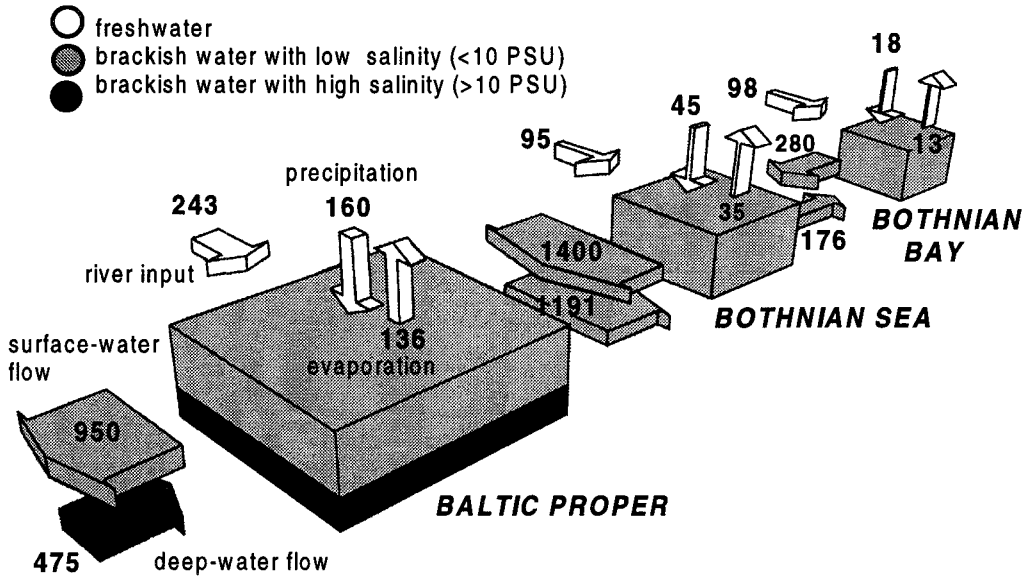


***Fig. 2.4.*** *Block diagram illustrating the water exchange in the Baltic. Data in $km^3$ per year. From HELCOM (1993).*

High-saline water, with salinity greater than 10 PSU is found only in the Baltic Proper. Intermittent saline water inflow, of different flowrate, duration and salinity, feeds the saline stratification which undergoes remarkable changes from year to year. Both diagnosis of the recent stagnation period and analysis of relevant key processes is given in a more detail in the next chapters.

# 3. STRATIFICATION CHANGES IN 1979-1995

*Jüri Elken*

Since the previous major inflow of saline North Sea water into the Baltic Sea occurring in turn of 1976/1977 (*e.g.* Matthäus and Frank, 1992), reduced salinity range of the inflowing waters had led to the stagnation of deep waters which period continued until 1993. Overall decrease of salinity and vertical stability was apparent in all the Baltic Proper sub-basins. Anoxic conditions prevailed in the Gotland Deep due to absence of effective deep water renewal. In January 1993 about 135 $km^3$ of highly saline (>17 PSU) and oxygenated water entered the Baltic Sea within a three week period (Matthäus and Lass; 1995). Due to the buffering effect of the western sub-basins, bottom water renewal in the Gotland Deep appeared only in spring of 1994. This Chapter presents detailed analysis of stratification changes during 1979-1995, based on the data from international HELCOM monitoring programme, a large number of historical CTD data by the Estonian Marine Institute, and additional data by the Baltic Sea Research Institute, Warnemünde and the Institute of Meteorology and Water Management, Gdynia.

## 3.1. Salinity

The most specific feature of the hydrographic regime of the Baltic Proper is the permanent saline stratification which is formed by intermittent inflow of saline water from the Belt Sea and the Öresund (Bergström and Matthäus, 1996), and by freshwater surplus {Bergström and Matthäus, 1996) from the adjacent diluted basins {Gulf of Bothnia, Finland and Riga) and draining rivers (Vistula, Odra, Nemunas etc.). Inflowing saline water is spread and mixed in the cascade of the deep sub-basins in the Baltic Proper. Overflow from one sub-basin to another is dependent on the halocline height above the sill depth of the connecting channel and the density/salinity difference between the basins (Stigebrandt, 1983, Omstedt, 1990) as well as by the direction and speed of dominating winds (Krauss and Brügge, 1992). Actual conditions are controlled by a complex of transport and exchange processes. Observations of the deep flow into the Arkona Basin in the beginning of January 1993 were performed and analysed by Liljebladh and Stigebrandt (1995). From CTD sections and ship-mounted ADCP records they were able to detect a dense bottom pool including baroclinic geostrophic currents along the northern flank of the pool. These observations are of great importance for the understanding how the deep water enters the Baltic Sea.

Saline water passing the entrances to the Baltic Sea spreads in the Arkona Basin as a bottom layer of variable thickness. Between 1989 and 1992 winter inflows were evident in each January-February, increasing the bottom salinity to 18-19 PSU and lifting the 14 PSU isohaline from the summer near-bottom position (about 43 m) to depths between 35 and 38 m. Autumn inflows appearing in August-September lifted the 10 PSU isohaline to depths above 25 m. Effects of more intense autumn and winter inflows were found in 1992. The major inflow in January 1993 (cf. Bergström and Matthäus, 1996, Matthäus and Lass, 1995) increased the bottom salinity to 23 PSU and shifted the 10 PSU isohaline up to 20 m depth. During the previous period since 1979, bottom salinity values exceeding 20 PSU were found only in winter 1980 and autumn 1986.

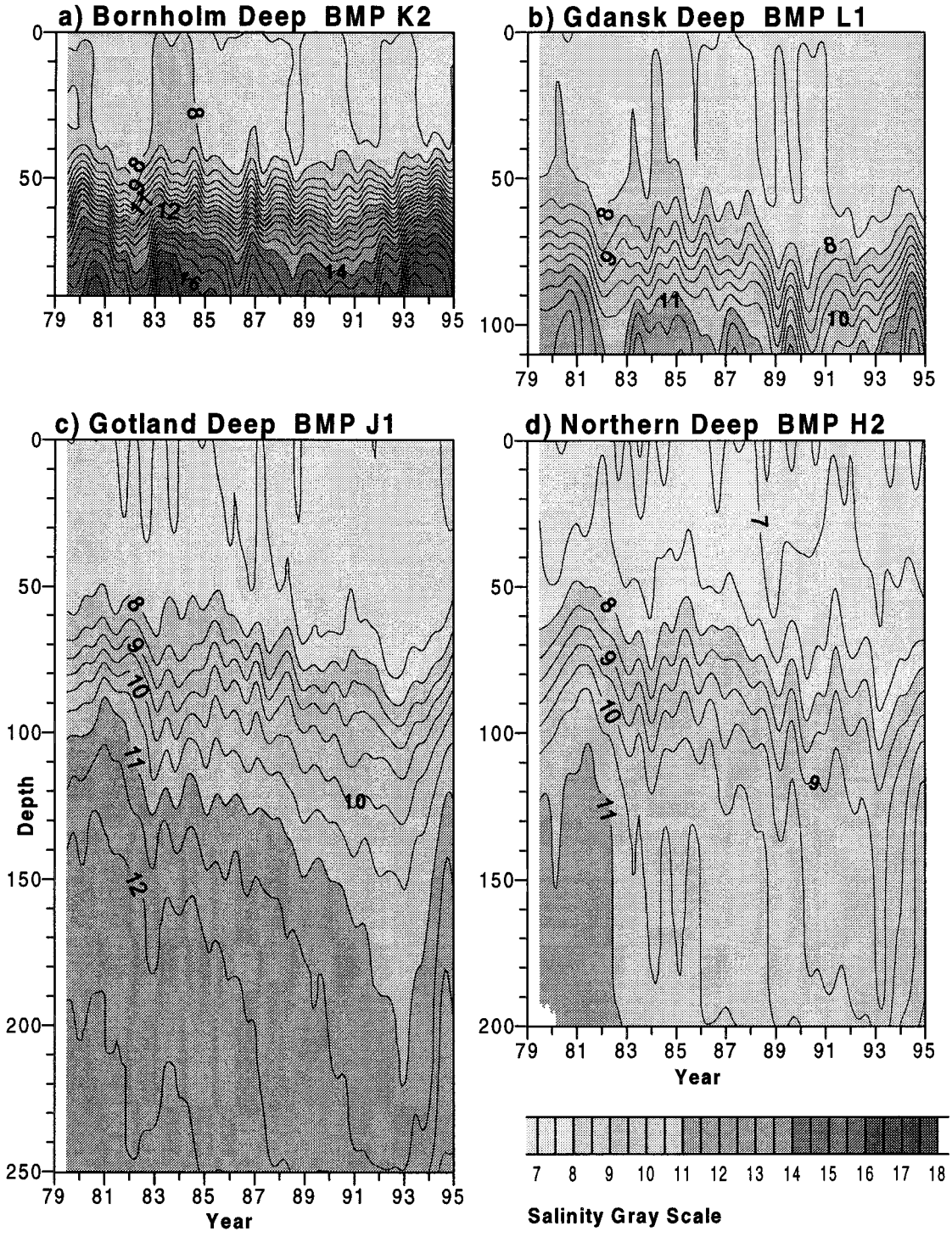


***Fig. 3.1.*** *Salinity as a function of time during 1979-1994 (x-axis) and depth (y-axis) at HELCOM BMP stations a) K2 - Bornholm Deep, b) L1 - Gdansk Deep, c) I1 - Gotland Deep, d) H2 - Northern Deep. Contour interval is 1 PSU.*

After passing the Bornholm Channel, saline and dense water sinks in the **Bornholm Basin** to the bottom or the level of neutral buoyancy, depending of the old stratification, while lifting up the above layers of lower salinity. Saline stratification (Fig. 3.1a) in the

period 1989-1991 is characterised by small temporal changes indicating that salt water overflow from the Arkona Basin took place into the different intermediate layers and was balanced by vertical mixing. Water of the bottom layer was renewed in winter 1991/1992 when bottom salinity was increased from 14 to 16 PSU following more elevated isohaline depths in the upstream Arkona Basin. After the major inflow in January 1993, bottom salinity increased to 19.5 PSU lifting the 16 PSU isohaline from the bottom (about 90 m) to 70 m depth. From the previous period, bottom water renewal is evident at inflows during winters 1980 and 1983 and autumn 1986. Seasonal summer decrease of the halocline salinity had maximal amplitudes in 1986, 1987, 1988 and 1992.

Overflow of saline waters from the Bornholm Basin to the Gdansk and Gotland Basins is limited by the **Stolpe Sill** which has a depth of 60 m. In 1989-1992 the layer above 60 m had salinity generally less than 10 PSU (see Fig. 3.1a), only in 1992 maximum of 11 PSU has been observed. Such an overflow situation for low saline water has been previously observed in 1981 and 1982. Since 1985 the overflowing water had salinity less than 11 PSU which has direct influence to the enhanced stagnation in the Gotland Deep. The major inflow in January 1993 increased the overflowing salinity range up to 12.3 PSU, and in winter 1993/1994 salinity at the Stolpe Sill depth exceeded 13 PSU.

Part of the saline water flowing from the Bornholm Basin layer above 60 m turns to the **Gdansk Basin** which is like the Bornholm Basin a buffer zone for the saline water pathway into the Gotland Deep. In 1989-1992 salinity of the bottom water did not exceed 10.5 PSU in the Gdansk Basin (Fig. 3.1b) which corresponds well to the low salinity in the Bornholm Basin at the Stolpe Sill depth. Strong storms during the winters 1989 and 1990 coupled with the weakened halocline caused temporary erosion of the halocline down to 80-90 m depth. After the 1993 inflow, bottom salinity increased to 11.8 PSU and increased further up to maximum value of 13.6 PSU in spring 1994.

Saline stratification in the **Gotland Deep** (Fig. 3.1c) exhibits decreasing salinity (deepening of isohalines) during the stagnation period until the major inflow in 1993. The bottom salinity decreased in 1980-1992 from 12.7 PSU to 11.3 PSU while the 11 PSU isohaline deepened from 90 m depth down to 230 m. Below the halocline, increased lateral transport of intermediate-saline waters (10-11 PSU) from the Bornholm and Gdansk Basins took place during 1985-1992 causing decrease of vertical stability of the intermediate waters. Long-term average dense water transport rate below the halocline has been estimated 33,200 $m^3/s$ (Kõuts and Omstedt, 1993). Deep waters were replaced by oxygenated new saline water in 1994 (cf. Bergström and Matthäus, 1996).

In the **Northern Basin** (Fig. 3.1d) the halocline centre followed generally the depth of the 8.5 PSU isohaline which deepened from its most shallow position found in 1981 at 60 m depth to the extreme depths of 110-120 m observed in 1993. Effect of the 1983 inflow into the Bornholm Basin can be found in all the downstream basins as elevated halocline during 1983-1986. Weakened vertical stability at the end of the stagnation period favoured winter-time erosion of the halocline to the greater depths and better aeration of deep layers. Below 150 m salinity decreased from 11.5 PSU in 1980 to 9 PSU in 1992 which is a result of decreased salinity in the Gotland Deep above the level of Farö Channel (115 m). In 1989-1992 the maximum salinity of overflowing waters decreased in the Gotland Basin from 10.3 to 9.3 PSU which corresponds to the salinity

of bottom waters of the Northern Deep. By the summer of 1994 bottom salinity increased to 9.6 PSU which is far below from the high values exceeding 11 PSU observed in 1979-1981.

### 3.2. Vertical stability

Vertical stability of the water column with respect to gravity is characterised by the Brunt-Väisälä frequency $N$, where

$$N^2 = \frac{g}{\rho_o}\frac{\partial \rho}{\partial z}, \qquad (3.1)$$

$\rho = \rho(T,S)$ is variable water density, $\rho_o$ is the mean density and $g$ is the gravity acceleration with the vertical co-ordinate $z$ directed downwards from the sea surface.

Fig. 3.2 presents the smoothed $N$ values calculated from the interpolated salinity (Fig. 3.1) and temperature time-depth $(t,z)$ distributions. Maximum $N$ values below the summer thermocline (about 20 m depth) are found in the halocline, which lies on the 55-65 m depth in the Bornholm Basin and below that at more variable depths in the downstream basins.

The strongest vertical stability with $N_{max}$ exceeding 0.05 $s^{-1}$ was observed in the **Bornholm Basin** (Fig. 3.2a) in 1980, 1983 and 1993 following intensive saline water inflows. Those years were characterised also by the shallow depths - about 55 m - of the $N_{max}$ layer. In 1989-1991 $N_{max}$ values decreased below 0.045 $s^{-1}$ which was accompanied by the deepening of the $N_{max}$ layer from about 55 m depth in 1988 to the depths below 65 m observed in summer 1990. As will be shown in Chapter 4, the halocline depth in the Bornholm Basin is effectively regulated by the gravity forced outflow through Stolpe Channel (sill depth about 60 m).

Large range of the halocline variation, compared with the Bornholm Basin, was observed in the downstream **Gdansk Basin** (Fig. 3.2b). Shallow positions of the halocline with the $N_{max}$ layer on about 70 m depth was observed in 1980-1981 and 1993-1994. The values of $N_{max}$ exceeded 0.035 $s^{-1}$. Strong winds have been capable of eroding the halocline down to 90 m in late autumn of 1982 and 1990 reducing the $N_{max}$ values below 0.025 $s^{-1}$.

In the **Gotland Basin** (Fig. 3.2c) the layer of $N_{max}$ controlling the cross-halocline mixing followed in general the depth course of isohalines 8.5-9 PSU (Fig. 3.1c) being in the range of 75-90 m. At the same time the halocline thickness (defined as a layer with $N$ exceeding 0.02 $s^{-1}$, typical values 20-30 m) did not change considerably. This is also valid for the small-scale vertical gradients derived from CTD profiles (Lips and Laanemets, 1994). However, larger values of $N_{max}$ exceeding 0.025 $s^{-1}$ were observed in 1980/1981 and 1994, and reduced vertical stability of the halocline with $N_{max} < 0.02$ $s^{-1}$ was observed in 1990-1991.

The vertical stability of the **Northern Basin** (Fig. 3.2d) repeated in general the features observed in the Gotland Basin, with the $N_{max}$ values being smaller by about 0.005 $s^{-1}$. Reduced vertical stability is a reason for more intense vertical mixing and larger depth excursions (65-100 m) of the halocline as compared with the Gotland Basin. The values

of $N_{max}$ decreased from 0.025 $s^{-1}$ in 1981 down to the low values of 0.015-0.017 $s^{-1}$ observed during 1990-1992.

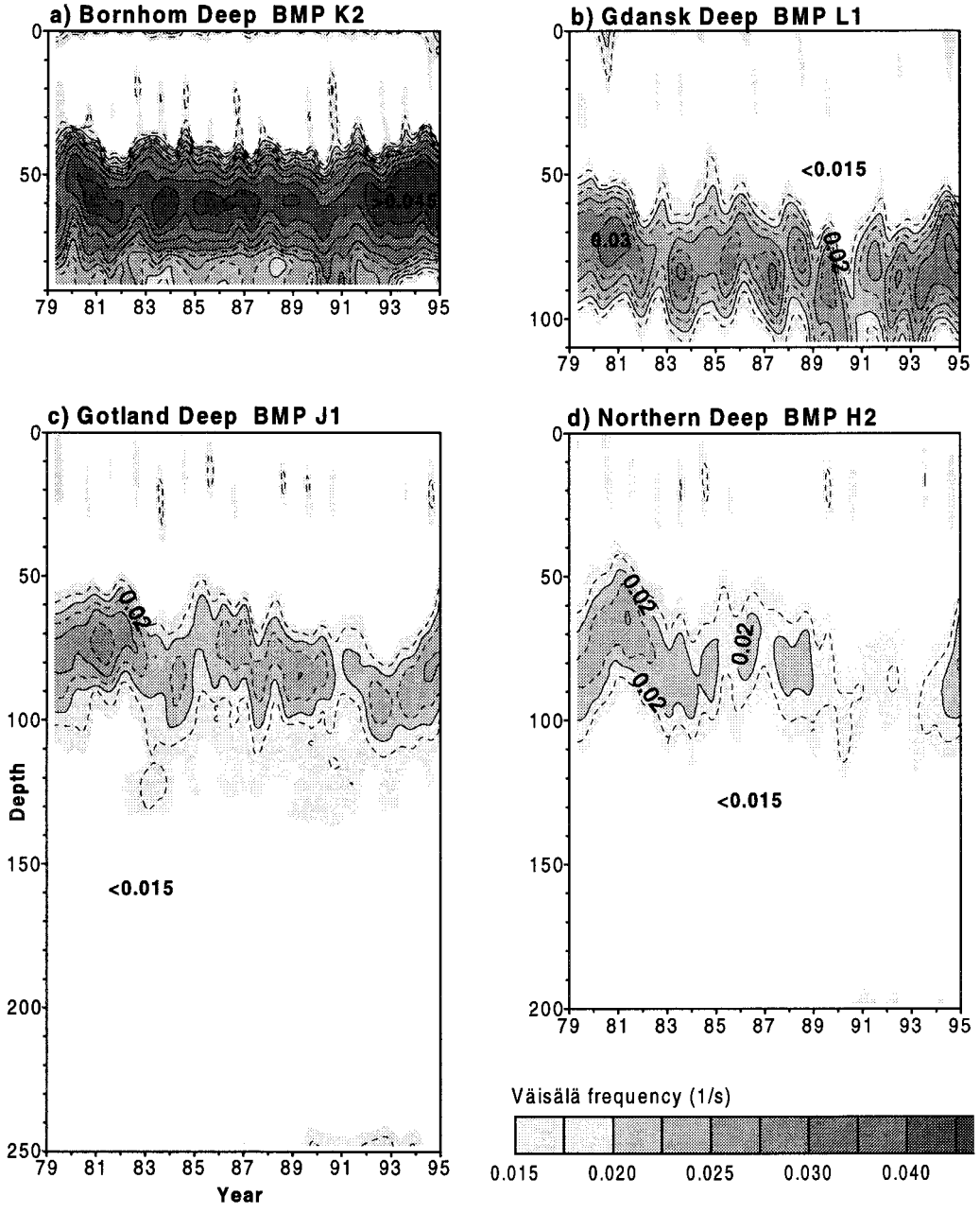


***Fig. 3.2.*** *Vertical stability (Brunt-Väisälä frequency) as a function of time during 1979-1994 (x-axis) and depth (y-axis) at HELCOM BMP stations a) K2 - Bornholm Deep, b) L1 - Gdansk Deep, c) J1 - Gotland Deep, d) H2 - Northern Deep. Contour interval is 0.005 $s^{-1}$, with the dashed lines inserted.*

### 3.3. Temperature-salinity relation

The end of the stagnation period (1989-1992) was characterised by abnormal increase of temperature of the intermediate layers. This warming-up is demonstrated in Fig. 3.3 on the basis of the contour plots of temperature drawn in the salinity coordinate.

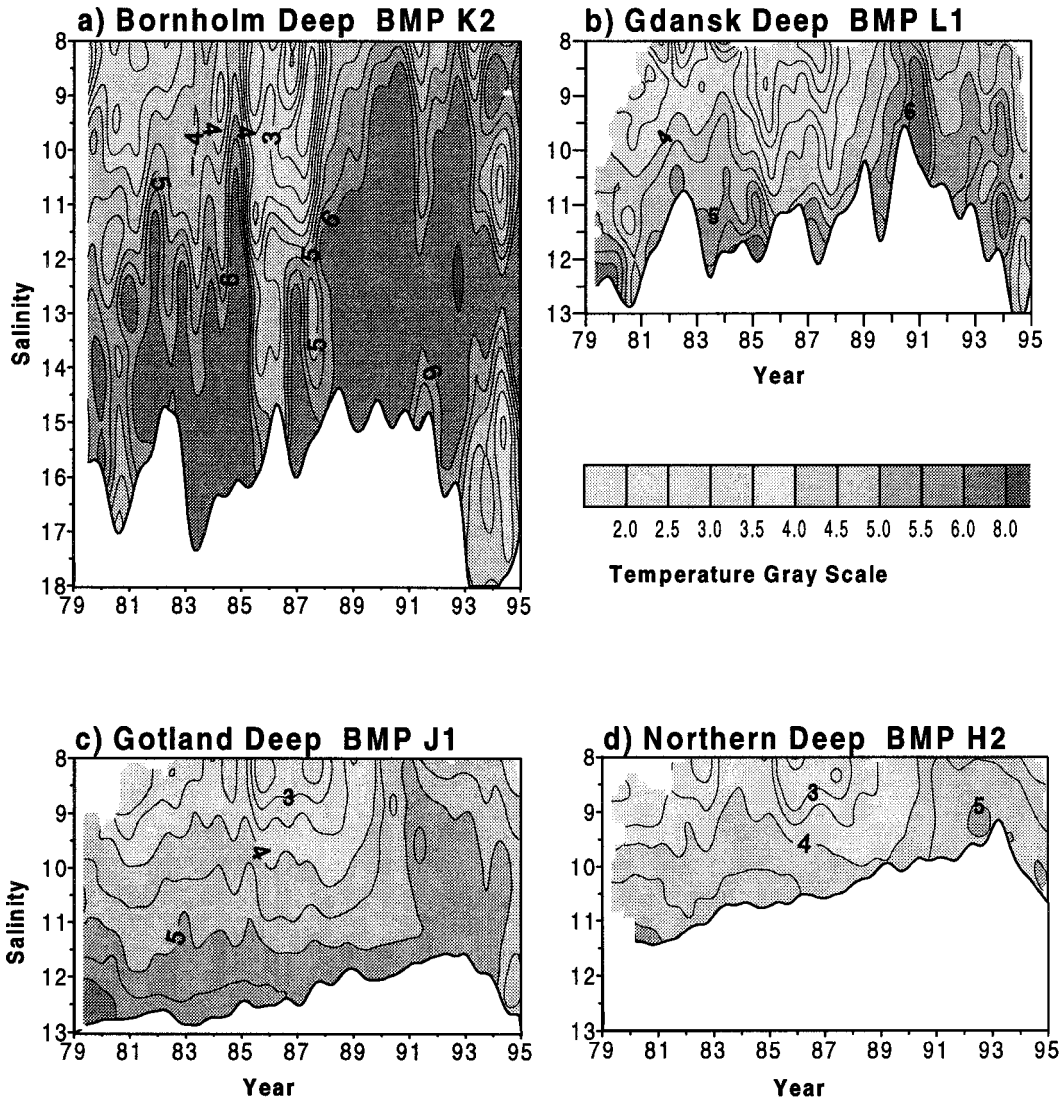


*Fig. 3.3. Temperature as a function of time during 1979-1994 (x-axis) and salinity (y-axis) at HELCOM BMP stations a) K2 - Bornholm Deep, b) L1 - Gdansk Deep, c) J1 - Gotland Deep, d) H2 - Northern Deep. Contour interval is 0.5°C.*

Salinity range 8-12 PSU of the **Bornholm Basin** (for the depth range of isohalines see Fig. 3.1) which is laterally transported through the Stolpe Channel into the Gotland Basin, was characterised by temperatures generally below 5 °C in 1979-1986 (Fig. 3.3a). In 1987 temperature started to increase reaching a peak value above 7°C in 1989-1990 between 10 and 13 PSU. In the layer 8.5-10.5 PSU of the buffering **Gdansk Basin** highest temperature exceeding 6 °C (Fig. 3.3b) was found in turn of 1990/1991. This abnormally warm dense water was transported further to the **Gotland** and **Northern Basin** where typical increase of temperature with salinity was replaced in winter

1990/1991 by homothermal conditions (Figs. 3.3c, 3.3d). Temperature at isohaline 9.5 PSU increased from a typical range of 3.6-4.2°C to a value of 5.4°C in the Gotland Basin and 5°C in the Northern Basin.

### 3.4. Oxygen

Oxygen depletion below 50 m was observed in the **Bornholm Basin** since the 1983 inflow until 1990. Low-oxygen bottom layer, with concentrations below 3 ml/l increased in the thickness and its upper boundary risen from about 75 m to 65 m during this period (Fig. 3.4a). Hydrogen sulphide appeared below 80 m in 1988 and 1989. Beginning from 1991, seasonal inflows created peak increases of the bottom oxygen concentrations, reaching 4 ml/l in 1992 and more than 5 ml/l during the 1993 major inflow. Depth range of 50-60 m which is overflowing to the Gdansk Basin, was characterised by concentrations 6-8 ml/l during 1983-1987, by 4-6 ml/l in 1988-1989 and by 5-7 ml/l in a period of 1990-1994.

**Gdansk Basin** reached the lowest oxygen concentrations in 1987-1988 while the waters below 3 ml/l occupied the layer from 75-85 to the bottom (Fig. 3.4b). Anoxic near bottom conditions were observed temporarily during 1987-1989. Highest near-bottom oxygen concentrations exceeding 4 ml/l at 105 m depth were observed in 1990 which is explained by a decay of vertical saline stratification (Fig. 3.1b) due to intensified mixing and by subsequent vertical aeration of deep layers. The year 1990 is characterised by the largest number of stormy and gale days during 1982-1994 (cf. Bergström and Matthäus, 1996, Fig. 2.7). The major inflow in 1993 had less effect on oxygen increase than the stratification erosion effect in 1990.

The boundary between oxygenated and anoxic waters in the **Gotland Deep** lied between 110-160 m depth during 1979-1992 (Fig. 3.4c), with a typical value of 130 m. The major inflow of 1993 intruded slightly oxygenated (less than 1-2 ml/l) waters into the deep layers. High oxygen values in the deep layers exceeding 3 ml/l were observed during 1994 (for the explanation see chapter 2.5.4). Intermediate layers (100-130 m) were more intensively oxygenated during 1984-1985 following the 1983 inflow and high oxygen conditions in the Bornholm Basin. The level of 2 ml/l which had a trend of deepening, from 80m in 1981 down to 110 m in 1993, went down to a depth more than 120 m during 1984-1985. By the end of the stagnation period, the deepened and more week halocline caused higher oxygen values at the depths 70-90 m.

In the **Northern Basin** (Fig. 3.4d) anoxic conditions were found in the deep layers in 1980-1984 and 1987-1990. Presence of near-bottom oxygen in 1985-1986 could be partly explained by transport of waters from the Gotland Basin above 115 m depth which had higher oxygen content in 1984-1985 (Fig. 3.4c). After 1991 decreased vertical stratification (Fig. 3.1d) facilitated more intense vertical mixing and hydrogen sulphide was not found in the deep layers.

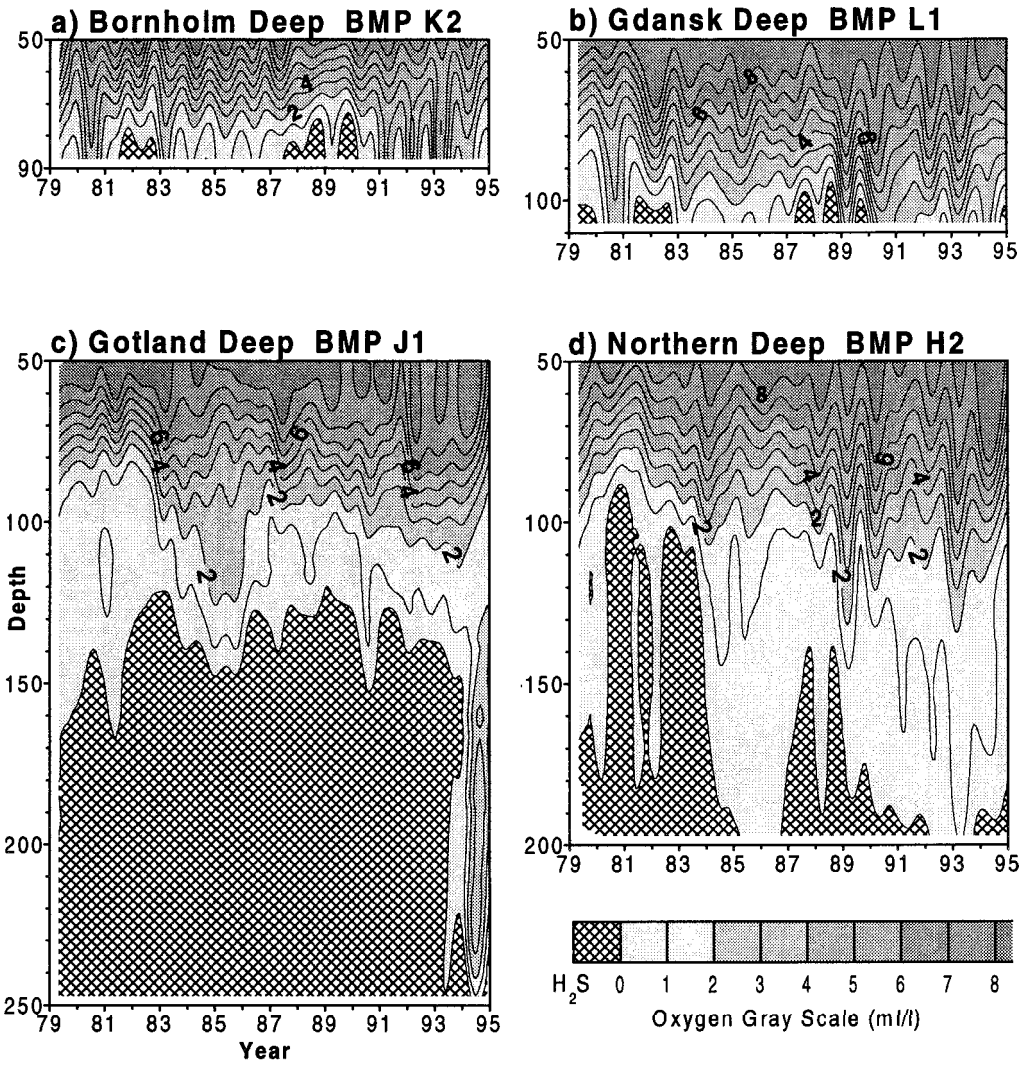


***Fig. 3.4.*** *Oxygen (ml/l) as a function of time during 1979-1994 (x-axis) and depth (y-axis) at HELCOM BMP stations a) K2 - Bornholm Deep, b) L1 - Gdansk Deep, c) J1 - Gotland Deep, d) H2 - Northern Deep. Contour interval is 1 ml/l, shaded area represents the depth range filled by hydrogen sulphide.*

# 4. LARGE-SCALE ESTIMATES OF EXCHANGE COMPONENTS

*Jüri Elken*

In Chapter 3 we have considered observed long term changes of stratification in the Baltic Proper sub-basins. Decrease of salinity, especially in deep layers, was evident until 1993 when the stagnation period was terminated by the major North Sea water inflow. Stagnation led also to oxygen depletion in deep waters. Mutual changes in different basins with respect to deep water overflow were qualitatively discussed. In the Chapter we use a simple box model to quantify the large-scale exchange components.

## 4.1. Box model approach

Let us assume that the sea consists of a sequence of stratified basins with horizontal surface area $A_i = A_i(z)$. Integration of the advection-diffusion equations for the heat and salt over the $A_i$, with a vertical co-ordinate $z = 0$ at the surface and increasing downwards, yields the following equations for the horizontally mean temperature $T_i = T_i(z,t)$ and salinity $S_i = S_i(z,t)$ in the $i$-th basin:

$$A_i \frac{\partial T_i}{\partial t} = \frac{\partial}{\partial z} A_i K_i^V \frac{\partial T_i}{\partial z} - \frac{\partial}{\partial z} A_i w_i T_i - q^-_{i+½} T_{i+½} + q^+_{i-½} T_{i-½} , \tag{4.1}$$

$$A_i \frac{\partial S_i}{\partial t} = \frac{\partial}{\partial z} A_i K_i^V \frac{\partial S_i}{\partial z} - \frac{\partial}{\partial z} A_i w_i S_i - q^-_{i+½} S_{i+½} + q^+_{i-½} S_{i-½} , \tag{4.2}$$

where $w_i$ is the horizontally mean vertical velocity, $q^+_{i-½}$ is the volume flow per unit depth at the connection line $i$-½ of the basins $i$-1 and $i$ on the side of the $i$-th basin, $T_{i-½}$ and $S_{i-½}$ are respective temperature and salinity. The bulk vertical diffusion coefficient $K_i^V$ (taken the same both for $T$ and $S$) is interpreted as parameterisation of horizontally mean turbulent fluxes of $S$ (similar also for $T$) by the standard gradient approach:

$$\int_{A_i(z)} (w(x,y,z,t) - (w_i(z,t))(S(x,y,z,t) - S_i(z,t))\, dA_i = -A_i K_i^V \frac{\partial S_i}{\partial z}. \tag{4.3}$$

In the case of narrow connections for the deep water, lateral heat and salt flux due to deviations from the mean values $q^+_{i-½}$, $T_{i-½}$ and $S_{i-½}$ on the connection line $L_{i-½}$ are assumed to be negligible.

For the vertical boundary conditions, exchange with the bottom is assumed to be absent. In the surface layer, the system (4.1)-(4.2) is usually coupled with the seasonal pycnocline model (*e.g.* Stigebrandt, 1987b; Omstedt, 1990) and appropriate surface flux conditions.

Vertical velocity $w_i$ is calculated from the continuity equation which takes the form:

$$w_i(z,t) = \frac{1}{A_i}\int_z^{H_i} (q^-_{i+½} - q^+_{i-½})\,dz, \tag{4.4}$$

where $H_i$ is the depth of the basin *i*.

We will further consider application of the model below the mixed layer as sketched in Fig. 4.1. The halocline depth $h_i$ may be defined, for instance, as a layer where $\Delta S$ per 1 m, starting from the surface, first time exceeds 0.05 PSU (Matthäus, 1979).

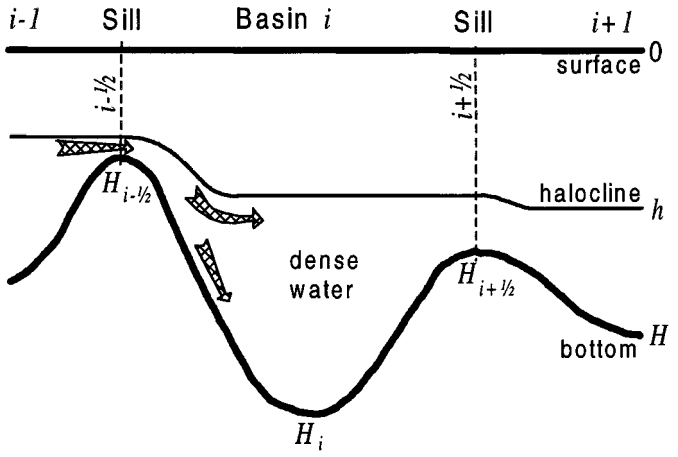


***Fig. 4.1.*** *A sketch of the box model approach.*

Above the sill with a depth $H_{i-½}$, below $h_{i-½} = \min(h_{i-1},h_i)$, the dense water volume flow (transport) per unit depth $q^-_{i-½}$ at the side of the basin *i*-1 may be calculated from the geostrophic relation,

$$q^-_{i-½}(z,t) = -\frac{g}{f\rho_o}\int_{h_{i-½}}^{z} (\rho_i - \rho_{i-1})\,dz. \tag{4.5}$$

with the assumption of the flow being absent at $z = h_{i-½}$. Here $\rho_i = \rho(T_i,S_i)$ is the water density, $g$ is the gravity acceleration and $f$ is the Coriolis parameter. The flow is driven by the gravity forces due to upstream-downstream density difference $\rho_{i-1}$-$\rho_i$ and balanced by rotational effects. More discussion about (4.5) is given by Stigebrandt (1987a).

In a two-layer approach, with $\rho_{i-1}$ and $\rho_i$ being constants, (4.5) turns into the Whitehead formula (Whitehead *et al.*, 1974)

$$Q^-_{i-½} = \frac{g'}{2f}(H_{i-½} - h_{i-½})^2, \tag{4.6}$$

where $Q^-_{i-½}$ is the volume transport and $g' = g\,(\rho_{i-1}$-$\rho_i)/\rho_o$ is the reduced gravity.

Frictional effects for the dense water overflow in the channel have been discussed in a number of papers (*e.g.* Pedersen, 1977; Lundberg, 1983; Pratt, 1986). Gidhagen and Håkansson (1992) showed by a two-layer numerical model that friction reduces the flow rate by about two times as compared with (4.6). The simplest way to encounter the friction is to introduce linear drag $rq^-_{i-½}$ which causes replacement of $f$ in (4.5) or (4.6) by $f+r$.

Considering further the continuous stratification formula (4.5), if dominatingly $\rho_{i-1}>\rho_i$ then the flow at the sill $q^-_{i-½}$ is sunk in the $i$-th basin down to the level of neutral buoyancy depending on the stratification $\rho_i(z,t)$ and the overflow continues at different depth levels as $q^+_{i-½}$. Therefore

$$q^+_{i-½}(z,t) = F_{\rho_{i-1},\rho_i}\{\ q^-_{i-½}(z,t)\ \}. \tag{4.7}$$

While $q^-_{i-½}(z,t) \neq q^+_{i-½}(z,t)$ then continuity of total volume transports $\int_{h_{i-1}}^{H_{i-½}} q^-_{i-½}dz = \int_{h_i}^{H_i} q^+_{i-½}dz$ is satisfied.

The coefficient of vertical diffusion $K_i^V$ of a stagnant ($w_i = 0$) semi-enclosed basin may be described as a function of the Brunt-Väisälä frequency $N$ (Gade, 1970). Hypsographic function $A_i(z)$ has a certain influence to the shape of $K_i^V$ (Gade, 1995). Following Stigebrandt (1987b) we use the form

$$K_i^V = \frac{\alpha}{N}, \tag{4.8}$$

where the value of $\alpha = 2*10^{-7}$ (± 35%) $m^2\ s^{-2}$ has been estimated. Discussion about the values of $\alpha$ can be found also in a recent paper by Stigebrandt (1995).

### 4.2. Diagnosis of salt and heat content in the intermediate layers

Taking the Gotland Basin as the basin $i$, the Bornholm Basin as $i$-1 and the Northern Basin as $i$+1, all the terms of equations of the system (4.1-2, 4.4-5, 4.7-8) may be directly estimated from the interpolated $z,t$ distributions of temperature and salinity (see Chapter 3) calculated from the "point" data (HELCOM BMP stations K2, J1 and H2) by the method of optimal interpolation with the time resolution of 1 month and depth resolution of 1 m. Having in mind the different sources of errors for the interpolated distributions (*e.g.* contribution of meso- and small-scale processes), and the problems of using the "point" data as representative for the horizontally mean over the basin value, the model equations are satisfied only approximately. The model coefficients may be varied to yield the best fit, *i.e.* to minimise the model disbalance on the given set of data.

The model coefficients have been optimised to diagnose the salt and heat content (total amount) changes in the intermediate layer covering the depth range from 90 to 150 m. Observed total amounts in the Gotland Basin were calculated as integrals of $A_iT_i$ and $A_iS_i$. Area function $A_i$ was taken as in Fig. 2.3, with the Gdansk Basin added to the

Eastern Gotland Basin. The modelled total amounts were calculated as time integration of the fluxes, which were determined from the right side of the equations (4.1, 4.2) by their vertical integration. With the fixed definition of the halocline depths $h_{i-1}$, $h_i$ and $h_{i+1}$, the best fit of the modelled total amounts to their observed counterparts is searched by variation of the sill depths $h_{i-½}$, $h_{i+½}$, the coefficient $\alpha$ of the diffusion parameterisation (4.8) and different formulations of friction.

The best fit to the observed salt and heat contents of the 90-150 m layer (Fig. 4.2) was obtained with the following set of parameters:

Stolpe sill depth: $h_{i-½} = 60$ m,
Farö sill depth: $h_{i+½} = 99$ m,
diffusion: $\alpha = 1.6*10^{-7}$ m$^2$ s$^{-2}$,
bottom friction: $r = 6*10^{-5}$ s$^{-1}$ for $\rho_{i-1}(z,t) > \rho_i(H_i,t)$.

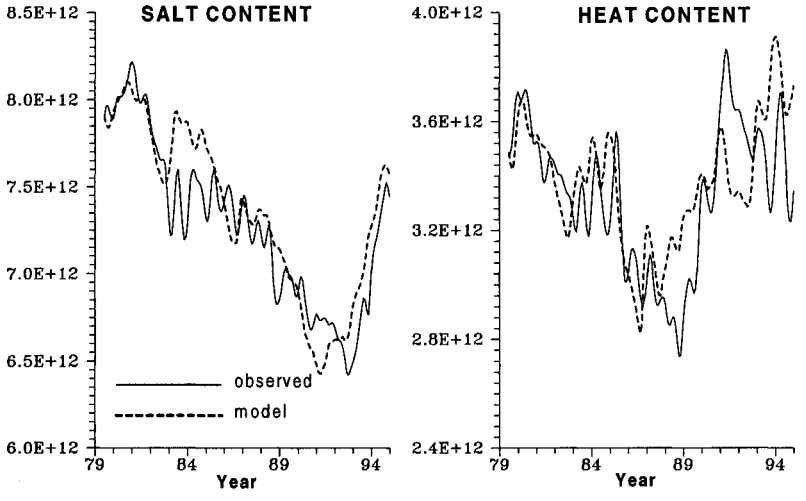


***Fig. 4.2.*** *Changes of salt and heat content in the Gotland Basin in the intermediate layer 90-150 m for the period 1979-1994 as observed (solid line) and calculated by modelling the fluxes (dashed line).*

The observed salt content changes are simulated by integration of the modelled fluxes rather well. Part of the mismatches can be directly attributed to the simplicity of the present model set-up, which can be easily accomplished. Since we have not taken into account the time lag (about 6-months by Fonselius, 1970) for advection of the inflowing water into the Gotland Basin, immediate response of the 1993 major inflow was modelled contrary to the observed salt content increase appearing only in 1994. Buffering role of the Gdansk Basin (see Chapters 3 and 8) is not considered. The modelled heat content followed closely the observed counterparts until 1987. Warming-up of the intermediate layers apparent from the observations during 1989-1991 was not reproduced by the model in such a detail. Those years at the end of the stagnation period were characteristic for appearing wintertime slope effects and deep lenses (see Chapter 5), probably not covered by the mixing scheme (4.8).

However, modelling of total amounts by the flux diagnosis have multiple parameter combinations allowing for the best fit of the nearly same accuracy. While increasing the friction at the Farö sill, the depth $h_{i+½}$ increased below 110 m. The parameter values given above were not suitable to estimate the fluxes in the bottom layer. Considerable increase of friction was necessary to mach the observed changes. Without having more basins in the model, we have not found any sense to deal more with tuning of the parameters. It is obvious, that the simple model is able to follow essential features of the stratification changes. Mutual response in the neighbouring basins, qualitatively described in Chapter 3, is further studied for quantitative relationships.

### 4.3. Lateral and vertical water transport

For the steady state of the Baltic Sea, Stigebrandt (1987a) has calculated the mean inflow rate into the Bornholm Basin of about 23 000 $m^3$ $s^{-1}$. Based on the two-layer approach which increases the salinity of the Bornholm Basin at the Stolpe sill depth (60 m) by more than 2 PSU, Kõuts and Omstedt (1993) estimated 33 200 $m^3$ $s^{-1}$ of the dense water flowing into the Eastern Gotland Basin.

Monthly water, salt and heat budgets of the non-steady stagnation period, terminated by the major saline water inflow in 1993, were calculated in the present study. The model uses continuous stratification and takes into account vertical circulation and mixing. Monthly inflow rates from the Bornholm Basin are highly fluctuative as displayed in Fig. 4.3.

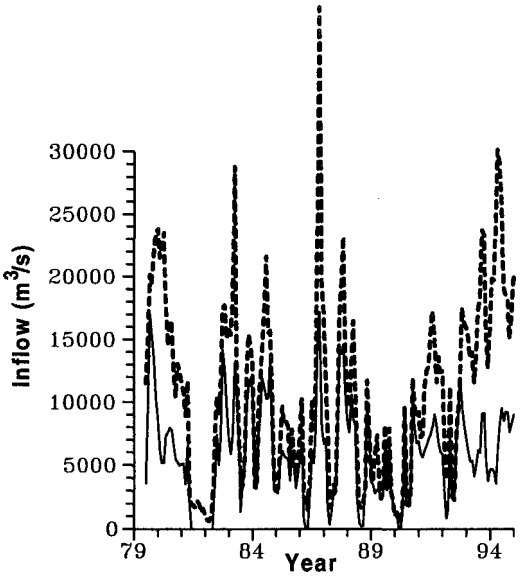


***Fig. 4.3.*** *Monthly inflow of the Bornholm Basin waters into the Gotland Basin for the intermediate layer 90-150 m (solid line) and the total depth range (bold dashed line).*

According to the equation (4.4), vertical velocity $w_i(z,t)$ equals to the net outflow below $z$ divided by the area $A_i(z)$, *i.e.* the net inflow below $z$ causes negative values of $w_i$. The water overflowing from the Stolpe Channel is sunk down to the level of neutral

buoyancy. If the overflowing water is not dense enough, it leaves into the intermediate layers and the deep layers remain stagnant with $w_i = 0$. Distribution of diagnosed $w_i(z,t)$ is given in Fig. 4.4. It is evident, that stagnant conditions below 150 m prevailed during 1981-1991. This is also consistent with the observed oxygen changes (Fig. 3.4). In the intermediate layers, upward velocity ($w_i < 0$) prevails. There have been cases of upward velocity enhancement when the normal outflow into the Northern Basin reversed to the northern inflow due to higher observed density values in the Northern Basin, see Fig. 3.1 and relation (4.5). Downward vertical velocity ($w_i > 0$) appeared from time to time above the Farö sill level ($z < 99$ m) when the outflow into the Northern Basin exceeded the inflow from the Bornholm Basin. Although the monthly vertical velocity is small (generally, $|w_i| < 2*10^{-6}$ m s$^{-1}$), vertical excursion in the intermediate layer may exceed 5 m during a month.

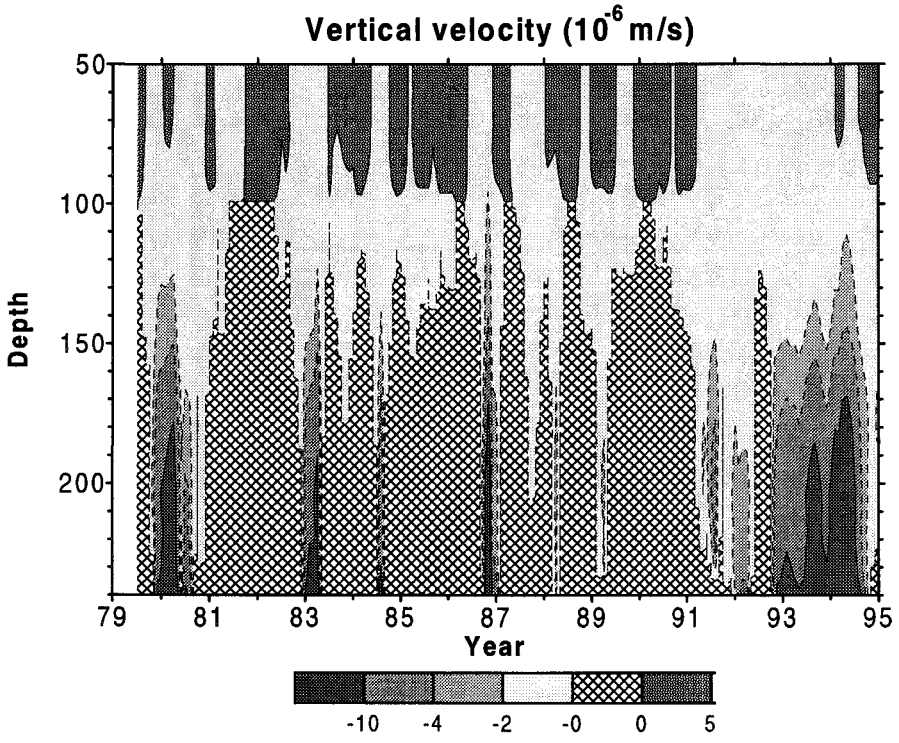


***Fig. 4.4.*** *Vertical velocity (negative upwards).*

Waters leaving the Bornholm Basin continue in the Gotland Basin at different depth levels, according to the isopycnal transformation (4.7). On the average for 1979-1994, the maximum inflow rates occurred around 100 m depth (Fig. 4.5). Below 150 m, only 17% of the net inflow occurred above the bottom. The minimum flow rate per unit depth around 200 m is explained by the low vertical stability observed there (see also Fig. 3.2), thus the inflowing waters tend to take either smaller or greater depths. About 12% of the inflow spreads on the bottom. Since it takes some 300 km for the densest water to spread on the bottom before reaching the Gotland Deep, introduction of friction for the inflowing bottom waters was necessary to simulate the salt content changes as described above. For the maximum inflow rate around 100 m, contact area with the bottom is rather small and already in the Hoburg Channel the waters spread above the bottom.

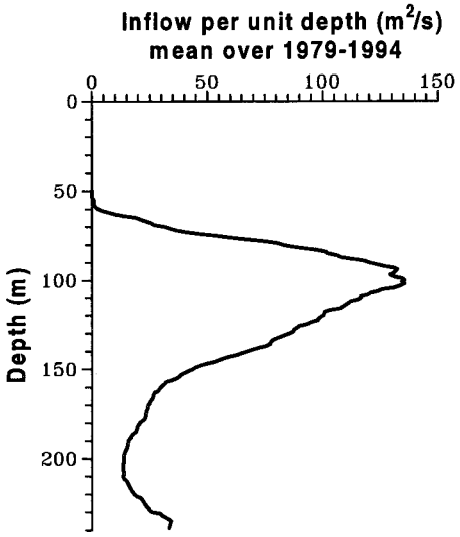


***Fig. 4.5.*** *Mean profile of the dense water inflow per unit depth entering the Gotland Basin from the Bornholm Basin. Mean flow reaching the bottom (not shown) is 1300 $m^3$ $s^{-1}$.*

The diagnostic model gives the mean inflow rate of dense water from the Bornholm Basin of 10900 $m^3$ $s^{-1}$ for the period 1979-1994. As given above, higher inflow rates have been estimated for different assumptions. A scheme of water exchange in the Gotland Basin is given in Fig. 4.6.

On the average, the inflow from the Bornholm Basin and the outflow to the Northern Basin are in approximate balance. Only 200 $m^3$ $s^{-1}$ of water is needed to come from the layers above the halocline to close the budget. The mean upward flow rate of 3200 - 3300 $m^3$ $s^{-1}$ is calculated for the intermediate layer 90-150 m. This yields the mean upward vertical velocity of 4.4 m $year^{-1}$ on the 90 m level and 23 m $year^{-1}$ on the 150 m level. Note, that the area of the Gotland Basin horizontal cross-section has been calculated $2.317*10^{10}$ $m^2$ on the 90 m depth and $0.438*10^{10}$ $m^2$ on the 150 m depth.

The end of the stagnation period, 1987-1990 was characterised by a different flow regime, based on the observed density differences in the three neighbouring basins. Decreased inflow from the Bornholm Basin - 6800 $m^3$ $s^{-1}$ , and increased outflow to the Northern Basin - 12400 $m^3$ $s^{-1}$, caused considerable downward flow of surface waters into the halocline. Thus 55% of the water flowing out to the Northern Basin came from the Bornholm Basin and 45% from the layers above the halocline. The mean sinking speed at the halocline depth (around 70 m) was estimated 5 m $year^{-1}$. This independent estimate of vertical advection is consistent with the observed halocline deepening (*cf.* Fig. 3.1). For the intermediate layer, 78% of the inflow came from the Bornholm Basin, 14% from the layers above and 8% from the layers below the selected depth range.

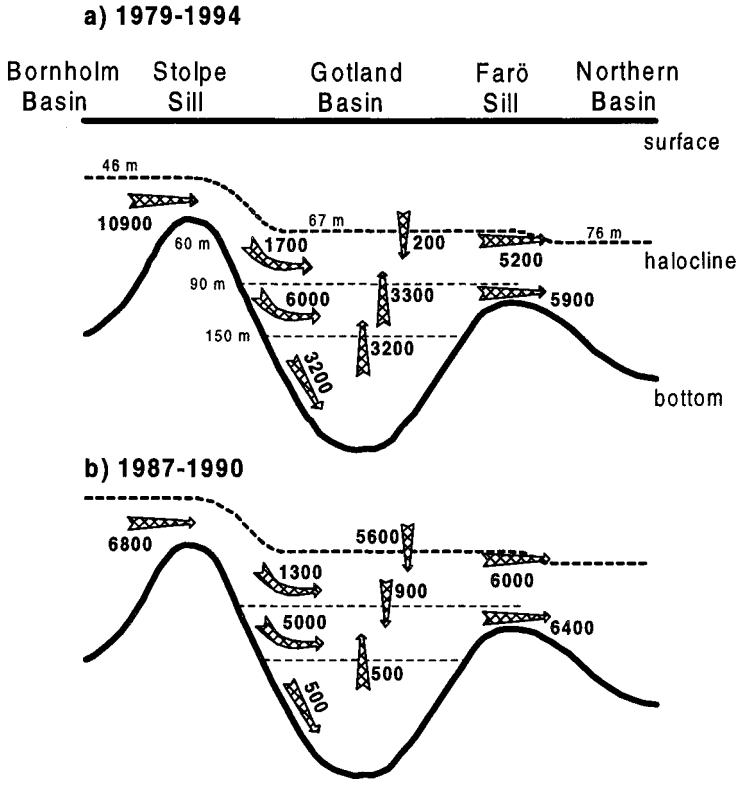


*Fig. 4.6. A scheme of mean water exchange in the Gotland Basin for the period 1979-1994 (a) and 1987-1990 (b). Bold numbers at the arrows represent volume transport in $m^3 s^{-1}$.*

### 4.4. Salt and heat exchange

Monthly advective transport of salt and heat is highly variable as the water transport (see Fig. 4.3) whereas both the horizontal and vertical components change the sign. On the longer time scale, diffusive effects become more important. Mean components of the salt and heat budget are presented in Table 4.1.

Within a period 1981-1992 the salt content of the 90-150 m layer decreased in the Gotland Basin from about $7.4*10^{12}$ kg to $6.1*10^{12}$ kg. Totally 11600 kg $s^{-1}$ of salt was exported from the layer due to vertical advection (21%) and vertical diffusion (79%). Import of salt due to horizontal advection comprised 71% of the salt loss. During the enhanced stagnation, 1987-1990 with the changed water exchange scheme (see above), the roles of horizontal and vertical advection in the salt import/export changed. The salt was lost by horizontal advection (52% of the 19000 kg $s^{-1}$) and vertical diffusion (48%). Salt supply was provided in this period by vertical transport (11400 kg $s^{-1}$) but increased salt loss caused more than a double salt amount decrease rate of 7600 kg $s^{-1}$.

Estimated heat content increased for the both periods of consideration, more for 1987-1990 and only a little bit for 1981-1992. For the warming-up period of the intermediate layers, 1987-1990, the heat was provided by vertical advection and lost by vertical

diffusion and horizontal advection. On the longer time scale, import by horizontal transport was nearly balanced with the export by vertical diffusion and advection.

***Table 4.1.*** *Components of the salt and heat budget of the intermediate layer 90-150 m of the Gotland Basin estimated for the stagnation period 1981-1992 and the sub-period 1987-1990.*

| | Salt budget components ($kg\ s^{-1}$) | | Heat budget components ($10^6$ cal $s^{-1}$) | |
|---|---|---|---|---|
| *(time period)* | 1981 -1992 | 1987 -1990 | 1981 -1992 | 1987 -1990 |
| Horizontal transport from the Stolpe Channel | 58100 | 51300 | 29500 | 27100 |
| Horizontal transport into the Northern Basin | 49900 | 61100 | 22800 | 28300 |
| **Total horizontal advective import** | **8200** | **-9800** | **6700** | **-1200** |
| Vertical transport from the layers below 150 m | 18000 | 6900 | 8100 | 3000 |
| Vertical transport into the layers above 90 m | 20500 | -4500 | 8900 | -4600 |
| **Total vertical advective export** | **2500** | **-11400** | **800** | **-7600** |
| Vertical diffusion from the layers below 150 m | 1100 | 1100 | 400 | 600 |
| Vertical diffusion into the layers above 90 m | 10200 | 10300 | 6100 | 4000 |
| **Total vertical diffusive export** | **9100** | **9200** | **5700** | **3400** |
| **TOTAL EXPORT** | **3400** | **7600** | **-200** | **-3000** |

Diffusive upward salt flux on the 90 m level has been estimated $0.45*10^{-6}$ kg $m^{-2}$ $s^{-1}$ which is a little less from the steady state estimate by Rahm (1985) who got $0.72*10^{-6}$ kg $m^{-2}$ $s^{-1}$. Matthäus (1990) summarised the limits for the known different salt flux estimates in a range of $0.12 \div 1.85*10^{-6}$ kg $m^{-2}$ $s^{-1}$.

### 4.5. Seasonal effects

Saline water inflow to the Baltic Sea has a seasonal maximum during the winter (Matthäus and Franck, 1992). This increases the dense water volume in the Bornholm Basin and lifts up the halocline, which is also evident from Fig. 3.1. Due to the absence of thermal stratification, wind mixing reaches the 40 m depth at wind speeds about 10 m $s^{-1}$ (Fennel *et al.,* 1986). At greater wind speeds, the waters from the top layer of the halocline are entrained into the surface layer. Another mechanism to loose the saline waters into the surface layer is convection due to negative vertical stability. While diffusion works towards smoothing of the halocline, convection and wind entrainment restore the rather sharp upper boundary of the halocline. Remaining part of the saline water - 10900 $m^3$ $s^{-1}$ by our calculations, is transported to the Eastern Gotland Basin. Density-driven outflow is practically not dependent on the stratification conditions in the Gotland Basin. Wind-driven transport superimposed on the persistent gravity current will be considered in Chapter 8.

Long-term vertical advection was found to be small at the halocline level in the Eastern Gotland Basin. During the summer, diffusion is not capable of making any effective export of heat and salt from the halocline to the cold layer just above. Therefore we assume that salt is convected and entrained to the surface layer mainly during the late autumn and winter. For the effective wind-induced entrainment, the speeds above 15 m $s^{-1}$ are needed. Between the two surveys made in the Gotland Deep in late autumn of 1986, the speed of westerly winds was dominatingly above 15 m $s^{-1}$ forcing a break in the measurements. During a 9-day period, the mean salinity of the layer 5-60 m had increased by about 0.1 PSU both in the plume of less saline northern waters and the Gotland Basin waters (Fig. 4.7). This yields the upward salt flux about $7*10^{-6}$ kg $m^{-2}$ $s^{-1}$ during the events of stormy entrainment which exceeds the maximum limits given by Matthäus (1990) by a factor of 4. Seasonal effects in the stratification appear due to coupling of inflow/outflow balance and wintertime halocline erosion. As a rule (*cf.* Fig. 3.1) the halocline goes deeper during the cold season.

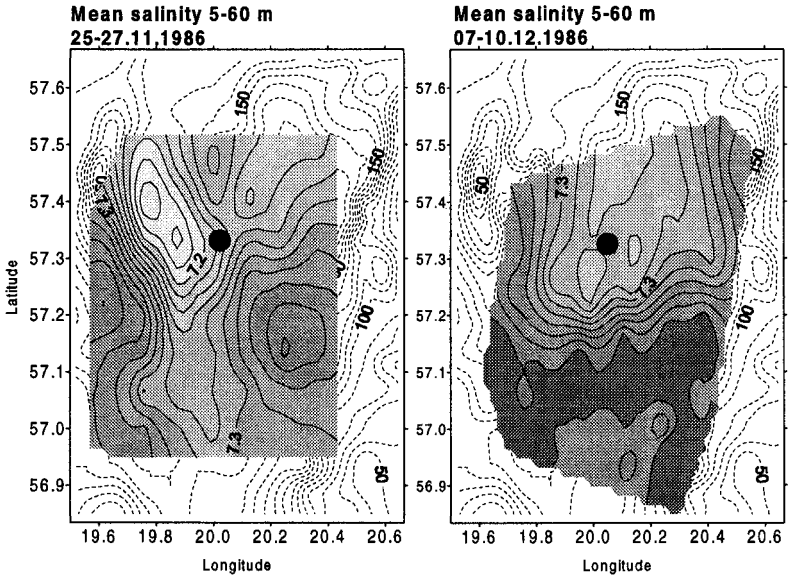


***Fig. 4.7.*** *Maps of mean salinity in the layer 5-60 m at two surveys in the Gotland Deep, with the bottom contours around the survey area given by dashed line. Heavy dot shows the position of the monitoring station HELCOM BMP J1.*

The Northern Basin is a region which splits into the two terminal areas of the saline water route - the entrance to the Gulf of Finland and the Western Gotland Basin. If we assume that 50% of the calculated mean inflow rate - 11000 $m^3$ $s^{-1}$ - is sunk down and another 50% spreads further to the terminal areas, then the halocline of the Northern Basin rises from the spring to the autumn by 8 m within 9 months. Without the halocline erosion during the cold season, the saline water sphere in the terminal basins would rise unrealistically. Significant vertical advection coupled with stronger halocline erosion (becuase the vertical stability is less than in the upstream basins) leads to the highest amplitudes of seasonal changes in the saline water (Matthäus, 1984). This is also seen from Fig. 3.1.

# 5. MESOSCALE HYDRODYNAMIC STRUCTURES

*Jüri Elken, Urmas Lips, Juss Pavelson and Madis-Jaak Lilover*

First polygon observations resolving mesoscale eddies in the open ocean (e.g. Koshlyakov and Grachev, 1973) changed the understanding of ocean dynamics. It became clear that oceanic motions with a length scale of the baroclinic Rossby deformation radius, $R_d = NH/f$ ( $\approx$ 50 km for the ocean), which are some kind of analogues to the atmospheric cyclones/anticyclones ($R_d \approx 2000$ km for the atmosphere), are of high energy and contribute essentially for the general circulation (Holland and Lin, 1975). In the Baltic deep basins $R_d \approx 10$ km, but smaller values are found in the shallow regions.

Research of mesoscale variability in the Baltic Sea followed the similar studies of the ocean. After first eddy indications on a polygon measured repeatedly by towed thermistors (Keunecke and Magaard, 1974), regular eddy-resolving polygon observations were introduced in the Baltic deep basins (Aitsam and Elken,1980,1982). Observational climax was reached by the international patchiness experiment PEX-86 (ICES, 1989) which hydrographic part took example from the ocean MODE and POLYMODE experiments. Since late eighties mesoscale investigations focused on deep lenses (Elken *et al.*, 1988, Kõuts *et al.*, 1990) which were found to be similar to the Mediterranean water lenses (Meddies) in the Atlantic, and on slope effects like the current jets and deep thermohaline anomalies. High-resolution transects with towed CTD were explored to study the hydrodynamic structures along the basins (Pavelson, 1988).

## 5.1. Statistical characteristics of mesoscale variability

Estonian Marine Institute with its predecessors has collected since 1978 a large CTD data set in different Baltic Sea areas by CTD Mark III NBIS. Considerable part of data (about 10000 CTD profiles) was collected within process-oriented studies at repeated mesoscale polygon surveys (with the space resolution a few miles) and time series. More details about the data is given in Chapter 6.

Available polygon data allow the estimation of mesoscale halocline heterogeneity by analysing the deviations of observed and derived properties from their horizontally mean (over the polygon) value. Eddy potential energy density per unit mass (*PED*) is calculated by the formula

$$PED = \frac{1}{2} \overline{N}^{\,2} \overline{\xi}^{\,2} \qquad (5.1)$$

where $N$ is the Brunt-Väisälä frequency calculated from the mean isopycnal depths and $\xi$ is the isopycnal displacement from the mean (over the polygon) depth.

In the Gotland Deep *PED* was determined in a layer 60-150 m on the basis of polygon observations in 1984-1992. Display of the *PED* values on a seasonal time scale (Fig. 5.1.1) reveals a clear signal that isopycnal displacements are smallest during the summer

and largest during the late autumn and winter. This cycle is also evident for thermohaline heterogeneity calculated as isopycnal temperature standard deviation, with the exception of two surveys in 1985 which also gave the high values.

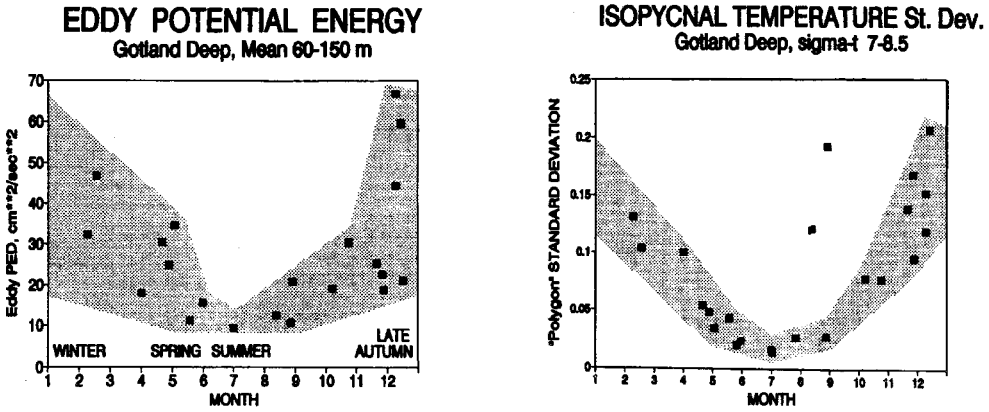


***Fig. 5.1.1.*** *Seasonal cycle of the eddy potential energy density (left) and standard deviation of isopycnal temperature (right) calculated from the polygon observations in the Gotland Deep.*

It is well known (*e.g.* Fennel and Lass, 1989) that variable wind forcing induces baroclinic Kelvin waves which amplitudes decay from the slope in a distance of $R_d$. The slope effects will be demonstrated in the following sub-chapters. The above statistical estimates included both the near-slope ($R_d$ distance from the 70-80 m isobaths) and off-slope regions. For the comparison of the model response (Chapter 8) it was necessary to recalculate the statistics for the interior, off-slope regions. Standard deviations of salinity were calculated by 5 m depth intervals and averaged in a layer from 60 to 90 m for the two areas containing mainly off-slope region. The results are given in Table 5.1.1. We may conclude that halocline in the off-slope regions of the Gotland Deep is by about 2 times less disturbed than in the Hoburg Channel.

***Table 5.1.1.*** *Salinity standard deviation in a layer 60-90 m by polygon observations*

| a) Hoburg polygon 56°00'-56°25'N, 18°40'-19°20'E | | |
|---|---|---|
| Date | No. sta. | St. dev. |
| 29-30.05.1979 | 22 | 0.26 |
| 05-06.08.1979 | 12 | 0.21 |
| 25-26.09.1979 | 13 | 0.23 |
| 30-31.05.1980 | 15 | 0.35 |
| 11. 06.1980 | 16 | 0.29 |
| 10-11.08.1980 | 16 | 0.19 |
| 08-09.06.1982 | 13 | 0.23 |
| 17-19.04.1985 | 24 | 0.25 |
| 01-02.04.1986 | 14 | 0.21 |
| 25. 04.1986 | 30 | 0.30 |
| 29. 04.1986 | 29 | 0.29 |
| 03. 05.1986 | 30 | 0.29 |
| 07. 05.1986 | 30 | 0.30 |

| b) Gotland Deep polygon 57°00'-57°30'N, 19°30'-20°10'E | | |
|---|---|---|
| Date | No. sta. | St. dev. |
| 25-27.11.1986 | 36 | 0.25 |
| 07-10.12.1986 | 28 | 0.37 |
| 26. 07.1987 | 6 | 0.13 |
| 04-06.10.1987 | 28 | 0.16 |
| 19-20.11.1987 | 8 | 0.13 |
| 05. 05.1988 | 9 | 0.30 |
| 29. 06.1988 | 8 | 0.13 |
| 17-18.12.1988 | 8 | 0.17 |
| 19-21.04.1989 | 16 | 0.12 |
| 10-11.07.1989 | 15 | 0.20 |
| 16. 09.1989 | 8 | 0.06 |
| 24-25.11.1989 | 26 | 0.11 |
| 12-14.12.1989 | 16 | 0.20 |

Empirical mode analysis of the polygon data revealed that two first EOF comprise more than 90% of isopycnal displacement (Elken, 1987). In the Hoburg Channel the depth of the sign change for the second EOF - around 80-85 m - is close to that of the theoretical mode of the Sturm-Liuoville problem for the vertical structure of wave solutions. Interesting feature is here that the second mode may have in a limited area snapshot more energy than the first mode. The second empirical mode comes from the lenslike eddies which have anomalous core around 80-m depth.

### 5.2. Structures in the up- and downstream sub-basins

*a) Upstream Bornholm Basin*

In the nearly circular Bornhom Basin the saline water is supplied in the west from the Bornholm Channel north of the Bornholm Island and is flowing out in the east through the Stolpe Channel. Variable inflow coupled with the wind forcing generates energetic mesoscale motions. Circular topography favours generation of topographic waves which propagate cyclonically along the slope, with the more shallow water remaining to the right (Kielmann, 1981). Saline water entering in the form of pulses is not spread instantaneously over the basin, but forms baroclinic eddies, either on the top of the halocline (Fig. 5.2.1) or anticyclonic deep lenses (Lehmann, personal communication). For the 20-km diameter cyclonic eddy found in June 1982 in the south-western part of the basin, isopycnals were elevated by more than 10 m compared with the basin background.

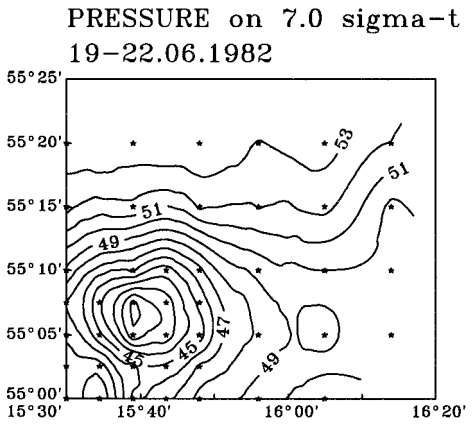


***Fig. 5.2.1.*** *A map of isopycnal depth (pressure) of 7 kg m-3 showing cyclonic eddy in the Bornholm Basin. Spacing between the stations (stars) is 2.5 and 5 miles.*

On the 60 m level which is controlling the saline water outflow over the Stolpe sill, salinity is rather variable as can be seen from the maps presented in Fig. 5.2.2. Salinity varies by more than 2 PSU whereas at the monitoring station BMP K2 (shown by a heavy dot) salinity may be often smaller than near the Stolpe Channel which is located in the eastern part of the maps.

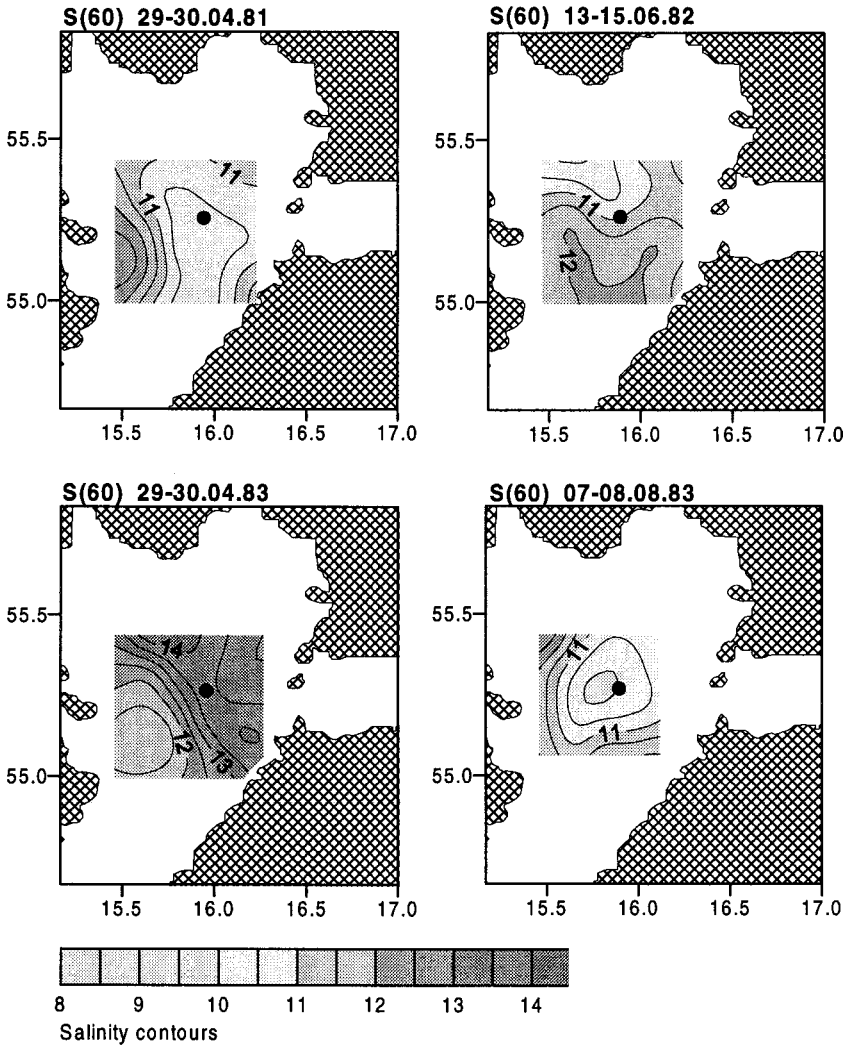


***Fig. 5.2.2.*** *Maps of salinity on the 60 m level in the Bornholm Basin by the data of mesoscale (gridspacing 5 miles) surveys. The area with depths less than 60 m is hatched. Heavy dot shows the position of the monitoring station BMP K2.*

*b) Downstream Northern Basin*

The Northern Basin receives on the average by more than 10000 $m^3 s^{-1}$ of saline water from the Gotland Basin. Remarkable bottom slopes and variable stratification give rise to several energetic fluctuations of the general cyclonic circulation in the form of synoptic eddies, topographic and inertial waves, fronts and unsteady jet currents, near-slope upwelling and downwelling *etc.*, modifying the mean deep flow of saline water into the Gulf of Finland and triggering this way the changes in the regime.

Mesoscale variability of the Northern Basin has been studied by a number of CTD surveys. In August-September 1982 the Estonian RV "Ayu-Dag" and the Finnish RV "Aranda" made hydrophysical measurements on a polygon near the monitoring station BMP H2. The main grid for CTD stations covered an area of 20 to 20 miles with a 5-mile grid step. Altogether six surveys were made. Current meters and a thermistor chain

were installed at three locations for the period of the experiment. More details of the results of the joint experiment are presented in a manuscript by Mälkki and Elken (1990).

In the halocline the salinity was increased at the southern flanks of the deep trench for the nearly one month period (Fig. 5.2.3). This corresponds to dominating saline water inflow towards the Gulf of Finland along the southern slope which is consistent with the mean circulation schemes in the area.

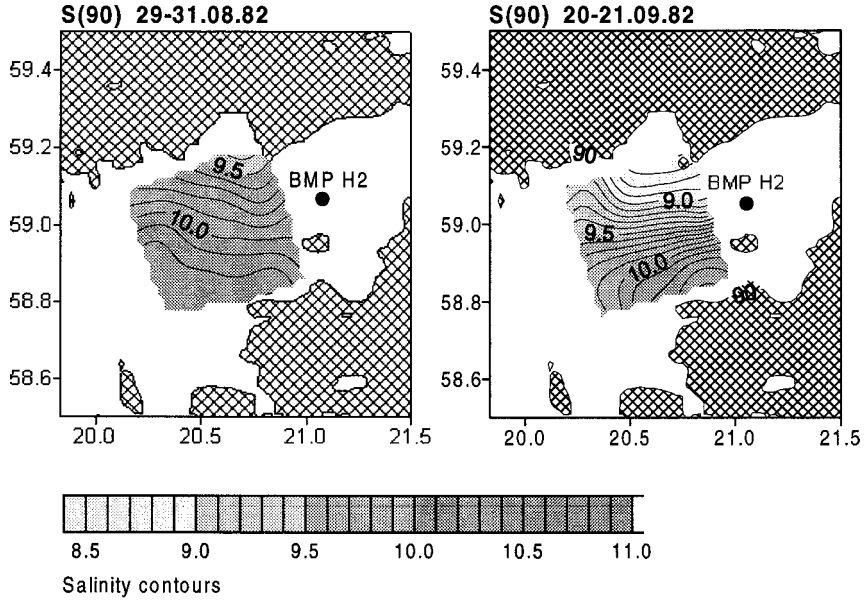


***Fig. 5.2.3.*** *Maps of salinity on the 90 m depth in the Northern Basin. The area with depths less than 90 m is hatched. Heavy dot shows the position of the monitoring station BMP H2.*

The halocline dynamics is displayed by dynamic topography of the 30 m level relative to the 90 m. The maps for the six surveys are presented in Fig. 5.2.4. The dynamic topography is proportional to the mean density in the layer, but in geostrophic approach it is also a streamfunction of the upper level currents relative to the lower layer. The first dynamic topography map reveals a system of cyclonic currents which is consistent with the upper layer salinity distribution. On the second and third survey the development of an eddy pattern centred at station D4 could be followed. In the eastern part of the polygon, an area with high dynamic topography values (corresponding to a decrease of the mean density or deepening of isopycnals within the halocline) started to develop and widen. On surveys 4, 5 and 6 a well-expressed jet-like structure of the dynamic topography with deeper halocline in the north and shallower halocline in the south could be observed. Also an anticyclonic eddy structure could be observed at stations E5 and D5. Looking at the dynamic topography of other levels of the first survey and the survey of the north-east subgrid it becomes clear that the anticyclonic eddy pattern observed in surveys 2 and 3 at station D4 (Fig. 5.2.4) started its development at station E5. Directly measured currents of the 30-m level relative to the 90-m level showed a general agreement with the geostrophic relation. In some cases, however, clear indication of ageostrophic movements was noted.

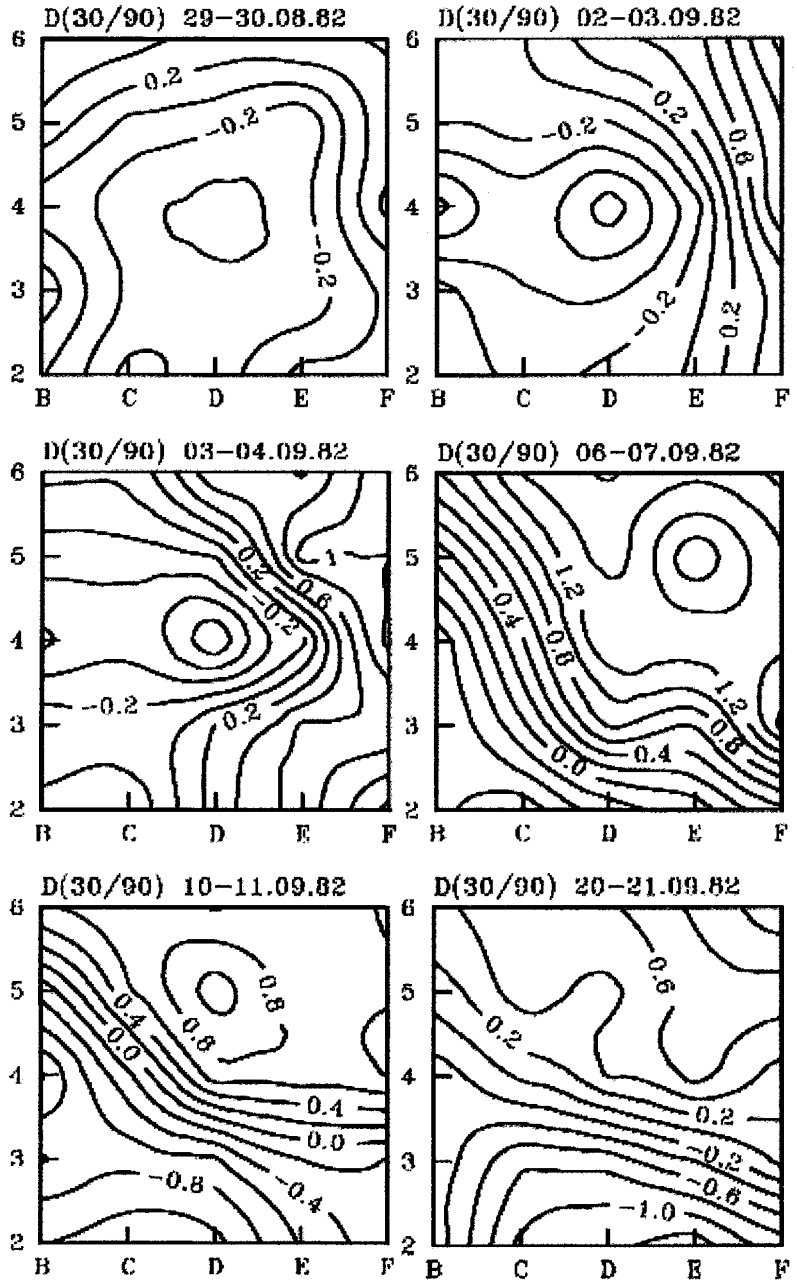


***Fig. 5.2.4.*** *Maps of dynamic topography of the 30-m level relative to 90 m for six CTD surveys in the Northern Basin. The grid spacing is 5 miles. Units are dynamic cm, with the negative values corresponding to the greater water density.*

Considering the isopycnal depths it became evident that the eddy observed by the dynamic topography on the first three surveys was of the lenslike, second mode structure, with the isopycnals raised in the top of the halocline and lowered in the deep layers. Anticyclonic currents were maximal at the "nucleus" level (80-90 m) and weaker above and below it. The eddy moved from the east (stations D4 and E4, survey 2) to the west (stations B4 and C5, survey 4). This explains the energetic current fluctuations observed at the 90-m depth at the mooring stations. High current speeds observed within the halocline are explained by the current jet and the anticyclonic westwardmoving lenslike eddy detected by the joint interpretation of current and density data.

### 5.3. Structures along and between the sub-basins

In the Baltic Sea, a great amount of measurements have been carried out in the limited areas (polygons) and different fixed (monitoring) stations. The horizontal resolution and frequency of these measurements is usually not sufficient for the investigation of meso-scale structures in the frame of Baltic sub-basins. Therefore, 12 synoptic transects from the period 1986-91, laying between the Gotland Deep and the entrance area to the Gulf of Finland were used in the further analysis (Fig. 5.3.1). Towed CTD data, with high horizontal resolution (about 1 km), represent the layer from the sea surface to the 70-80 m i.e. to the upper part of halocline. Two transects in September of 1989 and November of 1995 were made by the stations and they embraced the whole water column (Fig. 5.3.1).

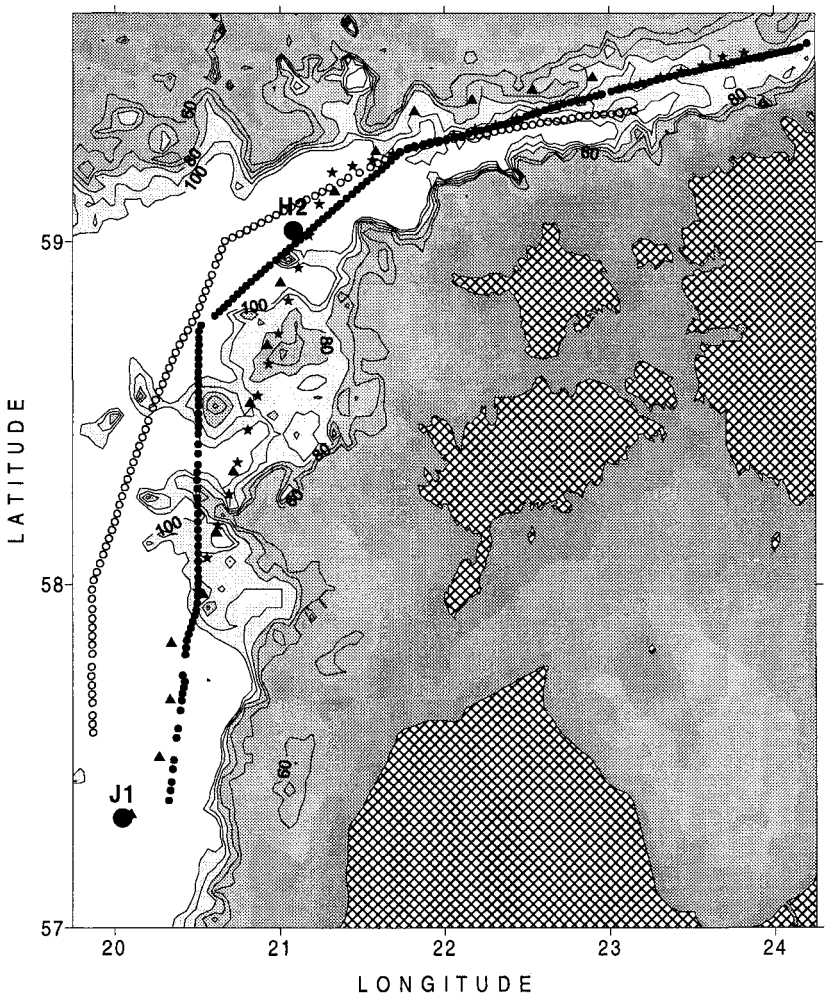


***Fig. 5.3.1.*** *Map of the study area with bottom topography in the transition between deep (>100 m) and shallow (<60 m) sea. Contour interval of isobaths is 10 m. Open and filled circles refer to the typical deeper and shallower sea towed CTD transects, correspondingly. Stars denote CTD stations in September 1989 and triangles in November 1995. Larger filled circles show the positions of long-term monitoring stations in the Gotland Deep (J1) and Northern Deep (H2).*

Due to the lack of major inflows, the period 1986-1991 is characterised by the descent trend of halocline at the stations J1 and H2 (Fig. 3.1). However, some stabilisation of the halocline depth occurred in 1989-90. The overall trend of halocline depth/salinity at fixed depth was modulated by the annual cycle. The salinity at fixed depths determined from the synoptic sections follow the changes in the interpolated monitoring data (not shown). Deviations from the interpolated curve were larger in the Northern Deep (H2) than in the Gotland Deep (J1). It can be explained by the smaller size of the Northern Deep and the position of H2 relatively close to the shallow areas, which makes it more sensitive to the external forcing.

The following general tendencies in the vertical course of halocline were found on the transects: lowering in the Gotland Deep, lifting above the Farö Channel and Northern Deep, and again lowering at the entrance to the Gulf of Finland (Fig. 5.3.2 and 5.3.3). Lowered halocline in the Gotland Deep was characteristic for all 'snapshots', except in December of 1990, when evident rising of halocline resulted from inflowing water. Clear dome-like halocline along the Farö Channel and Northern Deep was observed in 1986-87. Because of vertically limited data 8 PSU isohaline depth (uppermost halocline) was used to quantify vertical halocline excursions. Compared with Gotland Deep the halocline was risen 10-15 m, while 18 m in the most prominent case in May of 1986 (Fig. 5.3.3). During the following years due to the overall sinking trend of halocline this phenomenon was less expressive. In spite of that, at least 5-10 m doming was estimated. In March of 1991 the observational window was too 'shallow' to resolve the halocline.

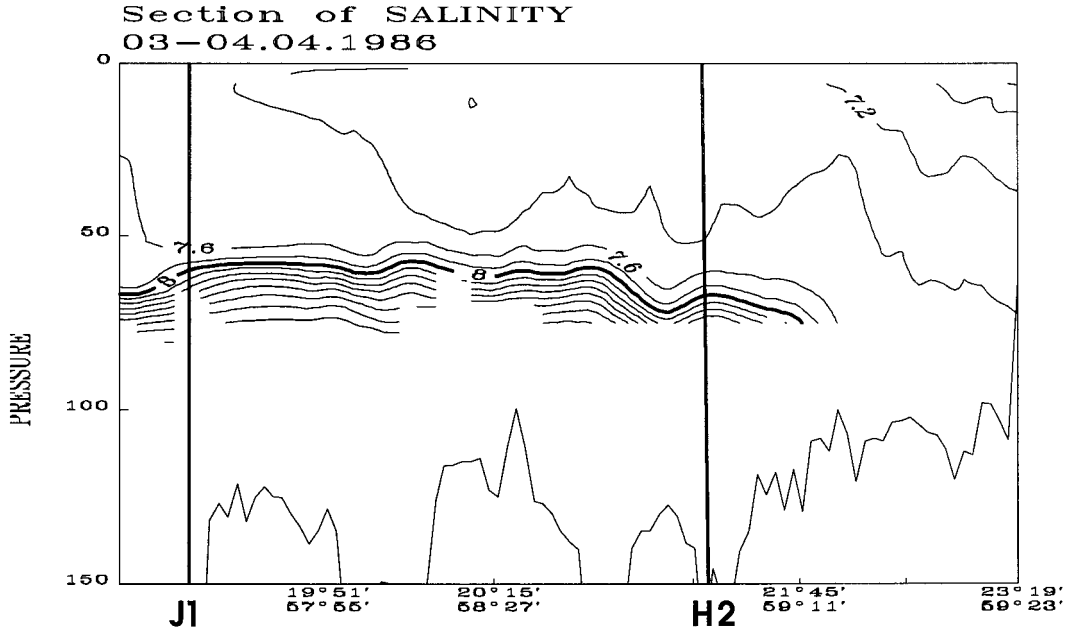


***Fig. 5.3.2.*** *Vertical distribution of salinity and bottom topography along the deeper sea transect in April of 1986. Contour interval is 0.2 PSU. Bold isohaline (8 PSU) marks the beginning of halocline. Bold vertical lines indicate the positions of long-term monitoring stations.*

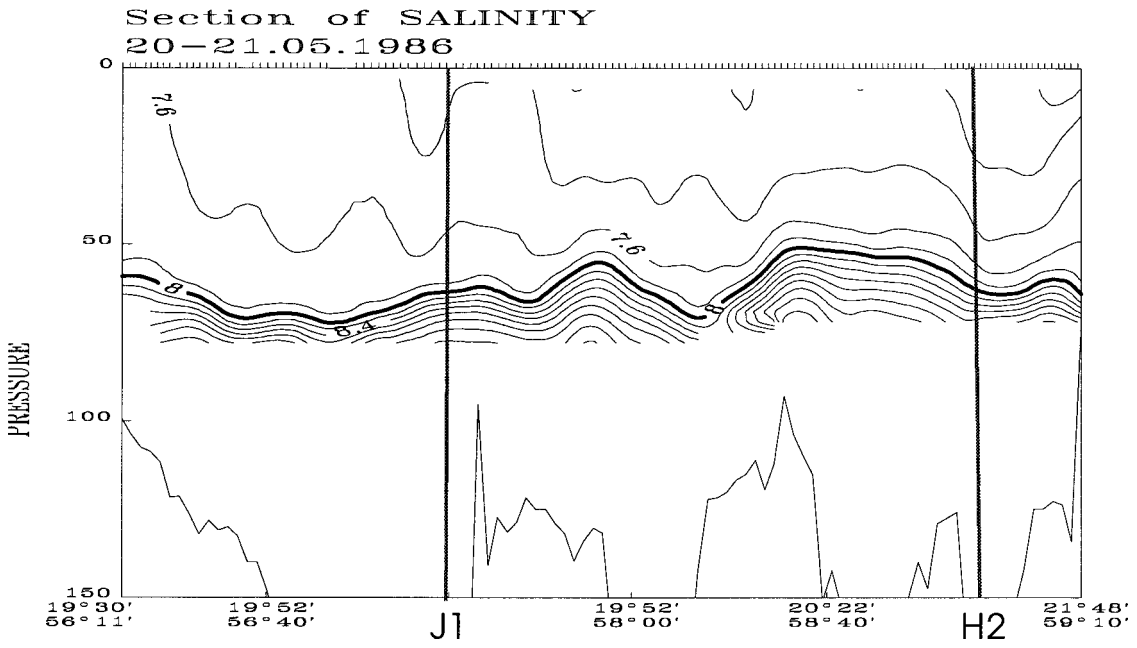


***Fig. 5.3.3.*** *Vertical distribution of salinity and bottom topography along the deeper sea transect in May of 1986. Contour interval is 0.2 PSU. Bold isohaline (8 PSU) marks the beginning of halocline. Bold vertical lines indicate the positions of long-term monitoring stations.*

The horizontal structure of halocline in the dome region was more complicated. Almost in all sections the dome was wave-like modulated. These sub-dome disturbances had different scales, vertical amplitudes and spacing. For example, our observations show a single strong disturbance with amplitude of about 15 m and 80 km long (Fig. 5.3.3), relatively regularly spaced 'waves' of 30-35 km length (Fig. 5.3.4) as well as domes with very weak disturbances (Fig. 5.3.2). The deeper transects (nearly along the axis of sub-basins) were predominantly smooth, whereas shallower ones (along the eastern part of sub-basins) appeared considerably modulated. Also, three shallower transects carried out by one week interval (September-October of 1989) had all different patterns of halocline without local preference of disturbances. All these examples support an idea that irregular modulation of the dome above the Farö Channel and Northern Deep, and also at the entrance to the Gulf of Finland reflects a complex of changing large-scale (sub-basin wide) flow over 'mounty' bottom. It is worth to mention that the problem is analogous to the effect of seamount group upon flow and thermohaline structure in the oceans (see *e.g.* Roden and Taft, 1985; Roden, 1991; Roden, 1994). According to these investigations generation of cyclonic and anticyclonic eddies, meandering jets and upwelling is common in the vicinity of seamounts.

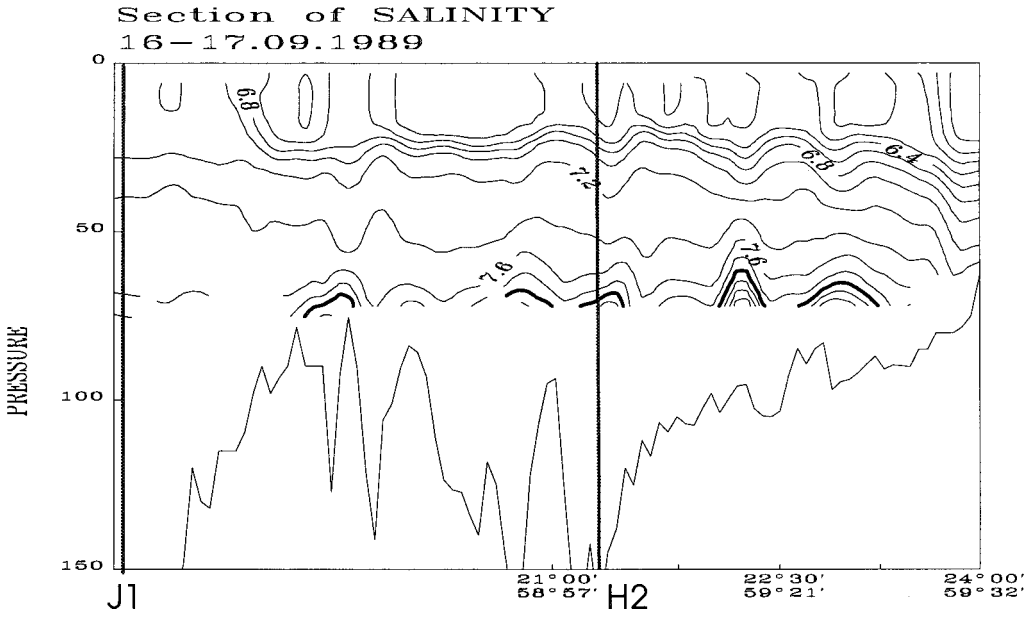


***Fig. 5.3.4.*** *Vertical distribution of salinity and bottom topography along the shallower sea transect in September of 1989. Contour interval is 0.2 PSU. Bold isohaline (8 PSU) marks the beginning of halocline. Bold vertical lines indicate the positions of long-term monitoring stations.*

Starting from the eastern part of the Northern Deep towards to the Gulf of Finland the halocline continuously lowered. The only exception are the transects of 1989, when halocline laid at the Northern Deep levels and trapped the rising slope of the entrance area to the Gulf at about 23°30'E in September (Fig. 5.3.5a) and 24°10'E (at Gulf axis latitudes) in December. Observations from other years (1986-1987, 1990) enable only to estimate indirectly the trapping locations between 21°30' and 22°30'E. Also, 'down to bottom' section made in November of 1995 showed trapping location in the same longitude range (Fig. 5.3.5b). This area, characterized by the rise of sloping bottom from 110 to 90 m, seems to be the mean border for the Baltic Proper halocline. Stronger intrusions of deep water into the eastern Northern Deep, as it happened in the autumn of 1989 and further eastward spreading may shift the end of halocline into the western Gulf of Finland.

In conclusion, observed structures of halocline in the different sub-basins enable to expect the following idealised general circulation scheme of deep waters. Lowered halocline in the Gotland Deep is likely to be the manifestation of anticyclonic gyre. Dome-like halocline above the Farö Channel and Northern Deep obviously reflects cyclonic circulation. This NE-SW orientated circulation extending to the entrance to the Gulf of Finland supports southern inflow of saltier waters and northern outflow of fresher waters. To verify this speculative scheme long-term current measurements as well as frequent synoptic mappings of halocline are requisite.

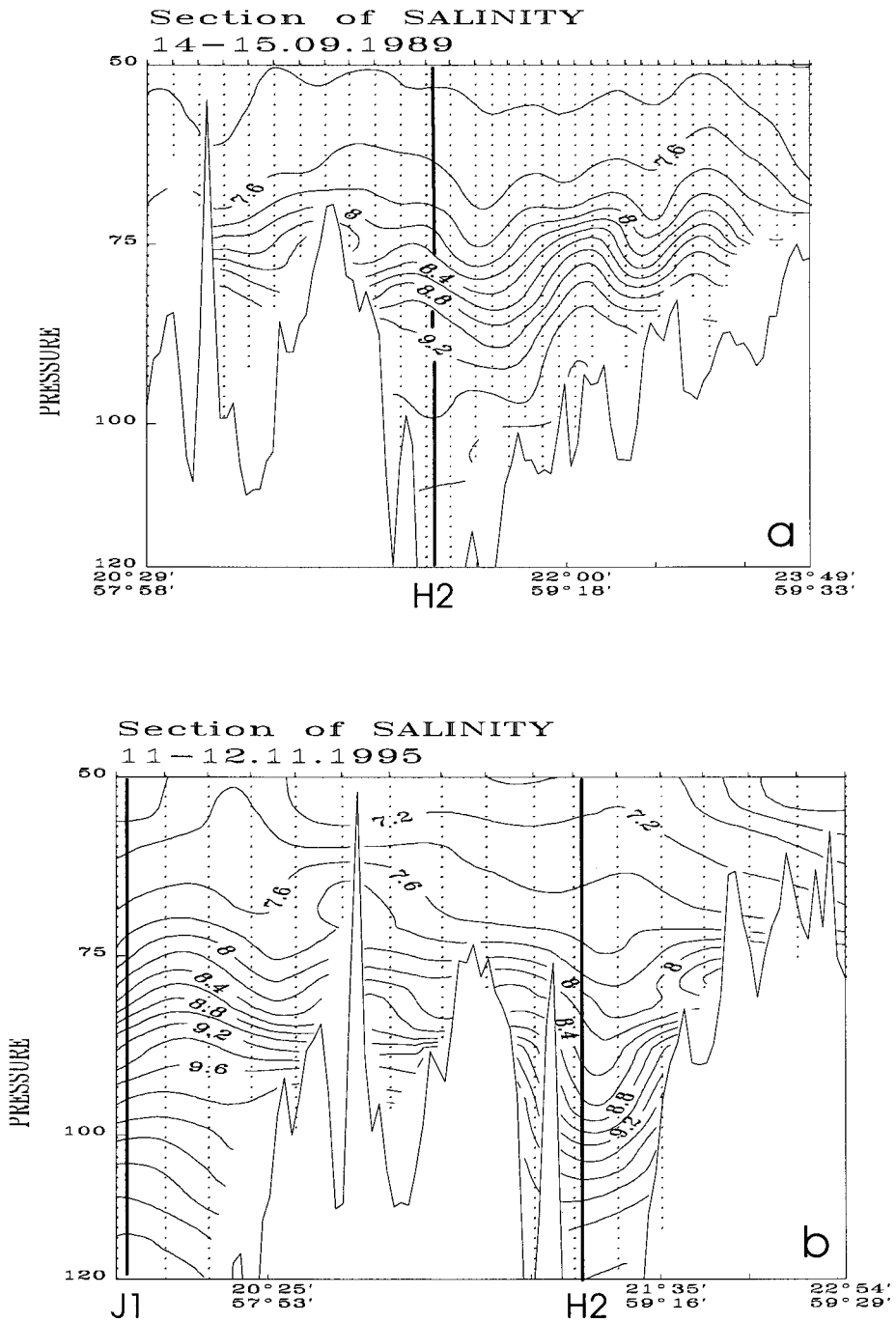


***Fig. 5.3.5.*** *Vertical distributions of salinity and bottom topography along the shallower sea transects in September of 1989 (a) and in November of 1995 (b). Contour interval is 0.2 PSU. Dotted vertical lines mark the positions of CTD stations. Bold vertical lines indicate the positions of long-term monitoring stations.*

### 5.4. Mesoscale eddies in the connecting channels

The Hoburg Channel, a site of two international experiments - BOSEX-77 and PEX-86, is about 70-km wide deep channel with a depth of 100- 30 m connecting the Stolpe Channel and Gdansk Basin with the Gotland Deep. Part of the saline water flowing from the Stolpe Channel is expected to pass directly to the Hoburg Channel while the other part is filling the deep layers of the Gdansk Basin. Intensive mesoscale eddies have been observed in this region (*e.g.* Aitsam and Elken, 1982; Horstmann, 1983; ICES, 1989).

Typical scenarios of the Hoburg Channel spring-time eddy structures are given in Fig. 5.4.1 by the maps of dynamic topography (providing geostrophic streamfunction of relative currents) and in Fig 5.4.2 by cross-channel sections of salinity through the eddy centres. The patterns of dynamic height of 10 dbar relative to 90 dbar, although being proportional to a layer mean density/specific volume anomaly, are mainly dependent on spatial variations in halocline depth. For a geographic/topographic reference of the maps (Fig. 5.4.1), depth contours outside the survey area are drawn in a standard box by a dashed line.

Comparing the dynamic topography patterns for the spring 1979 and 1986 (Fig. 5.4.1, a and c) we find similar mesoscale hydrodynamic situation. Without going into details of particular observations which can be found elsewhere (Aitsam and Elken, 1982, ICES, 1989), the common features include, first of all, "dynamic high" (geostrophically balanced by lowering of the halocline) found in the western and "dynamic low" (balanced by appraisal of the halocline) found in the eastern part of the channel. In the middle of the channel south-westward meandering current jet was observed above the halocline. In 1986 both the jet and the cyclonic eddy were well distinguished also on the satellite images (Fig. 5.4.3) and the western "dynamic high" region revealed an anticyclonic eddy by drifter data (ICES,1989). The main flow was parallel to the isobaths but some cross-isobath flow patterns were detected near the eastern slope. At the western slope direct current measurements did not show significant mean currents both in 1979 (Aitsam and Talpsepp, 1982) and in 1986 (ICES, 1989). This "high" west / "low" east situation was accompanied by a presence of well-defined quasipermanent salinity front at the western slope of the channel (see the salinity maps, Figs.4-12 and 4-13 by ICES, 1989).

Somewhat different hydrodynamic situation was observed at the end of May, 1980 (Fig. 5.4.1b). Strong cyclonic eddy with about 20-m appraisal of the halocline in its centre (Fig. 5.4.2b) was observed in the middle of the channel. This dominating eddy caused dispersal of the quasipermanent salinity front which is frequently observed at the western slope. Around the eddy centre current streamlines crossed with a more than 30-km wide band the channel/depth contours. As a result this eddy suffered later on rapid changes in its structure forming a lens-like (second mode) eddies. In contrast to the above described schemes anticyclonic activity was not found in the surveyed area. Near the western slope a mean 4-6 cm/s south-westward current was observed from beginning of May to beginning of July. The mean flow was superimposed by 6-8-day period slope-trapped oscillations (Aitsam and Talpsepp, 1982).

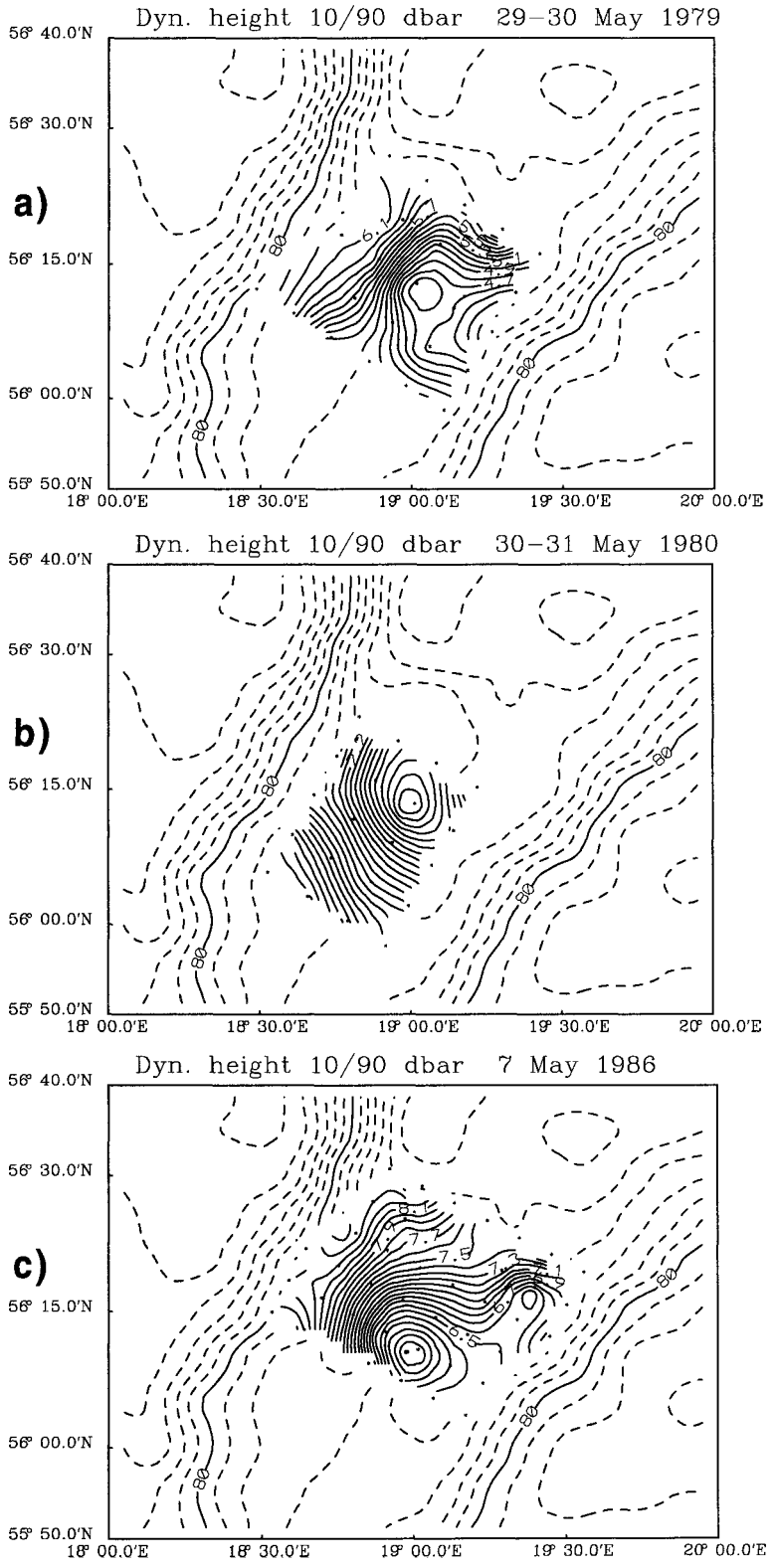


***Fig. 5.4.1.*** *Maps of dynamic height of 10 dbar relative to 90 dbar, in dynamic cm (solid lines) and depth contours (dashed lines) around the map area in the Hoburg Channel. a) 29-30 May 1979, b) 30-31 May 1980, c) 7 May 1986 (data from PEX-86).*

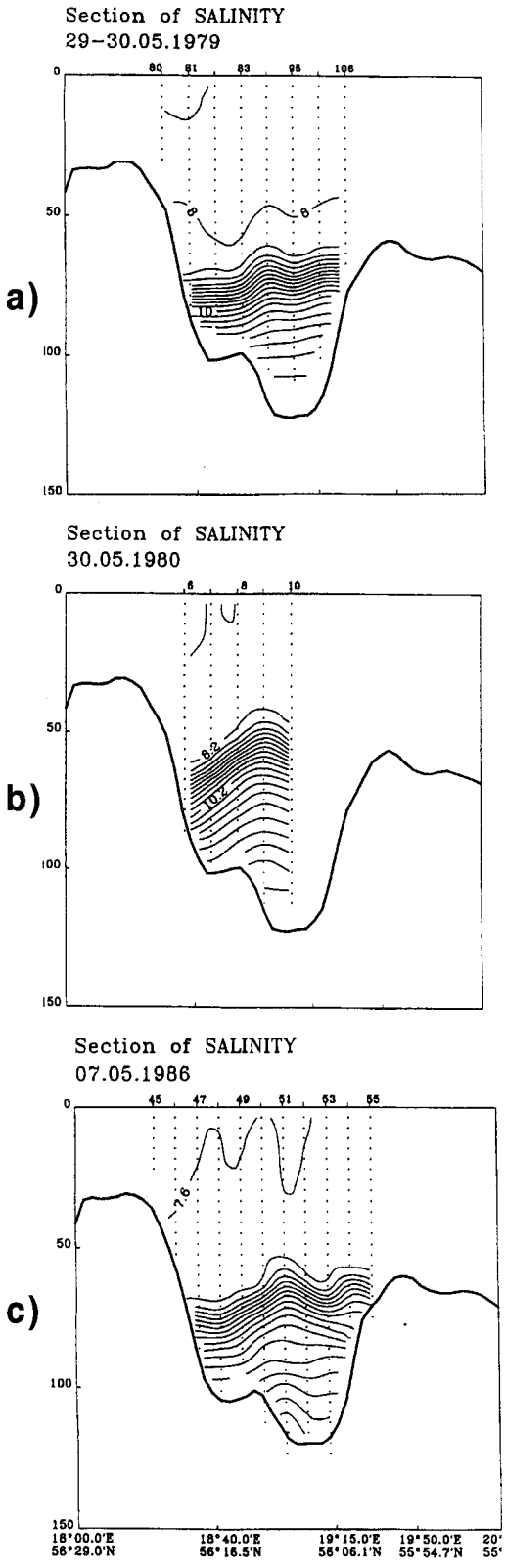


***Fig. 5.4.2.*** *Sections of salinity accross the Hoburg Channel through the mesoscale eddies shown in Fig. 5.4.1. a) 29-30 May 1979, b) 30-31 May 1980, c) 7 May 1986 (data from PEX-86).*

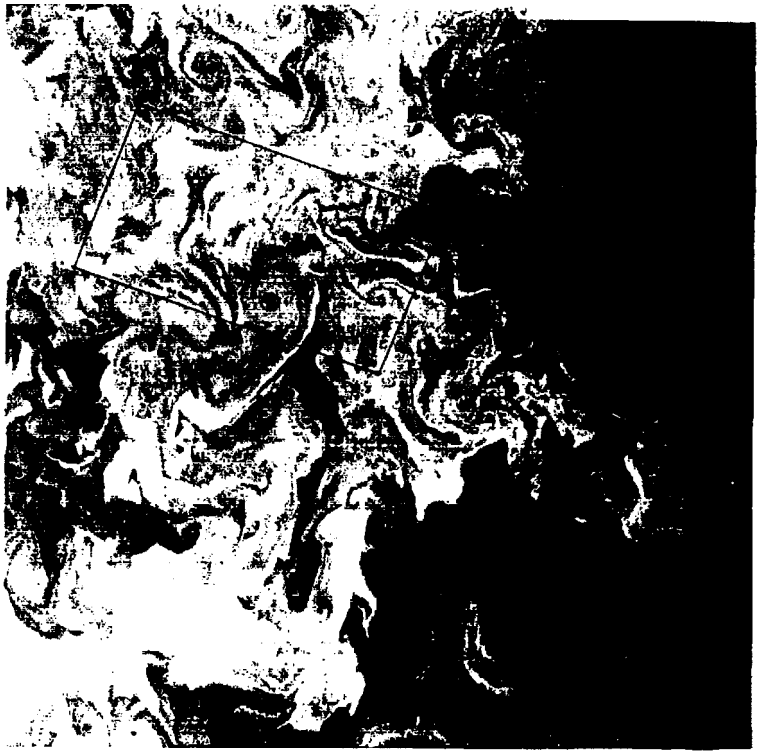

***Fig. 5.4.3.*** *Sea surface temperature of the Hoburg Channel region on 07 May 1986 during PEX-86 (ICES, 1989). The box denotes the PEX sampling grid (compare with the dynamic height map, Fig. 5.4.1c). The image was processed by U.Horstmann.*

PEX-86 documented clearly that phytoplankton spring bloom started within lenses/patches of slightly (by 0.02-0.06 PSU) less saline water floating at the surface above cyclonic and anticyclonic eddies (ICES, 1989). The cyclonic eddy had near the surface homogeneous (with salinity contrasts less than 0.02 PSU) 10-15 km wide core which extended down to 35-40 m. This is also proved by high-resolution measurements by means of towed CTD (see Fig. 4-16 in ICES, 1989). Local upwelling was evident just around the less saline core in a belt of maximum rotational eddy currents (coinciding with maximum slope of halocline depth) resulting in increase of salinity at fixed depth levels. Within the less saline eddy cores of PEX-86 the salinity was in a range of 7.54- 7.58 PSU. Three weeks before PEX upper layer salinity with the same range of 7.56-7.58 PSU as nearly constant down to the halocline. This implies that the weak background saline stratification was generated from the homogeneous state by mixing through the halocline which was prevented in the cores of eddies and enhanced in the upwelling belts around the eddy cores. Minor lateral and vertical exchange keeps their salinity constant while salinity of the surrounding water is increased by "normal" mixing. These isolated waters capture phytoplankton allowing them more exposition of light compared with background normally mixed waters. As a result the phytoplankton

spring bloom starts within hydrodynamically isolated lenses and spreads later on over the basin.

Stable baroclinic eddy structures in the BOSEX-PEX area may be summarized as follows (*e.g.* Elken, 1984):
- first mode eddies, with a diameter about 40 km, having dome-like density structure (isopycnals lifted up in the centre, displacement may exceed 20 m), cyclonic motion in the layer above the halocline;
- second mode eddies, with diameter about 20 km, having lens-like density structure (layer of undisturbed isopycnals lying at a depth between 80 and 90 m, above that ca 5-m upward displacement, below that ca 10-m downward displacement of isopycnals), anticyclonic motion within the lens core.

Generation mechanisms of the baroclinic eddies will be discussed in Chapter 8. Lifetime of a baroclinic eddy may exceed a week. Fast conversion of intensive first mode eddy into second mode eddies has been followed. In the second mode, lens-like eddies anomalous core have been found around 80-m depth, *e.g.* by nutrients (Fig. 5.4.4) indicating that eddies transport water from the place of eddy formation (Aitsam et al., 1984).

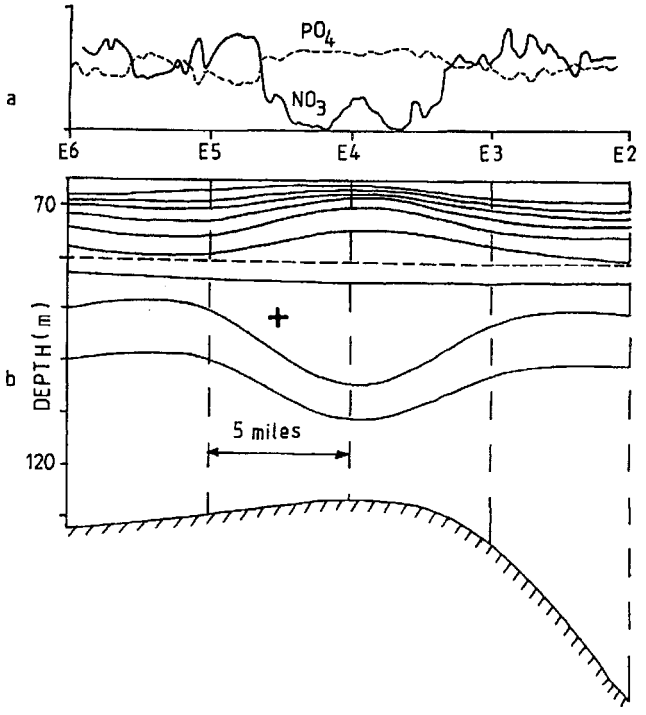


***Fig. 5.4.4.*** *Section of phosphates and nitrates (a) on 80-m depth through the core of the second mode eddy and the eddy density structure (b). Data from June, 1981 (Aitsam et al., 1984), nutrient data by Hans-Peter Hansen.*

### 5.5. Wintertime slope effects and deep lenses

During the warm season, May-September, thermal stratification in the Gotland Deep is rather continuous below the halocline. 'Spiky' profiles of temperature, characteristic for the intrusion cascade in the Bornholm Basin (Laanemets, 1984) but also in the Hoburg Channel are not found here at this period. Intensified field programme, started in the Gotland Deep in 1986 showed a clear seasonal cycle of late autumn intensification of deep thermohaline anomalies (Kõuts *et al.*, 1990). In November-December near-slope current jets (identified by tilted isopycnals) are formed and associated thermohaline anomalies go down to 130 m in a narrow band near the eastern slope of the Gotland Deep.

Deep intrusive lenses following vortex dynamics were found detaching from the near-slope jet flows, first in 1986 (Elken *et al.*, 1988) and subsequently in each year during late autumn and winter until 1991 when the observational programme terminated. The lenses have diameter about 10 km and they cover depths 90-130 m. Layer of undisturbed isopycnals 100-120 m is characterised by remarkable (1-2°C) anomaly of temperature. Origin of the anomalous water lies near the slope where halocline touches the bottom. The lenses are the main agents to carry isopycnally warmer (in 1986: colder) water from the slope regions to the basin interior forming to the next spring a new, intrusion-free stratification. It has been hypothesised that the isopycnally warmer water observed near the slope and in the lenses in 1988-1991 may originate from the Bornholm Basin and surface layers of the Arkona Basin via isopycnal advection. Another mechanism could be intensified cross-isopycnal mixing near the halocline slope during late autumn storms when surface waters are eroded down to the halocline.

Parameters of the near-slope water jet and the lenses given in Table 5.5.1 are rather similar for both the meso-scale phenomena which indicates their close relationship.

***Table 5.5.1.*** *Parameters of deep meso-scale thermohaline anomalies in the Gotland Deep.*

| Parameter | Near-slope water jet | Meso-scale lenses |
|---|---|---|
| Depth range | 90 - 140 m | 90 - 130 m |
| Thickness | 30 - 50 m | 25 - 30 m |
| Diameter (width) | 10 - 15 km | 8 - 12 km |
| Density range | 7.2 - 8.2 kg $m^{-3}$ | 7.2 - 8.0 kg $m^{-3}$ |
| Temperature anomaly | 0.5 - 1.5°C | 0.5 - 1.2°C |

Further on we will illustrate the observational findings, with a special focus on the results obtained during winter 1990/1991 when repeated wintertime surveys were made. Earlier 'snapshot' measurements did not provide any observational data about lifetime and time behaviour of deep thermohaline structures during the cold season.

Typical scheme of stations usually visited during 1986-1991 for the mapping of the thermohaline fields consists of cross-slope transects near the eastern slope of the Gotland Deep (Fig. 5.5.1).

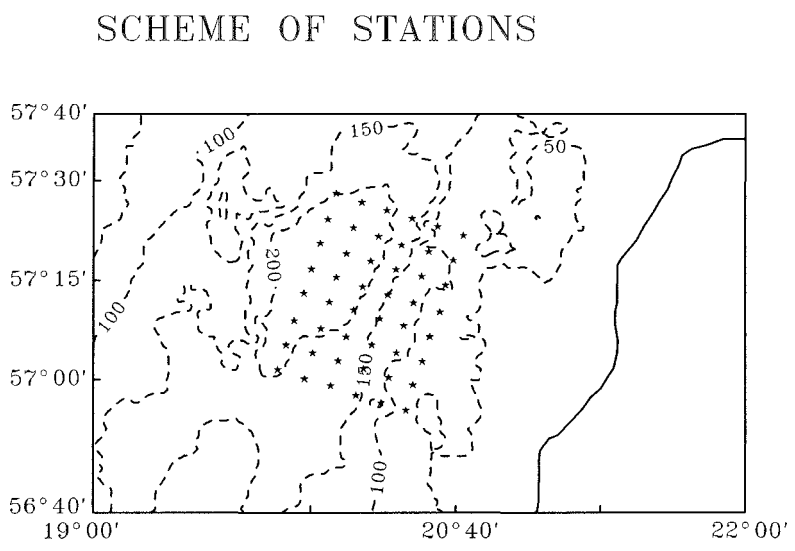


***Fig. 5.5.1.*** *Scheme of stations near the eastern slope of the Gotland Deep.*

Examples of observed near-slope deep temperature anomalies are given in Fig. 5.5.2. While in 1986 a cold anomaly was observed near the slope extending down from the top layers of the halocline then in the following years the warm-core anomalies were found. This tendency is correlated with the progress of the stagnation period, see Chapter 3.

Three measurement campaigns made in winter 1990/91 with one-and-half month interval (3-8 December 1990, 8-15 February and 21-30 March 1991) showed intensive meso- and small-scale thermohaline structures below the permanent halocline during the whole winter period. Surprisingly, the mean temperature had remarkably increased in the layer 100-120 m of the Gotland Deep in autumn-winter 1990/91 (cf. Fig. 5.5.3). Temperature ranging in between 4.8 - 5.4°C in December 1990 rose up to 5.4 - 5.8°C in March 1991. Because of vertical temperature stratification with maximum in this layer, the local vertical mixing was not able to produce the observed temperature growth. The isopycnal temperature below the permanent halocline had increased from December to March having maximum change (0.74°C) on 7.7 kg $m^{-3}$. Obviously there was no source for the warm water in the surface. By the monitoring data, this winter was abnormal for the temperature regime in all the Baltic Proper sub-basins. Temperatures above 6°C were observed in the saline water sphere of the Bornholm Basin and the Gdansk Basin (Fig. 3.3) which could have been transported to the area. In the warm deep water at the slope, indications *of Radioamoeba* were found on the 110 m depth (H.Kukk, personal communication). This freshwater amoeba was in a condition that it has not been in the saline water more than a half year.

Although, the observed increase in temperature and occurrence of lenses in the isopycnal range 7.2-8.4 kg $m^{-3}$ indicating intensive water input into this layer presumably from the southern basins of the Baltic Sea, the thickness of the layer was not remarkably increased. The latter could be explained by horizontal export to the Northern Basin and by intense diapycnal mixing. The observational results show that the intensified water exchange between the basins and enhanced vertical mixing starting in late autumn continues through the whole cold season.

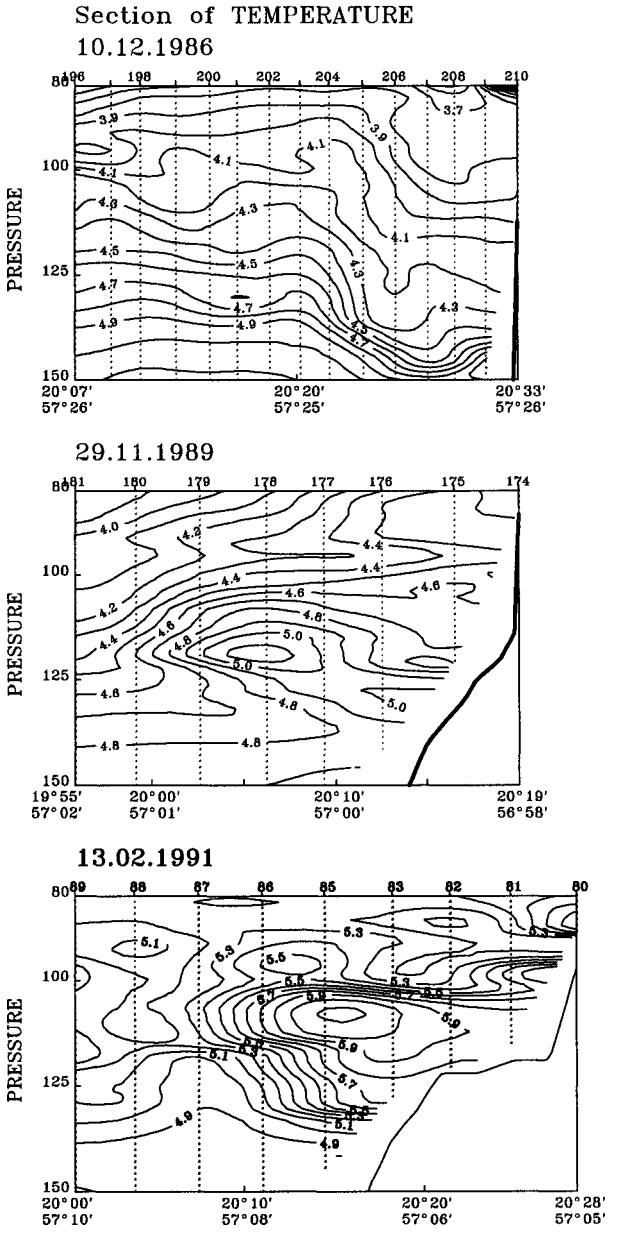


***Fig. 5.5.2.*** *Vertical sections of temperature in the Gotland Deep (across the eastern slope) during 3 different surveys exhibiting the presence of the anomalous water jet near the slope.*

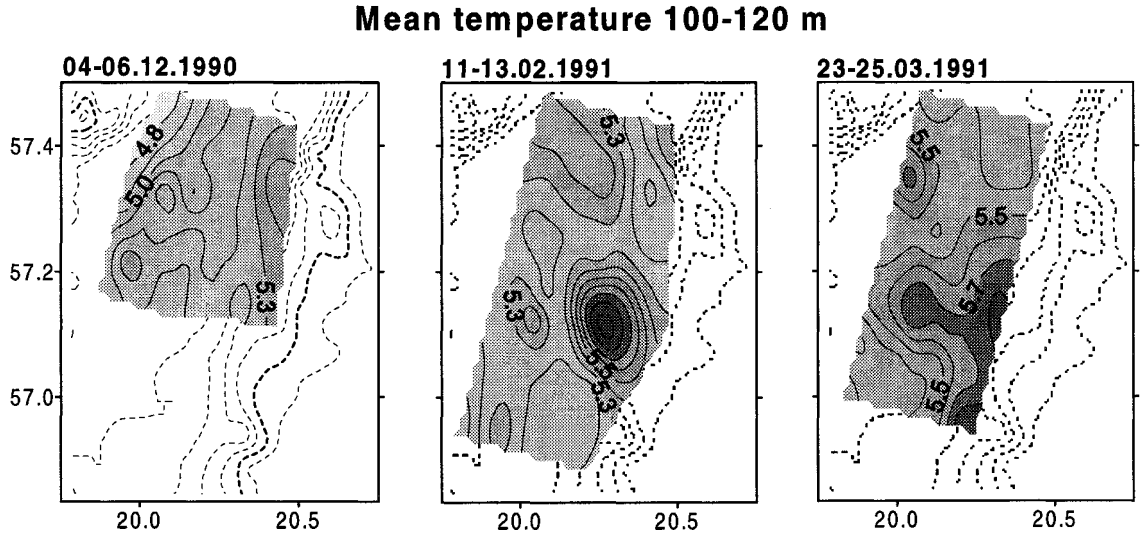


***Fig. 5.5.3.*** *Maps of mean temperature in layer 100-120 m in the near slope region of the Gotland Deep obtained during three successive surveys in winter 1990/91.*

Typical temperature and density structure of a deep lens obtained by continuous CTD scanning from a board of the slowly moving ship is shown in Fig. 5.5.4. The observed lenses always revealed well-drawn structure in density, with a diameter of 8-12 km, but thermal core of them had different anomalies and degree of homogeneity for different lenses. Comparing the positions of the lenses during the repeated surveys in 1986 and 1989 we can estimate the drifting speed of the lenses to be about 1 cm/s which is in the range of the speed of deep currents. Geostrophic calculations yielded the anticyclonic orbital speed in the lens more than 5 cm/s. Except of the lens presented in Fig. 5.5.4 the lenses could contain a lot of small-scale intrusions of surrounding water. The dynamic stability and thermal heterogeneity is indicating that the lenses could have been generated in the region of intensified mixing of different water masses. Hence, the formation mechanism of lenses appears to be related rather to meandering and baroclinic instability of intensive near-slope current than to entering of anomalous isolated water-body into the Gotland Deep.

Calculations made by Shapiro (1986) using a model of linearly stratified lens embedded in the water with stronger linear stratification suggest that the diameter of a vortex lens must be larger than a critical value $D_{min}$ which is determined as

$$D_{min} = 2h\,(N_B^2 - N_L^2)^{1/2}/f, \qquad (5.2)$$

where $f$ is the Coriolis parameter, $h$ - the thickness of the lens, $N_B$ and $N_L$ - Väisälä frequency in the surrounding water and in the lens, respectively. At $f = 1.25*10^{-4}$ 1/s, $N_B = 0.03$ 1/s, $N_L = 0.01$ 1/s and $h = 30$ m we obtain $D_{min} = 6$ km. In case of a smaller diameter the outward pressure gradient and centrifugal force cannot be balanced by the inward Coriolis force and the lens will decay rapidly. The life-time of a vortex lens is estimated to be about one month using parameters given in Tab. 5.5.1 and a three-layer model developed in (Kostyanoi and Shapiro, 1986). Such a long life-time allows to assume that meso-scale lenses could transport anomalous water over a long distance

from the slope region to the interior and play an important role in horizontal and vertical mixing in the deep layers.

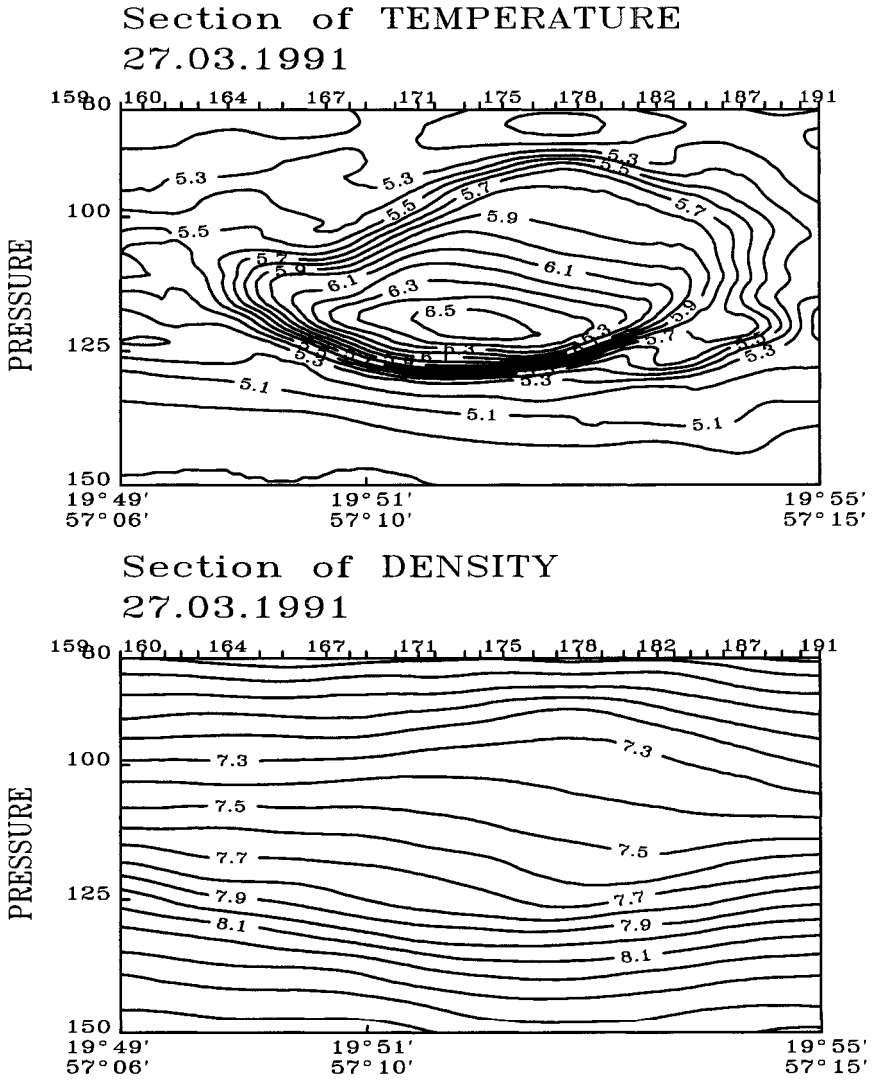


***Fig. 5.5.4.*** *Sections of temperature and density through a deep meso-scale lens observed in March 1991.*

Besides the lenses, the smaller scale intrusions of anomalous water were observed near the slope region and also in the interior (where they as a rule had lower intensity). Intrusion cascade was evident in the intermediate layers of the Gotland Deep in winter, what is characteristic for the contact regions of different water masses. The mean parameters of highly variable intrusions on the basis of vertical profiles obtained in November-December 1989 are: thickness 5-17 m (for the survey - 8.7 m) and intensity 0.24-0.47°C (0.35°C). Such intrusions could be interpreted as the signs of intensified mixing of the anomalous water carried into the Gotland Deep by the near-slope jet and meso-scale lenses.

Diapycnal mixing is seen on the vertical profiles of salinity and density as layers of low vertical gradients. In order to detect if there are significant differences in mixing intensity between the slope region and the interior, all the measurements performed on

the regular grid (see Fig. 5.5.1) in the Gotland Deep in 1986-1991 were analysed. The relative part of sub-layers having vertical gradient of salinity less than 0.005 PSU/m (10 times less than the minimum smoothed gradient in the halocline; see Chapter 6) was determined for each profile in the layer 80-120 m on the vertical basis of 1 m. The results presented in Fig. 5.5.5 show a remarkable tendency of the increased percentage of the mixed sub-layers near the slope.

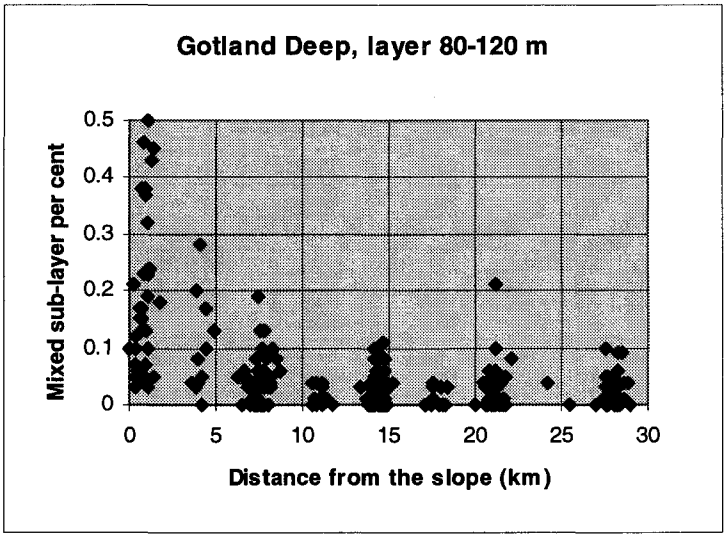


***Fig. 5.5.5.*** *Percentage of mixed sub-layers ($\Delta S/\Delta z$ < 0.005 PSU/m) in the layer 80-120 m in the Gotland Deep depending on the distance from the eastern slope (from the isobath 100 m).*

The background level of the selected parameter ($P_{ml}$ < 0.1, except a few stations) was exceeded only in the narrow near-slope band, where the mean percentage of low gradient sub-layers increased approximately exponentially. The mean and the standard deviation of $P_{ml}$ were estimated to be 0.03±0.03 in the interior (band 12.5 - 15 km) and 0.19±0.14 in the near-slope region (0 - 2.5 km). Interpreting the mixed sub-layers percentage as the measure of frequency of mixing events, a clear indication of the mixing source near the slope in accordance with previous discussions (Shaffer, 1979) is determined.

To conclude, it could be pointed out that the large amount of polygon data collected in 1986-1991 showed a clear winter-time intensification of water exchange between the sub-basins as well as the vertical mixing. The penetration of the seasonal thermocline down to the permanent halocline during autumn cooling and storms is the main prerequisite of direct influence of wind forcing in the halocline and the deep layer dynamics. The observed rather stable near-slope jet occurrence and the formation and decay of meso-scale lenses, leading to the remarkable temperature increase in and below the halocline in winter 1990/91, seem to be forced by the density difference between the sub-basins which was formed and presumably increased during the autumn rebuilding of the stratification. The local wind forcing and instabilities of near-slope current produce intensified diapycnal mixing in the slope region. Mixed water patches are carried to the interior what gives a large contribution to the vertical mixing of deep basins needed to close the salt budget (see in Chapter 6).

### 5.6. Kelvin waves propagating along the slopes

Wavelike structures of the thermocline and the halocline have been observed along the axis of the Baltic Proper in numerous occasions. For the low frequency range, with the period of the wave being larger than the inertial period $T_f \approx 14$ hours, both the internal gravity waves and the vorticity waves (effect of $\beta$, $f=f_o+\beta y$, is small in the Baltic) are trapped by the basin boundaries, *e.g.* the amplitude of the waves is decreasing from the coastline or slope. Therefore Kelvin waves appear near the basin boundaries (Fennel and Sturm, 1992). At the stratified bottom layers of the Hoburg Channel bottom-trapped waves have been observed (Talpsepp, 1982).

Repeated transects along the western slope of the Gotland Deep were made in August 1994 within the GOBEX project, with the aim of studying the slope-trapped mesoscale motions. The transect lied on a 10-15 km distance from the 80-m isobath thus being within the limits of the Rossby deformation radius from the halocline horizontal boundary. Sections of density measured by the towed undulating CTD are presented in Fig. 5.61. It is well distinguishable, that the thermocline and the layer below it were perturbed by a wavelike motion. On the transect of 17 August, the isopycnal 5.6 kg $m^{-3}$ had lowering at positions 56° 56'N and 57° 23'N. The estimated wavelength is therefore about 40 km. Two-and-half days later, the same wave pattern has migrated by 15 km to the south, which gives the estimate of the propagation speed about 7 cm $s^{-1}$.

Assuming the long internal wave propagating along the axis y, $\zeta = \zeta_o \exp i(kx+l(y-ct))$, in the case of two layer stratification the dispersion relation reads

$$l^2c^2 = g'h\,(k^2+l^2)+f^2\,, \qquad (5.3)$$

where $k$ and $l$ are the wave numbers, $c$ is the phase speed, $g'$ is the reduced gravity, $h$ is the thickness of stratified layer and $f$ is the Coriolis parameter. With the values taken from the observations, $c = 0.07$ m $s^{-1}$, $g' = 0.02$ m $s^{-2}$, $h = 15$ m, $l = 1.6*10^{-4}$ $m^{-1}$, we obtain $k^2 = -6.7*10^{-8}$ $m^{-2}$. This means that at the given values of the wave parameters, the cross-boundary wavenumber is imaginary and the wave amplitude decays exp(1) times in a distance of 24 km from the boundary.

The boundary-amplified Kelvin waves which are always exited at variable wind conditions, have the highest current speeds and isopycnal displacements near the slope. Since the vertical excursions of water particles may exceed 10 m during the passage of the wave nodes, motion above the sloping but rough bottom may create significant cross-isopycnal mixing there. However, clear signals of slope intensified mixing in the layers below the halocline were found only during the cold season as demonstrated in the previous Sub-Chapter.

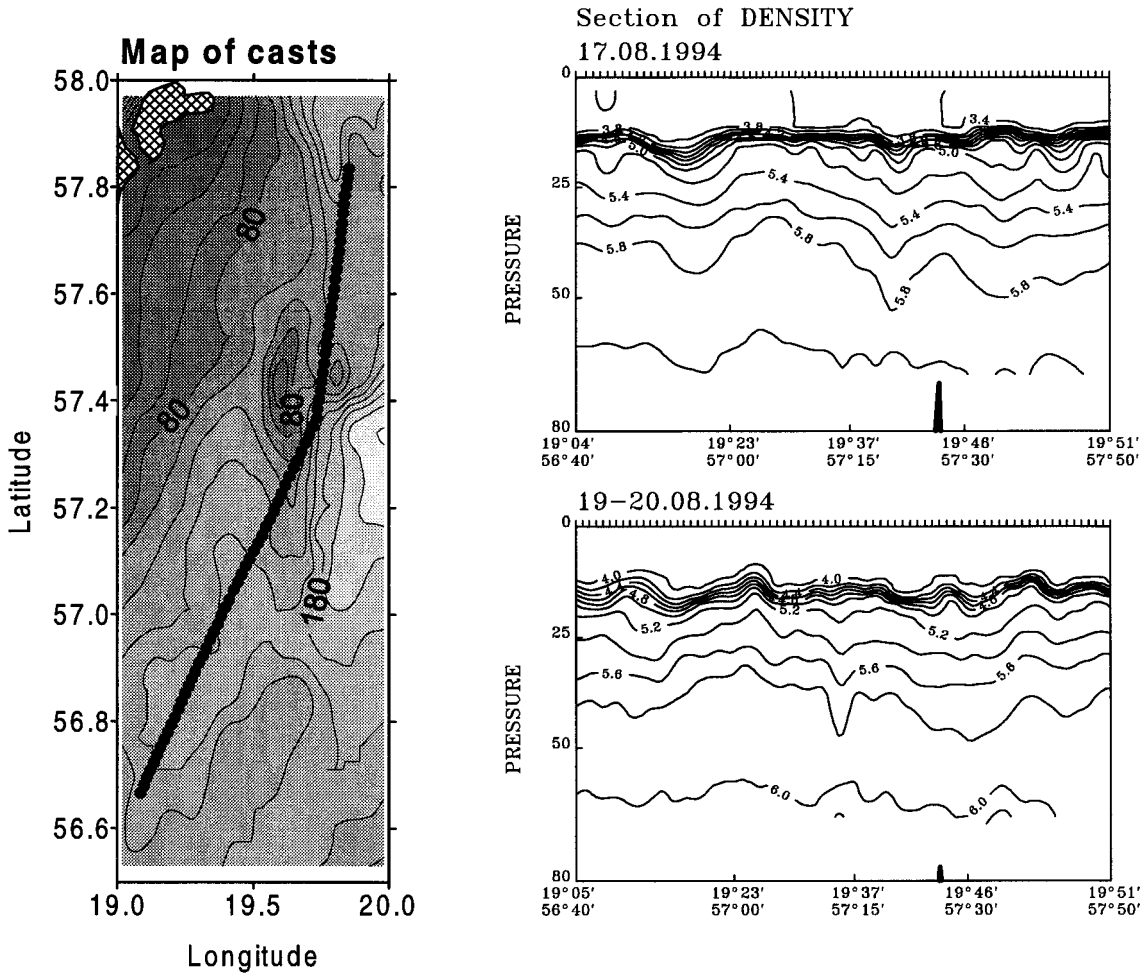


***Fig. 5.6.1.*** *Sections of density on the two consecutive transects along the western slope of the Gotland Basin (right) and map of casts made by the towed undulating CTD (left). Section length is 140 km. Data obtained during the cruise of RV "Alexander von Humboldt"(IOW, Warnemünde) by the equipment of EMI, Tallinn.*

# 6. SMALL-SCALE HALOCLINE STRUCTURE, VERTICAL MIXING AND POSSIBLE ENERGY SOURCES

*Jaan Laanemets, Madis-Jaak Lilover, Urmas Lips,*
*Mikk Otsmann and Tiit Kullas*

Renewal of the central Baltic deep water is caused by irregular large inflows of high saline and oxygen-rich North Sea waters, which are known as the major inflows. The frequency and magnitude of the major inflows depend on atmospheric forcing, sea level (Matthäus and Franck, 1992) and river run-off (Launiainen and Vihma, 1990). In the periods between the major inflow events, called stagnation periods, the decrease of salinity and oxygen concentration in the deep layer is observed (*cf.* Chapter 3). A positive long-term trend of oxygen concentration has been observed in the intermediate layers (around 100 m). The trend can be explained by the increase of vertical exchange across the permanent halocline due to the decreased stability of the stratification and significant shift of the halocline centre to the greater depths (Matthäus, 1990).

The small-scale turbulence is considered as the most probable physical process that is causing these changes. Turbulent kinetic energy dissipation rate ($\varepsilon$), describing the rate at which the mechanical energy is converted to the heat by friction, is a fundamental quantity which may be estimated from direct measurements of turbulence. The quantity $\varepsilon$ is proposed to be connected to the vertical eddy coefficient for momentum and mass and therefore enables to determine the vertical fluxes of momentum and mass as well. As the halocline by oneself is a layer restricting the vertical exchange, estimation of small-scale variations of the halocline structure is of great importance in our better understanding of the mixing in the Baltic Sea.

## 6.1. Direct measurements of turbulence and current shear

Turbulence measurements with fast-response sensors are of great value for the mixing problem. In the Baltic Sea only a few direct measurements of turbulence have been made due to the technical difficulties. Joint measurements of turbulence and the background current and density fields were carried out at the eastern slope of the Gotland Basin in 1987. Turbulence characteristics were registered with free-falling dropsonde BAKLAN, designed in the Atlantic Branch of P.P. Shirshov Institute of Oceanology. Vertical structure of current and density were measured by the Neil Brown CTD/ACM profiler with the acoustic current meter system. Details of the technical parameters of BAKLAN, calibration and data processing techniques are presented in Lilover *et al.,* (1993).

Significant jet current was observed on the eastern slope of the Gotland Basin in October, 1987. The jet showed up in deepening of the thermocline and lifting up the halocline closer to the slope (Fig. 6.1.1). In the slope region $\varepsilon$ got its maximum value of $10^{-4}$-$10^{-3}$ $Wm^{-3}$ which corresponds to the values of turbulent eddy coefficient for heat and salt in a range $10^{-5}$-$10^{-4}$ $m^2s^{-1}$ (Lilover and Nabatov, 1990). Towards the basin interior, the characteristic $\varepsilon$ values decreased to $10^{-5}$-$10^{-4}$ $Wm^{-3}$ in the thermocline and $10^{-6}$-$10^{-5}$ $Wm^{-3}$ in the halocline.

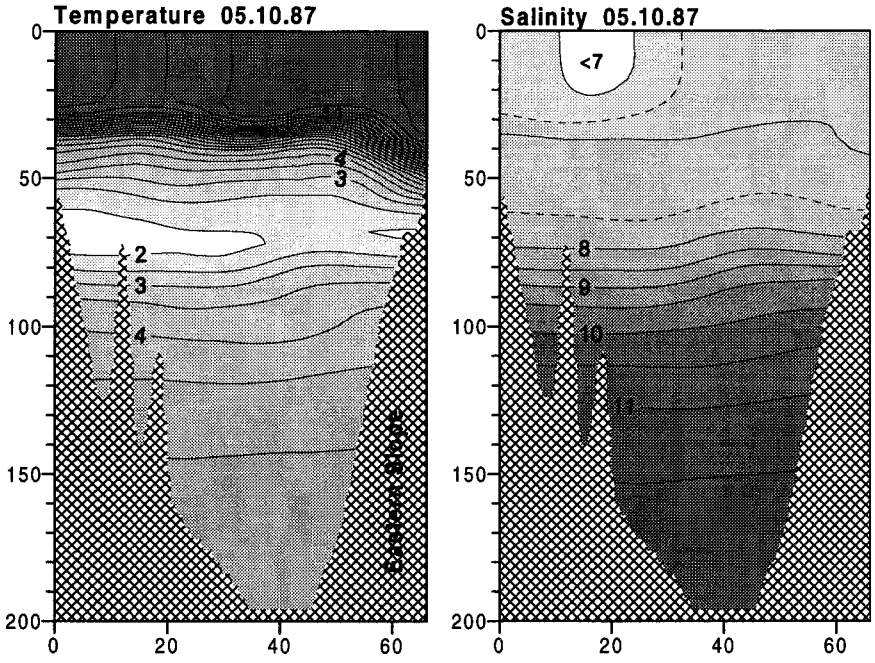


***Fig. 6.1.1.*** *Section of temperature (left) and salinity (right) showing a jet current at the eastern slope of the Gotland Basin.*

Vertical mixing may be generated by breaking of the internal waves. The Richardson number is a measure of the tendency for the occurrence of turbulence in the stratified fluid and is defined as the square of the buoyancy frequency divided by the square of the shear ($Ri=N^2/s^2$ , $N^2 = - \rho_z\, g/\rho$, $s^2=u_z^2+v_z^2$, where $u_z$ and $v_z$ are vertical gradients of the current velocity east and north components respectively). If the *Ri* drops below the critical value (~ 0.25) the vertical mixing due to shear instability can take place.

Intensive patches of turbulence were well correlated with the low values of gradient Richardson number (*Ri*) calculated from the background current and density fields (Fig. 6.1.2). The simplest way to parametrize the vertical turbulent mixing is to relate the turbulent eddy coefficient *K* to a single parameter of the mean hydrophysical field, i.e. *K=K(Ri)*. The examination of the *Ri* dependence from the averaged turbulence levels revealed the gradual increase of the observed eddy coefficients with decreasing Richardson number (Peters *et al.* 1988). As the vertical fluxes are proportional to eddy coefficients the *Ri* distribution (or the amount of small *Ri* values) therefore can characterize the vertical fluxes as well. However, the calculated values of the shear and *Ri* are specific to the vertical scale resolved by the data.

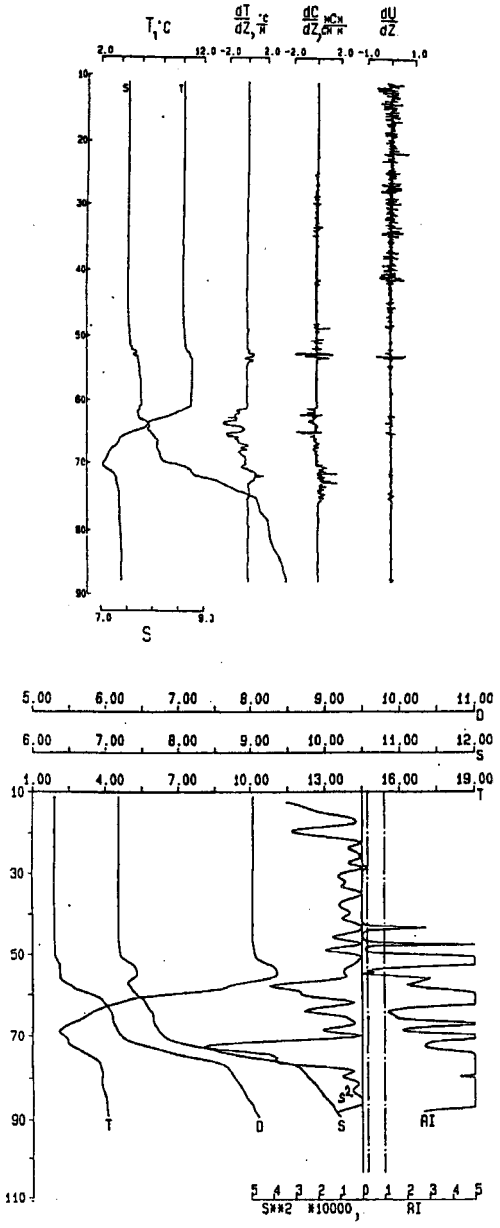


***Fig. 6.1.2.*** *Background temperature (T) and salinity (S) vertical distributions and profiles of temperature, conductivity and current velocity vertical gradients in the near-slope region (upper panel). Background temperature (T), salinity (S) and density (D) vertical distributions and profiles of current shear ($s^2$ ) and Ri (lower panel). Patches of turbulence at about 55 and 65 meters are well correlated with low values of Ri in case of near-slope current.*

During the 32. cruise of R/V Aju-Dag, April 1983, a series of measurements with the Neil Brown CTD/ACM profiler were carried out in the Bornholm Basin. These measurements are now reviewed considering near-inertial waves as possible source of energy for small-scale turbulence in the halocline. For the mesoscale structures observed during the experiment, see Chapter 5.2 (Fig. 5.2.1).

Outside the slope regions the larger scale circulation and mesoscale dynamical processes (*e.g.* mesoscale eddies, intrusive vortex lenses) are responsible for the background vertical shear. In the cases where the shear of near-inertial waves allied to the background shear, the enhanced total vertical shear resulted in patches of weak hydrodynamic stability. In these patches the Richardson number was more frequently below the critical value and turbulence could take place (Lilover, 1987, Lilover *et al.*, 1989). The *Ri* distributions without and with the presence of near-inertial waves are compared in Fig. 6.1.3.

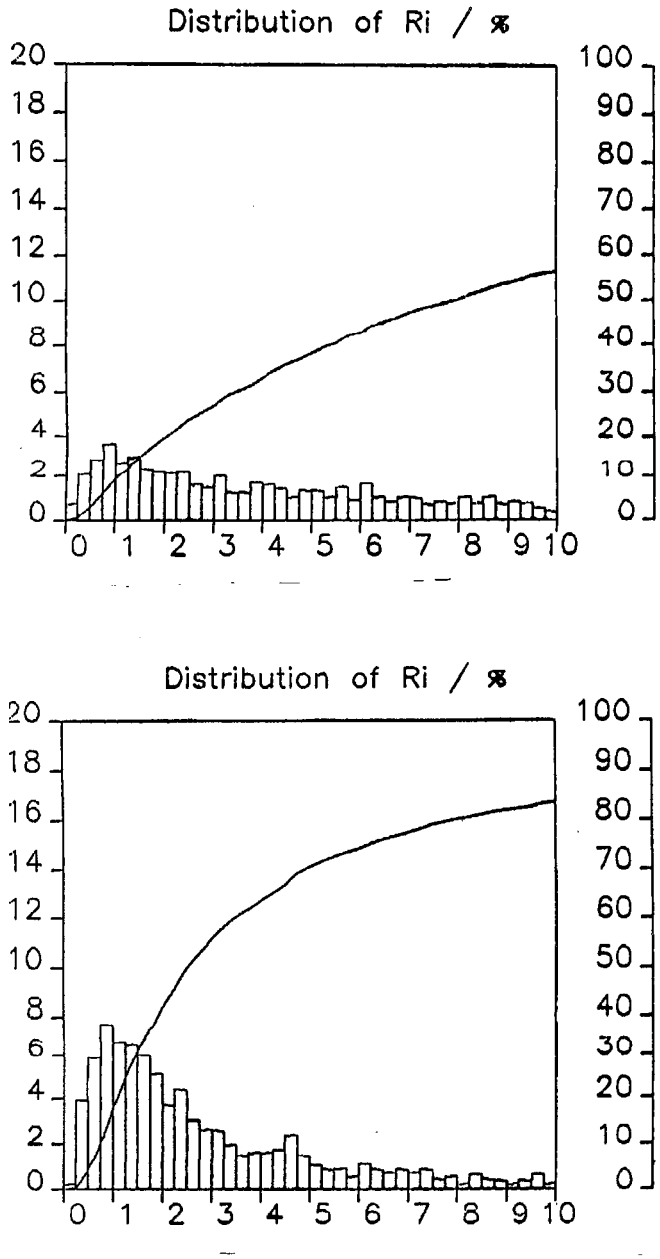


***Fig. 6.1.3.****The distribution of Ri (Ri is calculated with 1 m step in vertical) in the case of absence of near-inertial waves (upper panel) and in the case of presence of near-inertial waves (lower panel). The curve represents the cumulative distribution. Measurements were done during the R/V Aju-Dag cruise 32 in the Bornholm Basin.*

When the signal of near-inertial waves was not detected the amount of *Ri* values below 1 was only 9%. In the case when the shear caused by near-inertial waves was superimposed to the background current field shear the amount of corresponding *Ri* values was considerably higher (18%).

We may conclude from here that the rare direct measurements of turbulence confirmed the gradual mechanism of vertical mixing for deep basins: a) small-scale turbulent mixing near the sloping bottom, and b) following advection of mixed water masses into the interior of the basin. Measurements made in the Bornholm Basin point to the possibility that near-inertial waves can be considered as the most likely physical phenomena supplying the deep layers with energy.

### 6.2. Evolution of the halocline structure and estimates of vertical salt fluxes

This sub-chapter is based on the data collected during the cruises of R/V Aju-Dag, R/V Arnold Veimer (at present Livonia) and R/V Marina in the period May 1984- May 1995. Study area (60x40 km) was located around the HELCOM BMP station J1 (Fig. 2.2). Measurements were mainly performed as hydrographic surveys with the grid step 8 km by using NBIS Mark lll CTD profiler. Two surveys consisted of single transects. Additionally we have used two CTD surveys carried out during the cruise of R/V Prof. Shtokman (Russia) in the spring 1993. Analysed CTD data-set consisted all together 18 surveys with the total number of casts 321. The preliminary data processing for the whole CTD data-set was realised by a scheme which follows the main steps proposed in a Report of SCOR Working Group 51 (UNESCO technical papers in marine science, UNESCO, 1988). The laboratory calibration of temperature and conductivity sensors as well the field comparison of CTD conductivity with *in-situ* conductivity (Rosette salinity is inverted to an *in-situ* conductivity using the CTD temperature and pressure) were carried out. After correction procedures temperature and salinity data were interpolated to depth interval 0.5 m.

*a) Changes of the halocline small-scale structure in 1984-1995*

The characteristic vertical distributions of temperature, salinity and density in the cold season of the year display the two-layer structure of the water column on the study area. Also, due to the water properties (low salinity and low temperature) changes in the density distribution are mainly caused by salinity. The beginning of halocline starts from the depths of 60-80 m.

To estimate the changes of halocline structure, the following survey averaged halocline parameters and their standard deviations were determined: depth of the beginning of halocline, thickness of halocline, total salinity difference across halocline, maximum vertical gradient of both smoothed and non-smoothed salinity profile and corresponding depths of maximum gradients. The halocline was determined as a layer where the vertical gradient of smoothed salinity profile exceeds 0.05 PSU $m^{-1}$ (Matthäus, 1979). The salinity profiles were precedingly smoothed with 2- meter running mean.

First of all, in most cases the variations of the calculated parameters from survey to survey and within a particular survey are significant compared with long-term changes.

Top of the halocline displays variations in its depth without clear trend during the whole period and probably reflects the dynamic balance between the erosion of halocline (winter convection and entrainment) and vertical transport of salt from deeper layers (Fig. 6.2.1a). Obvious deepening of isopycnals below the halocline until the major inflow in January 1993 were observed (Fig. 3.1c, 6.2.1a) reflecting the freshening tendency of the whole Baltic deep-water body during the stagnation period. Taking into consideration that and halocline definition the decrease and mutual dependence of halocline thickness and salinity difference were expected (Fig. 6.2.1b). The evident and expected rise of isopycnals and increase of halocline thickness and salinity difference followed the propagation of new water into the Gotland Deep after inflow. The maximum salinity gradients of both smoothed and non-smoothed profiles and the corresponding depths have no distinguishable trends on the background of large scatter in the whole period of the study (Fig. 6.2.1c).

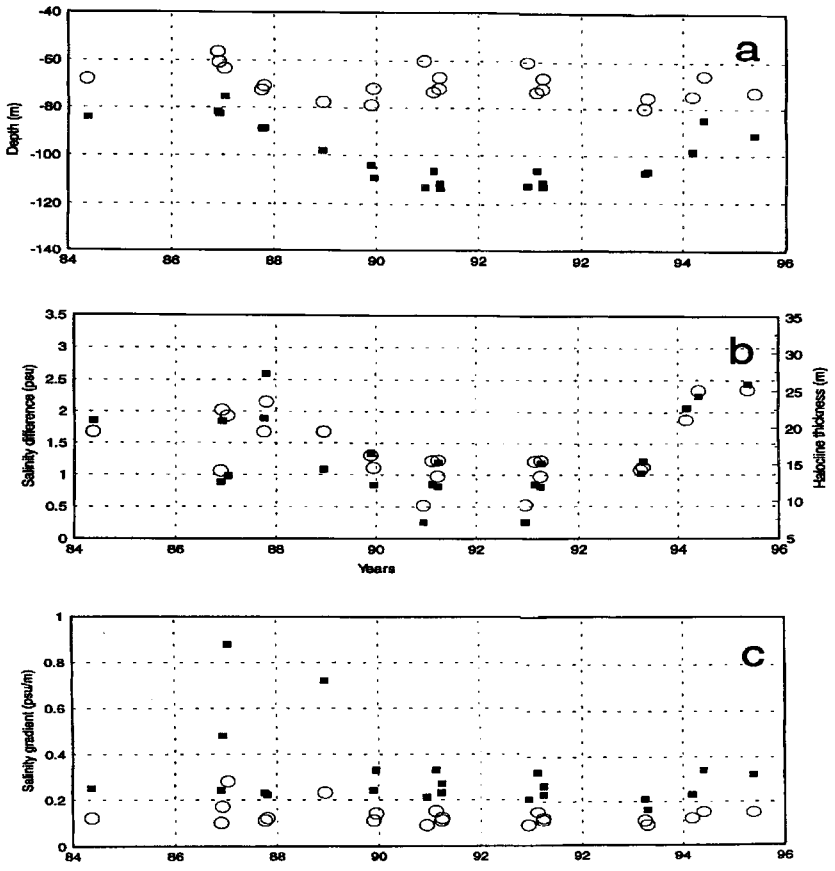


***Fig. 6.2.1.*** *The time changes of the survey-averaged halocline parameters during the period 1984-1995. a) halocline depth (circles) and depth of isopycnal 7.5 kg m $^{-3}$ (filled square), b) halocline thickness (circles) and salinity difference across this thickness (filled square), c) maximum of the smoothed salinity gradient (circles) and maximum of the non-smoothed salinity gradient (filled square).*

The occurrence of turbulent mixing events depends on the halocline stratification. The total difference of salinity and density in the halocline have decreased during the stagnation period. However, the turbulence occurrence probability is determined rather

by the distribution of the small-scale (about 1 m) vertical density gradients than by the total difference of density, because the order of magnitude of the Ozmidov length scale $L = (\varepsilon N^{-3})^{1/2}$ is O(10 cm) in the Baltic halocline. Here $\varepsilon$ is the turbulent kinetic energy dissipation rate and $N$ is the Väisälä frequency. For estimation of evolution of small-scale background stratification, the averaged over survey distributions of the vertical non-smoothed density gradients were calculated. The general shape is similar for all distributions and retains in the halocline over the whole observation period (Fig. 6.2.2, uper panel). The distributions vary from survey to survey, hence the background conditions for turbulence change, but no unidirectional changes in the distributions were observed, *i.e.* no trends were observed for relative weights of weak and strong gradient relative frequency.

*b) Estimates of the salt flux*

Turbulence in the sea is intermittent due to the non-uniform stratification and energy input. It was found from laboratory experiments that the value for transition turbulent kinetic energy dissipation rate is $\varepsilon_{tr} = c\nu N^2$ below which turbulent mixing does not occur, where $\nu$ is kinematic viscosity. The values of the dimensionless coefficient $c$ were found to be in the limits from 16 to 25 ( Peters *et al.*,1988 ). The value $c$=20 was applied to the ocean as the lower boundary of "active" mixing by Peters *et al.*(1988). Proceeding from the above given formulae $\varepsilon_{tr}$ value in the halocline was estimated for every point of CTD profile (depth interval $\Delta z$ =0.5 m). The Väisälä frequency $N$ was calculated from non-smoothed density profile with $\Delta z$=1 m. The values of eddy coefficient $k_z=0.2\varepsilon N^{-2}$ (Peters *et al.*, 1988) and of the corresponding salt flux $Q_S = k_z dS/dz 10^{-3}$ were estimated for different predetermined turbulent kinetic energy dissipation rates ( varying from $10^{-9}$ to $5 \cdot 10^{-7}$ W kg$^{-1}$). The survey-averaged salt flux per "active" mixing point $Q_S$ and the ratio $n$ of "active" mixing points number to the all halocline data points number for each survey were calculated. Assuming that the probability of occurrence of turbulent mixing events in every point of halocline is equal, the quantity $nQ_S$ may be considered as the mean salt flux through the halocline. There exist only a few estimations of dissipation rates from velocity microstructure measurements in the open Baltic halocline . The dissipation rates estimated from velocity microstructure profiles in quiet meteorological conditions varied between $10^{-9}$-$10^{-8}$ W kg$^{-1}$ in the halocline (Lilover and Nabatov, 1990). The salt fluxes corresponding to those dissipation rates are practically zero (Fig. 6.2.2, lower panel). It means, that $\varepsilon_{tr} > 10^{-8}$ W kg$^{-1}$ in most points of halocline. Rapid salt flux growth is characteristic for the Baltic halocline stratification if $\varepsilon > 10^{-8}$ W kg$^{-1}$ (Fig. 6.2.2, lower panel). No trends of the salt flux estimates were observed for the predetermined dissipation rates and for the real stratification. The salt fluxes comparable with those from budget calculations, 0.01-0.16 kg m$^{-2}$ day$^{-1}$ (Matthäus, 1990), occurred if $\varepsilon > 10^{-7}$ W kg$^{-1}$. It follows, that if the small-scale turbulent mixing is regarded as the main process, which causes the across halocline transport, the extreme conditions with high energy input levels, *e.g.* storms or winter convection, are needed.

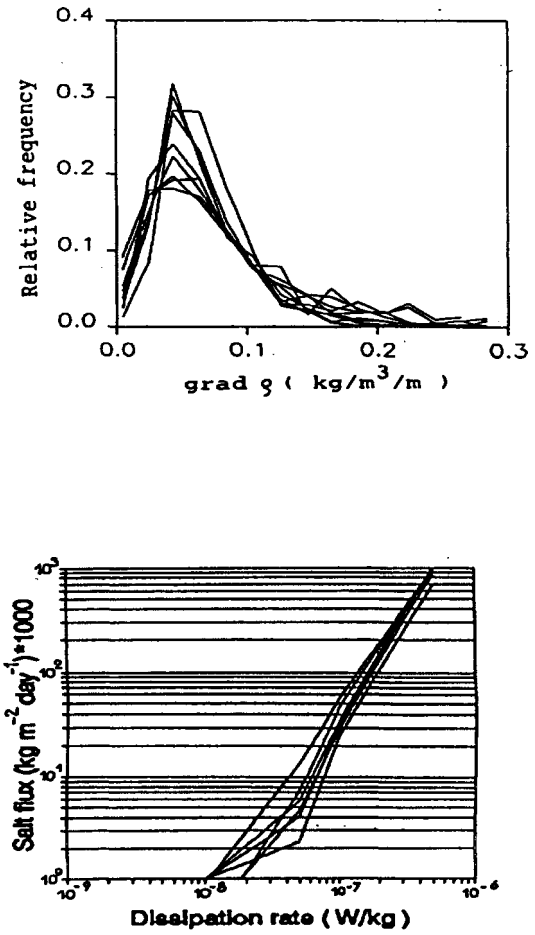


***Fig. 6.2.2.*** *Distributions of survey-averaged small-scale vertical density gradients (uper panel) and dependence of salt fluxes on predetermined dissipation rates in the cases of real stratification (lower panel).*

*c) Discussion and conclusion*

The analysis of the last decade CTD measurements on the central Baltic area demonstrated variations of the mean and maximum salinity gradients and distributions of small-scale density gradients, however no trend was observed. Winter convection re-establish sharp gradients, restricting the diffuse of halocline. Also, the vertical turbulent salinity flux (and water exchange between basins) do not allow remarkable deepening of halocline. It follows, that background stratification conditions in aspect of small-scale turbulence have no regular change during the stagnation period as well after the inflow. Accordingly salt fluxes (in the cases of predetermined different dissipation rates) vary but there is no obvious trend too. It should be emphasized here that the two essential assumptions were made for the salt flux estimations: probability of turbulent events in every point of halocline is equal and energy transfer from larger scale processes to turbulence does not depend on stratification decrease.

Practically equal to zero calculated turbulent salt fluxes in the cases of $\varepsilon < 10^{-7}$ W kg$^{-1}$ (that correspond to quiet meteorological conditions) and their rapid growth at the

dissipation rates $\varepsilon > 10^{-7}$ W $kg^{-1}$ were characteristic for the Baltic permanent halocline. The latter also points to the relatively uniform structure of the halocline. Therefore, the bulk of turbulent salt flux across the halocline depends to a great extent on the mixing under special hydrometeorological conditions (storms, winter convection and rapid movement of wind front, which generates inertial waves that lead to turbulence (Itsweire et al., 1989)) and/or occurs in the specific areas, such as slope regions (Shaffer, 1979, Kõuts *et al.,* 1990).

On the other hand, the across-halocline exchange could be partly related to the large-scale processes, the vertical scale of which is comparable with the halocline thickness, *e.g.,* upwelling /downwelling, meso-scale eddies, ventilation *etc.* The observed decrease of halocline thickness and salinity/density difference during the stagnation period would be then the reason for the increased across-halocline transport by these processes and for the corresponding positive long-term trend of the oxygen concentration in the intermediate layer. The superimposed short-term changes in oxygen concentration (as well as in temperature) in the intermediate layer are probable caused by the intensive water exchange between the basins of the Baltic Sea, expressed by intensive intrusions and meso-scale lenses observed in the Gotland Deep in cold seasons during last years (Elken *et al.,* 1988; Kõuts *et al.,* 1990).

Consequently, the changes of hydrographic conditions and oxygen concentration in the central Baltic deep layer during the stagnation period, cannot be explained by a small-scale turbulent transport across the halocline only. It is a rather complicated phenomenon comprising different scale physical processes.

### 6.3. A model for generation of near-inertial waves

The wind-induced drift current vanish in the upper mixed layer and is therefore not directly responsible for the mixing and vertical salt transport in the deeper layers. Also, current shear in the deep layers is too week to create turbulence by oneself. Near-inertial oscillations dominate in the velocity spectrum almost always, i.e. these oscillations possess considerable amount of kinetic energy. Therefore, inertial gravity waves are considered as possible mechanism, which transport energy from subsurface layer (energy input from atmosphere through wind stress) into the deeper layers. In the following we propose the model which describes the generation of inertial gravity waves.

In the numerical model proposed here the external forcing is represented by the moving wind front. The response of the sea is divided into two different motions. First, the wind-induced drift current, which is modulated by the horizontally propagating wave with inertial frequency. The wave length is determined by the speed of movement of wind front. Second, inertial gravity waves propagating in the whole water column. These waves are able to carry energy from subsurface layer into the deep stratified layers and thus create large vertical gradients of horizontal velocity, i.e. shear instability.

We start from the following equations:

$$
\begin{aligned}
&\frac{\partial u}{\partial t} - fv + \tilde{f}w - \frac{\partial}{\partial z} A_H \frac{\partial u}{\partial z} + \frac{1}{\rho_0}\frac{\partial p}{\partial x} = 0, \\
&\frac{\partial v}{\partial t} + fu - \frac{\partial}{\partial z} A_H \frac{\partial v}{\partial z} + \frac{1}{\rho_0}\frac{\partial p}{\partial y} = 0, \\
&\frac{\partial w}{\partial t} - \tilde{f}u + g + \frac{1}{\rho}\frac{\partial p}{\partial z} = 0, \\
&\frac{\partial u}{\partial x} + \frac{\partial v}{\partial y} + \frac{\partial w}{\partial z} = 0, \\
&\frac{\partial \rho}{\partial t} - \rho_0 N^2 w = 0.
\end{aligned}
\qquad (6.3.1)
$$

The following boundary conditions are applied:

on the sea surface ($z = 0$) :

$$
\begin{aligned}
&A_H \frac{\partial u}{\partial z} = -\tau_x, \\
&A_H \frac{\partial v}{\partial z} = -\tau_y
\end{aligned}
$$

and at the bottom ($z = -H$):

$u = v = w = 0$.

Here $x$ and $y$ are the horizontal co-ordinates, $z$ is vertical co-ordinate ($z$=0 at sea surface) and positive upward, $u$,$v$ and $w$ are the horizontal and vertical velocity components, $f$ is the horizontal Coriolis parameter, $\tilde{f}$ is the double horizontal component of the angular velocity of the Earth, $g$ is the acceleration due to gravity, $A_H$ is the horizontal eddy diffusion coefficient, $N$ is the Väisäla frequency, $\rho$ is the density of sea water, $\rho_0$ is the reference density, $p$ is the pressure, $\tau_x$ and $\tau_y$ are the wind stress components.

The system of equations (6.3.1) is linear, but considers the full rotation of the Earth. The solution of the system of equations (6.3.1) is $\varphi = \varphi_1 + \varphi_2$ , where $\varphi_1$ satisfies the simplified system of equations (6.3.1) with predetermined wind stress:

$$
\begin{aligned}
&\frac{\partial u_1}{\partial t} - fv_1 - \frac{\partial}{\partial z} A_H \frac{\partial u_1}{\partial z} = 0, \\
&\frac{\partial v_1}{\partial t} + fu_1 - \frac{\partial}{\partial z} A_H \frac{\partial v_1}{\partial z} = 0, \\
&\frac{1}{\rho_0}\frac{\partial p_0}{\partial z} = -g, \\
&\frac{\partial u_1}{\partial x} + \frac{\partial v_1}{\partial y} + \frac{\partial w_1}{\partial z} = 0.
\end{aligned}
\qquad (6.3.2)
$$

Some solutions of system (6.3.2) in the case of moving wind stress front $\tau(x,t) = \tau_0\ \eta(u_a t - x)$, where $\eta$ is the unit step function and $u_a$ is the speed of the wind front, are presented in Fig. 6.3.1. The solution is modulated by the horizontally propagating wave with inertial frequency. The amplitude of the wave decreases with depth. The phase velocity of wave is equal to the speed of the wind front.

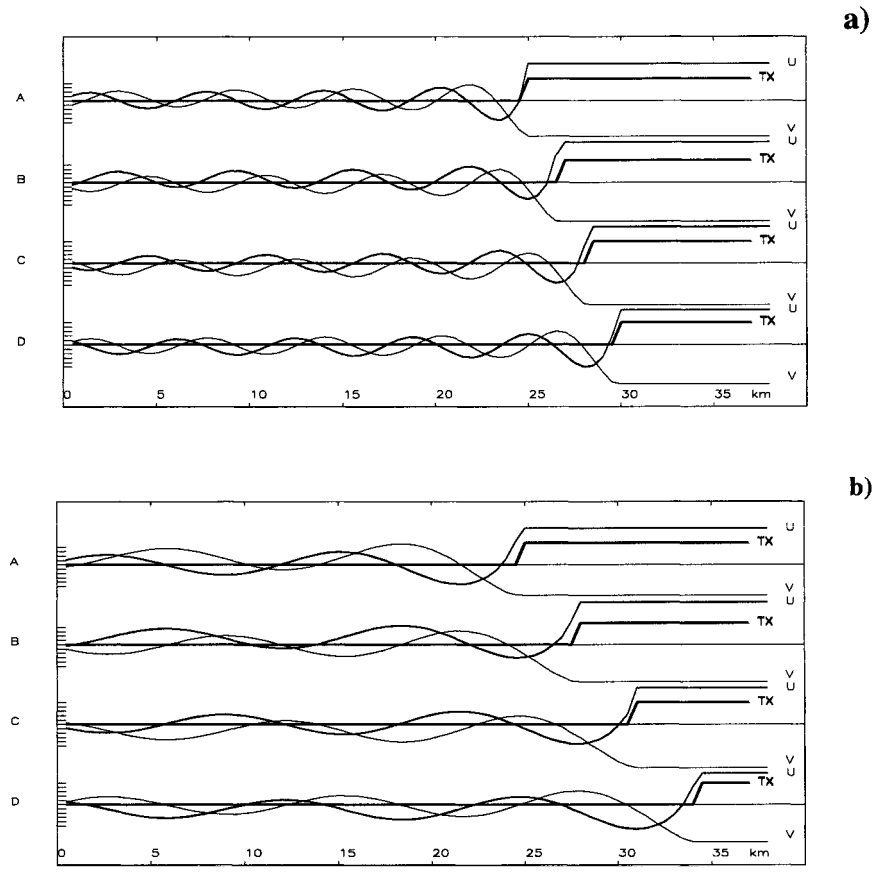


***Fig. 6.3.1.*** *Horizontal distributions of surface current components $u_1$ and $v_1$ generated by moving wind front a) $u_a$=12.5 cm $s^{-1}$, wave length L is 6.28 km and b) $u_a$=25 cm $s^{-1}$, wave length L is 12.57 km. Time steps: A) $t = t_0$; B) $t = t_0 + 0.25T_i$; C) $t = t_0 + 0.5T_i$; D) $t = t_0 + 0.75T_i$; where $T_i$ is inertial period ($2\pi/f$).The bold line represents the shape of wind stress $\tau_x$ and position of wind front. Wind front covers the distance from starting point to podition at time step A with $t_0$.*

In the second stage we find analytical solution $\varphi_2$, which satisfies equations (6.3.1) and the solution $\varphi_1$ is considered as external forcing. The solution $\varphi_2$ consists of waves, which have the vertical phase velocity and frequency $\omega$ satisfies the dispersion relation in stratified and rotating fluid.

The simulations with developed numerical model (system (6.3.2)) and analytical investigation of system (6.3.1) demonstrate that:

1) the moving wind front generated horizontal wave $\varphi_1$ modulated by inertial frequency and with the wave length $L = 2\pi u_a/f$. This wave is considered as the external forcing for $\varphi_2$.
2) the solution $\varphi_2$ has vertical phase velocity $c=\omega k_z/k^2$ and the same length $L$. Here $k^2 = k_x^2 + k_y^2 + k_z^2$, where $k_x$, $k_y$ and $k_z = k_y f \tilde{f} /(\omega^2 - f^2)$ are the wave numbers of corresponding axis. The amplitude of the wave is modulated by the inertial frequency. Notice, that wave $\varphi_2$ exists only in the case when the full rotation of the Earth ($f\neq0$, $\tilde{f} \neq0$) is considered. The wave $\varphi_2$ is enable to create the vertical gradients of the velocity sufficient to produce instability.

# 7. MODELLING OF VERTICAL MIXING AND TRANSPORT PROCESSES

*Jaak Heinloo and Üllar Võsumaa*

Turbulent mixing is an important factor in forming the vertical distribution of water quality parameters in the sea. Dictative role of relatively large scale eddies for the mixing processes is evident (*e.g.* Turner, 1986). Conventional methods of turbulence modelling are not able to take into account the specific feature of turbulent environment - rotational anisotropy, caused by large-scale eddies. General theory of rotationally anisotropic turbulence - RAT theory - has been worked out (Nemirovski and Heinloo, 1982; Heinloo, 1984), allowing also applications for the problems of marine turbulence (Heinloo and Võsumaa, 1987, 1992; Võsumaa and Heinloo, 1989; Toompuu *et al.*, 1989). The main aim of the present project was to develop and calibrate the hydrodynamic model of vertical structure of the sea water quality parameters in the form suitable for its ecological use.

## 7.1. The model

According to the RAT theory turbulent environment is defined as rotationally anisotropic, what means that the moment of momentum **M**, defined as

$$\mathbf{M} = \langle \mathbf{v}' \times \mathbf{R} \rangle \tag{7.1}$$

differs from zero ($\mathbf{v}'=\mathbf{v}-\langle\mathbf{v}\rangle$ is the velocity pulsation, **R** - the curve radius for $\mathbf{v}'$ vector lines).

Let us presume all the fields (expect the pressure field) to be horizontally homogeneous. The vertical structure problem formulated on the RAT theory leads to the following set of equations:

$$\rho_0 \frac{\partial \mathbf{v}}{\partial t} = -\nabla p + (\mu + \gamma)\frac{\partial^2 \mathbf{v}}{\partial z^2} + 2\gamma\nabla\times\Omega + 2\rho_0 \mathbf{v}\times\omega^0 \tag{7.2}$$

(the equation of balance of momentum),

$$\rho_0 J \frac{\partial \Omega}{\partial t} = \Theta J \frac{\partial^2 \Omega}{\partial z^2} + \left\{4(\gamma+\kappa) + k^{(2)} g \frac{\partial \rho}{\partial z}\right\}\Omega + 2\gamma\nabla\times\mathbf{v} + 2\rho_0 J\Omega\times\omega^0 \tag{7.3}$$

(the equation of balance of moment of momentum, $\mathbf{M}=J\boldsymbol{\Omega}$ and $J$ is the effective moment of inertia of the large-scale turbulent eddies),

$$\rho_0 \frac{\partial K}{\partial t} = c\frac{\partial^2 K}{\partial z^2} - \left\{\frac{\rho_0}{t_K} + k^{(0)} g \frac{\partial \rho}{\partial z}\right\}K + 2\mu\left|\frac{\partial \mathbf{v}}{\partial z}\right|^2 + 4\gamma\left|\frac{1}{2}\nabla\times\mathbf{v} - \Omega\right|^2 + \Theta J\left|\frac{\partial \Omega}{\partial z}\right|^2 + 4\kappa\Omega^2 \tag{7.4}$$

(the equation of balance of the energy of the small scale turbulence),

$$\rho = \rho\,(C_1=T, C_2=S, .., C_p=q_1, C_{p+1}=q_2, ...) \tag{7.5}$$

(the equation of state),

$$\frac{\partial C_i}{\partial t} + a_i \frac{\partial C_i}{\partial z} = \frac{\partial}{\partial z}\left[\left(k_{C_i} + k^{(0)} K + k^{(2)} \Omega^2\right)\frac{\partial C_i}{\partial z}\right] + F_i(C_1, C_2, ...) \tag{7.6}$$

(the balance equation for $C_i$);

where $T$ is temperature, $S$ is salinity, $K$ is small-scale turbulent energy, $\rho_0$ is the characteristic density of the environment, $p$ is the mean thermodynamic pressure; $\mu$, $\gamma$, $\kappa$ are the coefficients of shift viscosity, friction of the turbulent eddies at their relative rotation, and loss of the mean orientation of eddies in the random process of their interaction respectively; $\Theta$ is the coefficient describing the diffusion of the internal moment of momentum $\Omega$; $k$ and $c$ characterize, respectively, the diffusion of substance and momentum due to small-scale turbulence; $t_K$ is the characteristic time of decay of the small-scale turbulence; $k^{(0)}$ and $k^{(2)}$ are the coefficients describing the transport processes caused by the large-scale turbulence; $C_3, ..., C_{p-1}$ are the other water quality parameters of "non-suspension" type; $C_{p+1}=q_1$ are the concentrations of "suspension type" parameters; $k_{Ci}$ are the molecular diffusion coefficients of $C_i$; $a_i$ are sedimentation velocities for $C_i$ ($a_i$=0 for $i$=1,...$p$); $F_i(C_1,...)$ is the term describing the mutual changes of $C_i$; $\vec{\omega}^0$ is the angular velocity of the Earth; $g$ is the modulus of the gravity acceleration, and $z$ is the vertical coordinate directed downward.

Boundary conditions for Eqs. 7.2-7.6 are specified corresponding to meteorological conditions at the sea surface and sedimentation situation in bottom.

The physical situation described by the model is pictured in terms of energy balance in Fig. 7.1. According to the model the turbulent energy is divided into the energies of large-scale and small-scale turbulence, with coupling effects between the energies of the mean flow and the large-scale turbulence.

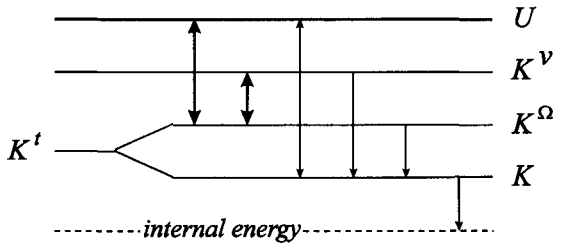


***Fig. 7.1.*** *The energy balance described by the model.*

Here $U$ is the potential energy, $K^v$ is the energy of the mean flow, $K^\Omega$ is the energy of large-scale turbulence and $K^t$ is the total turbulent energy.

### 7.2. Seasonal development of thermocline

The model is numerically investigated in different initial and boundary conditions. Firstly the problem of seasonal thermocline development is addressed. Since in the

Baltic lateral advection plays significant role, then the model is first tested in more simple oceanic conditions. Simulation has been made on the basis of data obtained at the Ocean Weather Station (OWS) Papa, Gulf of Alaska and Long term Upper Ocean Study (LOTUS), Sargasso sea. The proposed model is compared with the model of Gaspar (1990).

In the case of oscillating heat flux (daily heating oscillation), the shallow thermocline appearing during the heating period alternates with the deeper mixing during the cooling period (Fig. 7.2).

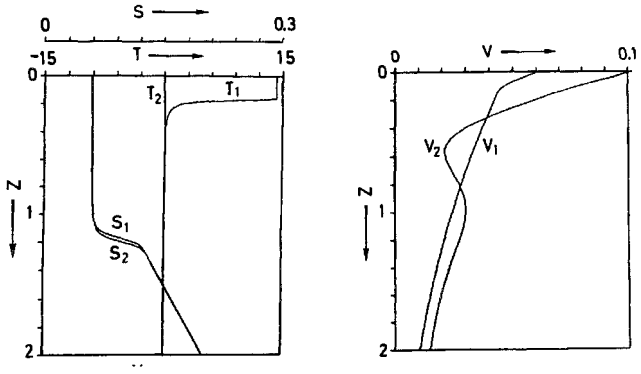


***Fig. 7.2.*** *Typical calculated profiles of T, S and mean velocity components, during the daily heating (index 1) and cooling (2).*

In the case of steady heating and wind conditions, the mixed layer depth approaches its characteristic value $H$ being a function of heat flux and wind stress (Fig. 7.3).

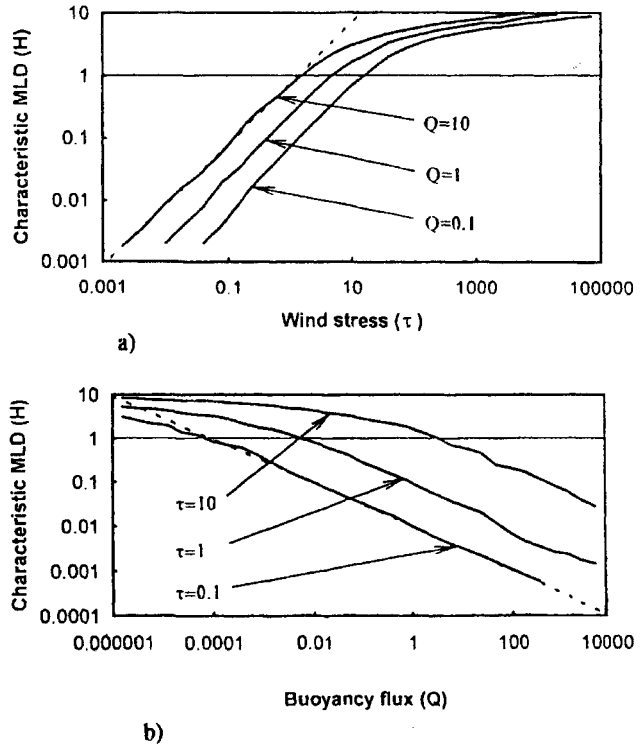


***Fig. 7.3.*** *Dependence of the mixed layer depth (MLD) from the wind stress and the buoyancy flux.*

These results are in good accordance with the results following from the Richardson number parameterisation of the mixing process (Price *et al.*, 1986).

The results of the comparison of the present model with the observational data obtained at the Ocean Weather Station Papa, Gulf of Alaska, and the Long Term Upper Ocean Study (LOTUS), Sargasso Sea, are presented in Figs. 7.4 and 7.5.

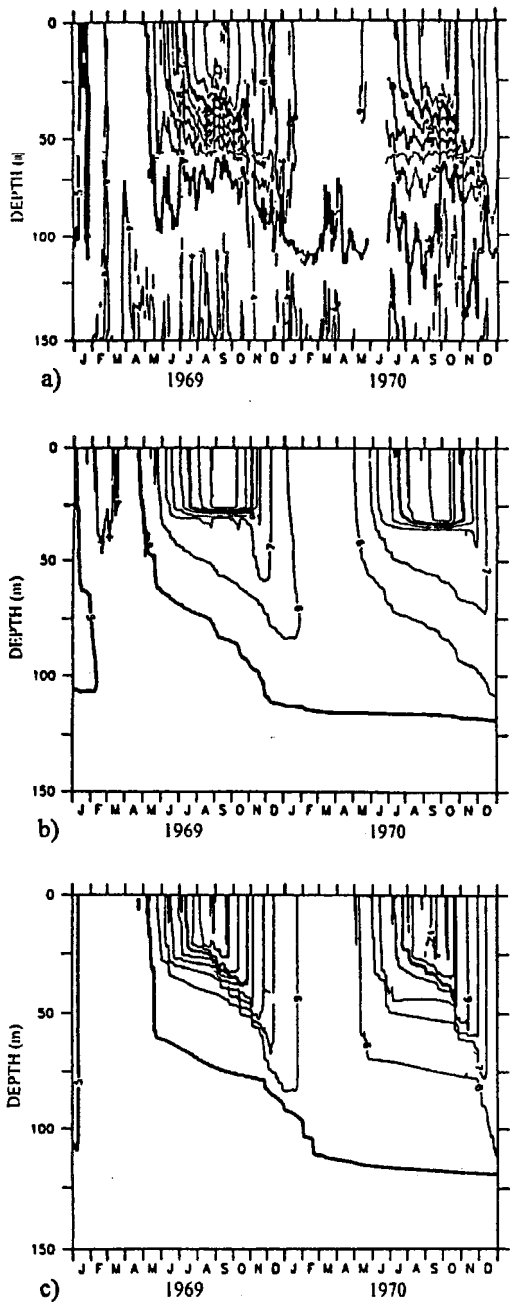


***Fig. 7.4.*** *Temperature isolines at the OWS Papa during 1967-1970 determined from measurements (a), calculated with the help of proposed model (b) and the model of Gaspar (1990) (c).*

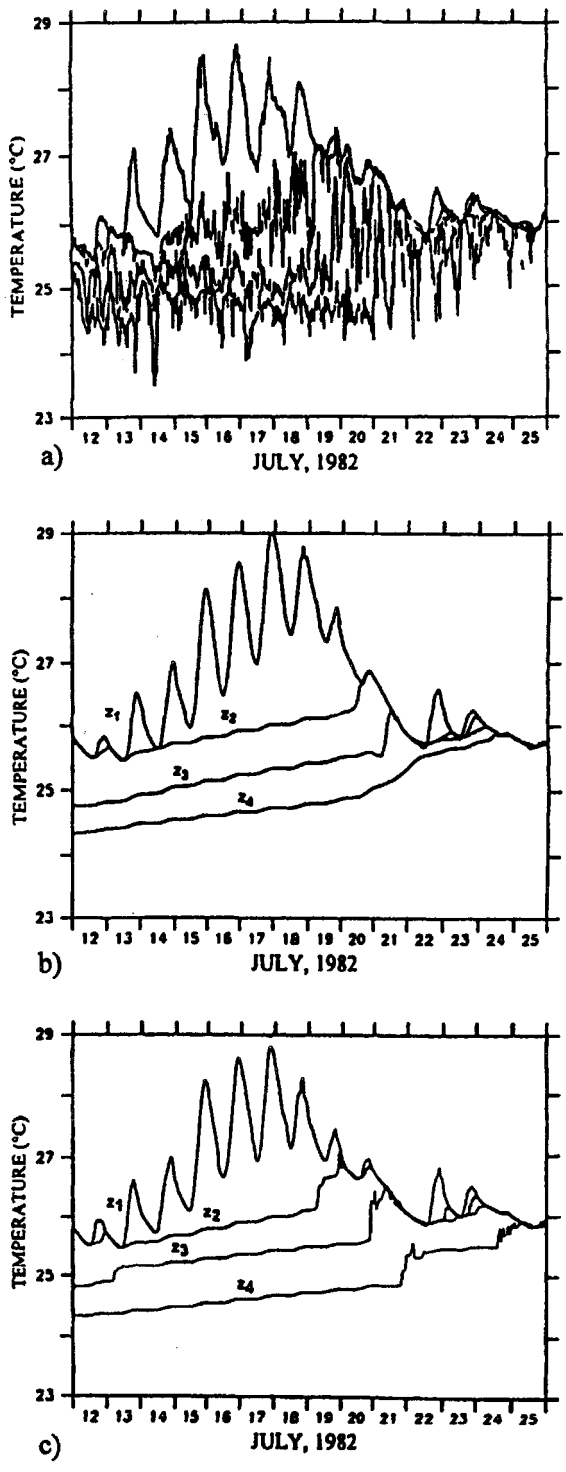


***Fig. 7.5.*** *Evolution of temperature during the LOTUS at four depth: 0.6, 5, 10 and 15 m determined from measurements (a), calculated with the help of the proposed model (b) and the model of Gaspar (1990) (c).*

### 7.3. Development of step-like finestructure

In the situation where the relatively warm and salty water is overlaid by colder but less salty water mass, the overall stable stratification can be still achieved. However, due to difference in the molecular diffusivities of the stratifying substances, instabilities will appear locally. That brings to the local mixing events and to the corresponding changes in stratification. Described process is pictured as the appearance of the system of well-mixed and the step layers in Fig. 7.6.

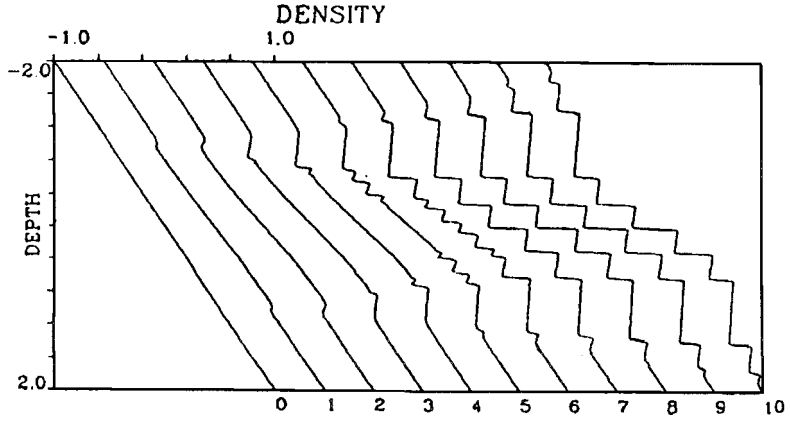


*Fig. 7.6. Development of initially smooth stratification, favourable for double diffusion, into a staircase-like structure.*

The demonstrated effect is known from a number of oceanographic observations, both in the ocean (Swallow and Creace, 1956; Siedler, 1968; Padman and Dillon, 1989) and in the Baltic Sea (see Chapters 5 and 6).

### 7.4. Ecological applications of the model

Series of investigations have been carried out for testing the different model situations in the near-bottom layer where the resuspension effect of sediments is important. Some aspects need a further study, in particular the influence of different sediment properties (*e.g.* the buoyant effects) on the near-bottom flow and turbulence regime. This necessitates also more co-operation with the sedimentological observational programmes (*e.g.* the Gulf of Riga Project, EU BASYS).

The model gives unique treatment of the vertical structure from the sea surface to the bottom. Improved turbulence description used in the model is capable of simulating both the thermocline development and the finestructure formation. The model can be coupled with the ecological block of the FINEST model and incorporated into the regional hydrodynamic circulation model described in Chapter 8. Another straightforward application in the Baltic regional context is within the one-dimensional 'filling box' models (*e.g.* Stigebrandt, 1987) which diagnostic case was considered in Chapter 4.

# 8. CIRCULATION MODELLING

*Jüri Elken*

The present Baltic Sea circulation modelling was initially motivated by the study of generation and decay mechanisms of mesoscale eddies, based on the observational data highlighted in Chapter 5. However, with the progress of the numerical experiments, problems of deep circulation and water exchange were addressed. The model was used also for the study of salinity fronts at the surface (Elken, 1994).

## 8.1. Model description and setup

*a) The model*

Specific estuarine inflow-outflow features of the Baltic Sea coupled with the multi-basin topography had accomplished the use of isopycnic and sigma co-ordinate models and more success has been obtained by using of the fixed level models. Modelling activities in the Baltic Sea have been recently reviewed by Lehmann (1992).

We have chosen the free surface version of the GFDL ocean circulation model (Killworth *et al.,* 1989) which is based on the Bryan-Cox-Semtner code developed at the Princeton University. The rigid lid version of the model has been used in the Baltic by Krauss and Brügge (1992). The free surface model is presently used for the Baltic Sea regional studies at IfM, Kiel (Lehmann,1992, 1994; Meier and Krauss, 1994), at IOW, Warnemünde (Seifert and Fennel, 1994) and at EMI, Tallinn (Elken, 1994; Raudsepp and Elken, 1995).

The GFDL model is the primitive equation model based on the three-dimensional (3D) conservation equations for the components of momentum, the mass field and the conservative tracers (temperature, salinity *etc.*). Vertical component of the momentum is treated by the hydrostatic approach which filters out short internal gravity waves. Mass conservation for incompressible fluid leads to non-divergent current velocity field. Equation of state is used to calculate the water density from temperature, salinity and pressure. Turbulence is considered as viscosity for the momentum and as diffusion for the tracers. For solving the equations, velocity field is decomposed into the depth-independent, barotropic mode and the remainder depth-dependent baroclinic mode. The barotropic mode is used to calculate the pressure at the surface. Kinematic boundary condition at the surface used in the free surface version encounters the long barotropic gravity waves.

The equations are solved numerically on the grid following fixed longitude, latitude and depth. In a horizontal plane, the points for calculation of tracers, vertical velocity, pressure and surface elevation are placed in the centre of the grid cells and the points of horizontal velocity are placed in the centre of the grid cell walls. In a vertical plane, the points for vertical velocity are placed on the upper/lower walls of the grid cells and all the other variables are placed in the centre. Time integration of the model is done by the explicit second-order scheme which for a variable $\psi$ is written as

$$\frac{\psi^{n+1}-\psi^{n-1}}{\Delta t}+Adv(\psi^n)=Diff(\psi^n)+F^n, \tag{8.1}$$

where $n$ denotes the time step index, $\Delta t$ is the time step, *Adv*( ) and *Diff*( ) are the advection and diffusion operators and $F$ is the source/sink term. Barotropic mode is solved by a different time step $\Delta t_B$ which is much smaller than $\Delta t$. Numerical formulation of the model satisfies integral conservation of mass, momentum and tracers. Although the total energy is also conserved by the second-order advection scheme based on the central differences, a certain amount of viscosity and diffusion is needed in the model to suppress the 'overshooting' effects apparent due to numerical dispersion (*e.g.* Gerdes *et al.*, 1991). Bottom friction was taken into account by a quadratic drag formulation adopted from Lehmann (1992).

The original model code by Killworth *et al.* (1989) has included the forcing only due to wind stress. At the bottom and lateral boundaries both the advective and diffusive flux through the boundary is assumed to be absent.

We have implemented the budget-type boundary conditions for rivers and open sea boundaries. For numerical simplicity, normal to the boundary velocities were kept zero, thus the export/import fluxes were taken into account without the kinematic effects for the velocity field near the boundary. On Cartesian $x,y,z$ coordinates, assume $Q$ to be an external, prescribed volume transport into the horizontal grid cell with a surface area $A_{xy}$. Then the surface elevation $\xi^{n+1}$ at time step $n$+1 is calculated as

$$\frac{\xi^{n+1}-\xi^{n-1}}{\Delta t_B}=\frac{\Delta U^n}{\Delta x}+\frac{\Delta V^n}{\Delta y}+\frac{Q\,\Delta t_B}{A_{xy}}, \tag{8.2}$$

where $U$, $V$ are the total barotropic transports along $x$ and $y$ and $\Delta$ denotes the finite difference operator. At the rivers and sea boundaries with the barotropic inflow $Q$>0, at the barotropic outflow $Q$<0.

Salt flux at the rivers and open sea boundaries was treated as a prescribed volume transport $Q_S$ (>0) of water with a prescribed salinity $S^*$ into the 3D grid cell with a volume $V_{xyz}$. Note, that 2D integral of $Q$ and 3D integral of $Q_S$ are equal. At the boundary of barotropic outflow (Q<0), saline water ($S^*>S^n$) with $Q_S$>0 is inserted in the bottom layers and at the barotropic inflow, less saline or freshwater is inserted in the surface layers. Mixing of the salt amounts $Q_S\,\Delta t\,S^*$ and $V_{xyz}\,S^n$ during the time step $\Delta t$ yields a nudging formula

$$F^n=\frac{Q_S}{V_{xyz}+Q_S\,\Delta t}(S^*-S^n), \tag{8.3}$$

where $F^n$ is the source/sink term of the salt conservation equation following (8.1). Due to dispersive effects of the advection scheme, it is necessary to distribute large inflow rates over the number of neighbouring grid cells that $Q_S\,\Delta t << V_{xyz}$.

For the dense water overflow problem it is very important to modify the convection scheme. In case of hydrostatic instability appearing in the model, mixing of the vertically adjacent *T,S* grid cells is performed in the original code. Therefore, if dense water is advected over the sill into the deeper basin then it cannot sink to the level of neutral buoyancy but is vertically mixed with the surrounding water. As a result, artificially high mixing of the overflowing water and false eddy formation appears in the standard code. In order to suppress these effects, sinking option was implemented in the convection scheme where the *T,S* grid cells in the deep water were mutually replaced until hydrostatic stability was achieved.

*b) Regional implementation*

While $R_d$ = ca 10 km and the observed eddies have diameter 20-60 km, it was necessary to take the horizontal grid step several times smaller than the eddy size. A grid step of 2.5 miles (4.66 km) was chosen. Limited area test runs gave too much barotropic and baroclinic disturbances generated at closed boundaries. Therefore it was necessary to include the whole Baltic Proper with the Gulf of Riga and the Gulf of Finland, with the narrow connections to the North Sea and the Bothnian Sea closed. Initially it was assumed that water exchange has minor effect on mesoscale dynamics. The selected model domain covers the area 12°00'-30°20'E, 54°00'-60°30'N. In order to properly resolve the isopycnal displacements within the halocline which was of primary interest with respect to the observations, vertical grid step was taken 5 m in the depth range 0-130 m, and larger steps, from 10 to 30 m were used below this level down to 200 m. With the eastern part of the Gulf of Finland converted to the free land points, the model grid has altogether 157x157x30 grid points. The model grid was created using digitised topography with 5'x5' resolution provided by F.Wulff.

*c) Initial data, forcing and coefficients*

From the model test runs with fluctuating wind forcing it became clear, that starting the model from the horizontally homogeneous stratification, baroclinic Kelvin waves are generated at the slope and baroclinic response in the off-slope regions is underestimated several times as compared with the observations. Actual stratification of the Baltic Sea follows estuarine differences between the sub-regions, with the forcing of gravity currents and dense water overflow from one basin to another (see Chapters 3 and 4). Therefore it was necessary to include the observed T,S values in the different basins as the initial conditions. However, on the longer time scale it was necessary to include also the volume and salt fluxes from the rivers and the adjacent sea regions to maintain the stratification against the salt loss from the deep layers by diffusion and transport.

For the initial conditions, sub-basins were selected in the model domain by the area masks as depicted in Fig. 3.1. In addition, river influence areas were selected at large rivers. Initial T,S data were taken from HELCOM BMP, winter 1985/1986 by adopting horizontally uniform distribution within each of the 11 selected Baltic sub-basins and 5 river influence areas, allowing initial fronts at sub-area boundaries. Selected salinity profiles are given in Fig. 8.1. In transition between the sub-areas smoothing was applied to the initial distributions to avoid numerical problems. The initial salinity distribution is demonstrated in Fig. 8.2 by a transect along the deepest positions.

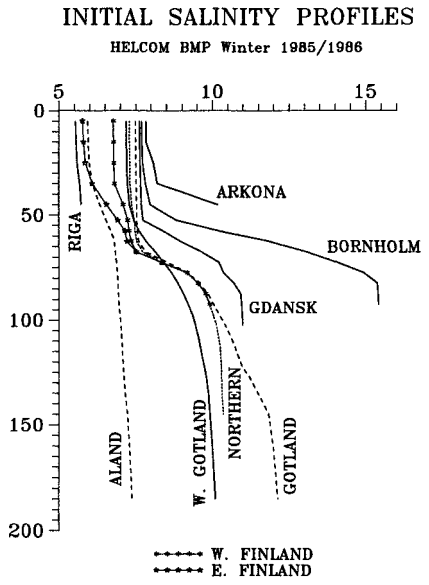


***Fig. 8.1.** Initial profiles of salinity in the model sub-basins taken from HELCOM BMP, winter 1985/1986.*

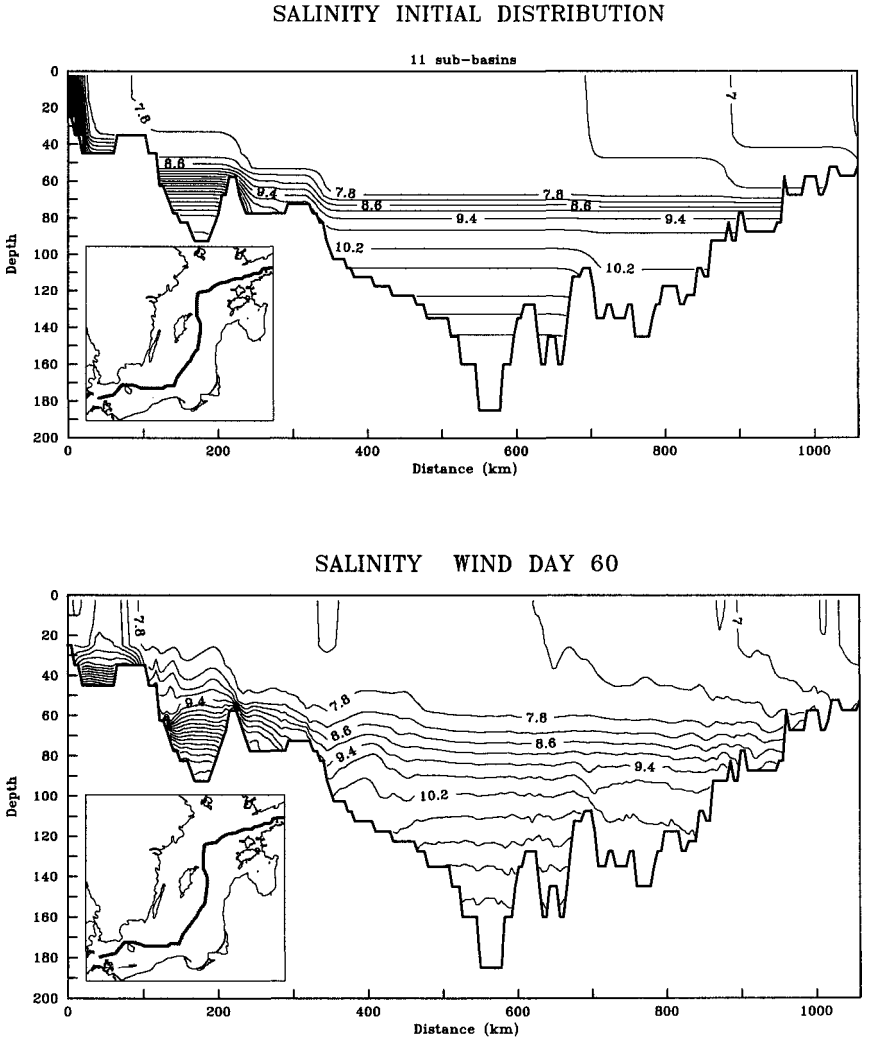


***Fig. 8.2.** Salinity distribution in a transect shown on the inserted map, for the model initial conditions (above) and the model response after 60 days of calculation with variable wind forcing (below).*

For the comparision with the actual distributions, an example of the salinity section observed during the PEX-86 experiment is given in Fig. 8.3.

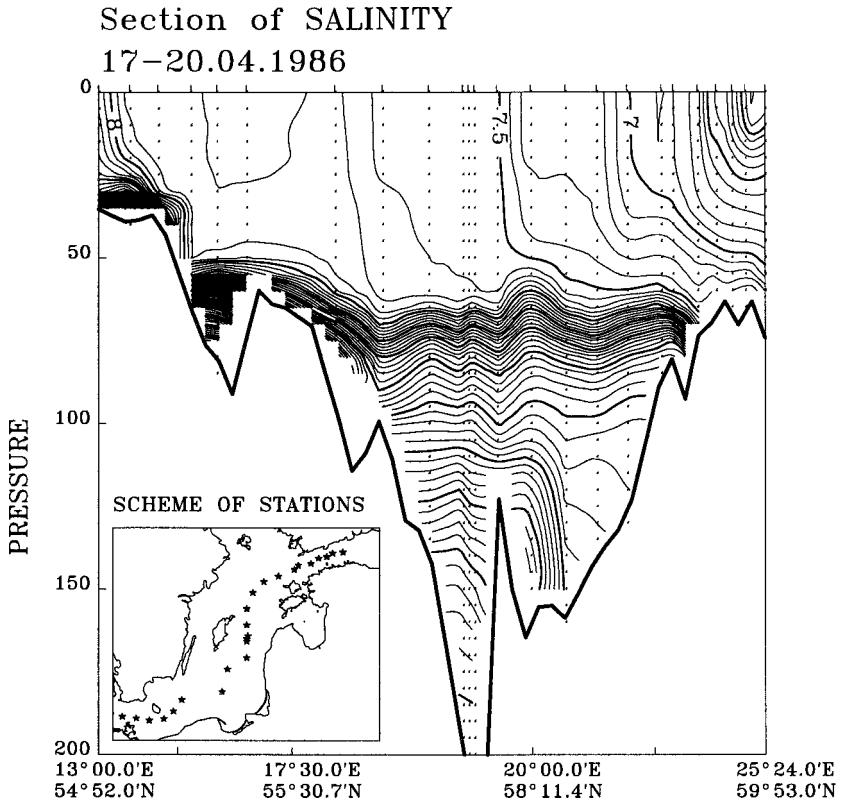


***Fig. 8.3.*** *Section of salinity observed in a transect shown on the inserted map. Data from PEX-86.*

Initial stratification given above is hydrodynamically not balanced. Therefore the model was first calculated without the wind forcing allowing only for the density driven flows. Time period of 10 days was found to be sufficient for a decay of inertial oscillations generated during the adjustment towards the quasi-geostrophic state.

The model was forced by fluctuating but spatially uniform wind observed at Hoburg (SMHI) which was switched on after 30 days of density driven adjustment phase Two wind periods were used, starting from 01.10.85 and 01.03.86 respectively. Water level and salinity were forced at the boundaries by the schemes (8.2) and (8.3) using the climatic mean flow rates and salinity at the rivers and semi-open sea boundaries (Åland Sea, Belt Sea, Sound).

Constant coefficients of horizontal viscosity $\mu = 0.7*10^6$ $cm^2s^{-1}$ and diffusion $\mu_T = 1.3*10^5$ $cm^2s^{-1}$ were adopted. Coefficients of vertical viscosity and diffusion were taken as depth-dependent functions, with the values $\nu = 25$ $cm^2s^{-1}$ and $\nu_T = 5$ $cm^2s^{-1}$ at the surface layer and 0.3 $cm^2s^{-1}$ and 0.07 $cm^2s^{-1}$ below 20 m, respectively.

*d) Numerical experiments*

A number of preliminary experiments were made with respect to different wind forcing (*incl.* constant winds), initial stratification (*incl.* spatially uniform and two-basin approach), viscosity and diffusion (*incl.* larger coefficients), bottom topography (*incl.* smaller width of the Stolpe Channel). With the two wind forcing time series, abbreviated as W85 and W86, calculations were made both for the closed basin and for the volume and salt flux forcing from the rivers and the semi-open sea boundaries. Transport calculation was made at selected sections during the model run. At some of the experiments, a tracer was inserted in deep layers of the Bornholm Basin in order to study the dense water overflow through the narrow Stolpe Channel.

### 8.2. Reproduction of mesoscale eddies

It has been shown that Baltic Sea baroclinic eddies have non-dimensional parameter values close to that of the ocean eddies (Elken, 1985), with $R_d$ ($\approx$ 10 km) as a scaling unit. However, the role of beta-effect which controls the Rossby waves and eddy kinematics in the ocean, is negligible in the Baltic (Kielmann, 1981, Aitsam and Elken, 1982) and mesoscale dynamic balance is affected by the bottom slope leading to topographic waves (Talpsepp, 1982).

Regarding the eddy generation mechanisms, role of baroclinic instability of the mean flow has been evaluated on the basis of linearized models (Aitsam and Elken, 1982, Aitsam and Talpsepp, 1982). At this stage no reasonable assumption of the origin of the mean flow was given. Wind generation of eddies has been studied by numerical models which produced eddies above topographic features during a period of ceasing wind following strong wind events (Kielmann, 1981, Krauss and Brügge, 1992). Generation of wind forced waves has been analyzed by Fennel and Lass (1989) using analytical theory. In contrast to the wind forcing concepts based on the approach of horizontally uniform background stratification, observed baroclinic eddies were found to be not very sensitive to changing winds. Recently Lehmann (1992) has implemented a realistic eddy-resolving Baltic Sea circulation model which produced eddies at the areas of eddy observations, *e.g.* the PEX polygon in the Hoburg Channel.

Preliminary model experiments attempted to generate the eddies by the wind forcing only, with the large-scale potential energy being absent in the system. Multiple highly variable eddy patterns were produced, but the baroclinic response was dominated by the Kelvin waves and the baroclinic amplitudes in the halocline interior were very small. While in the off-slope 'check boxes' (Table 5.1.1) the observational r.m.s. deviation of salinity was in the range of 0.19-0.35 in the Hoburg Channel and 0.11-0.37 in the Gotland Deep, then only about 0.05 was produced by the model with simplified initial conditions. Full implementation of the initial conditions raised up the model baroclinic amplitudes to the level of their observed counterparts.

From the ocean models it is well known that baroclinic eddies are generated if there is enough large-scale potential energy (Holland and Lin, 1975) which is produced by the curl of wind stress and/or thermodynamic effects. In the Baltic Sea the large-scale potential energy is produced by a complex of water and salt/heat exchange processes which may be called as estuarine dynamics.

Initial deep density front between the Gdansk and Gotland Basins transformed into the saline water plume spreading towards the Gotland Basin until it got arrested at a transition to the more wide and more deep Gotland Basin. The dense water blocking is accompanied by formation of the channel-wide strong baroclinic eddy as can be seen from the current field (Fig. 8.4). This eddy was persistent in the model over more than 15 days and was not destroyed by the strong winds in between. In the Stolpe Channel the flow pattern depends a lot on the wind forcing. While at the smaller wind speeds dense water overflow into the Gdansk Basin is dominant, with the flow intensification at the southern slope of the channel (Fig. 8.4.a), then stronger winds, especially of the western and southern directions may cause the flow reversal in the upper layers of the saline water. Due to baroclinic rotational effects in the channel, bi-directional flow and eddy formation may be found in the channel (*e.g.* Fig. 8.4c).

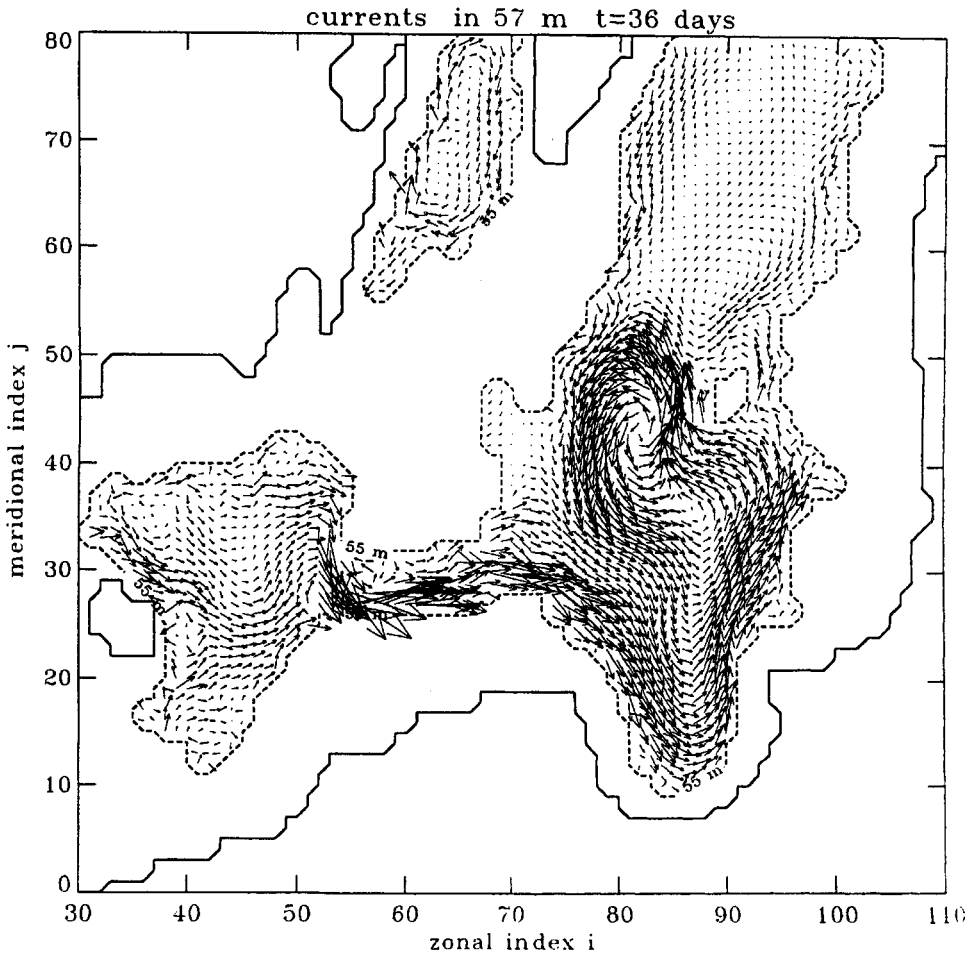


***Fig. 8.4.*** *Modelled current vectors in a layer 55-60 m. (a) model wind day 6.*

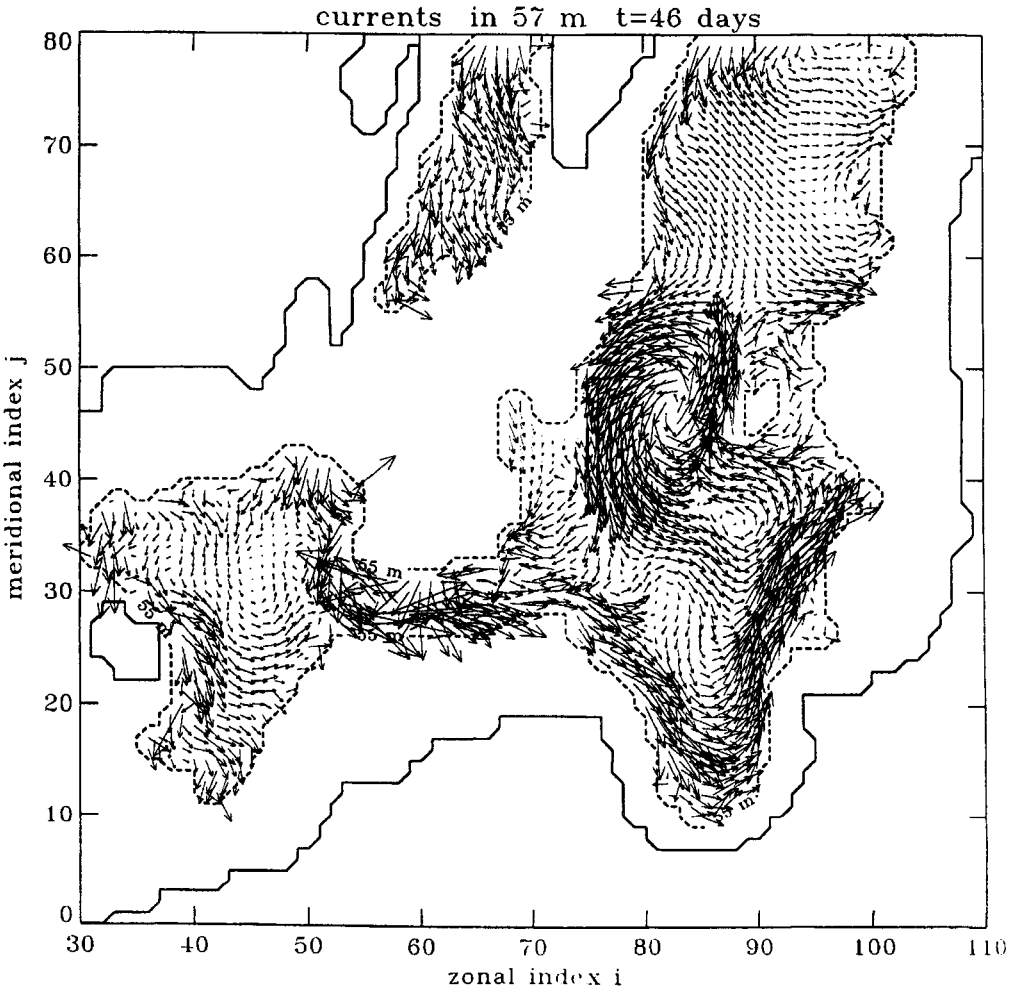


***Fig. 8.4.*** *Continued. (b) model wind day 16.*

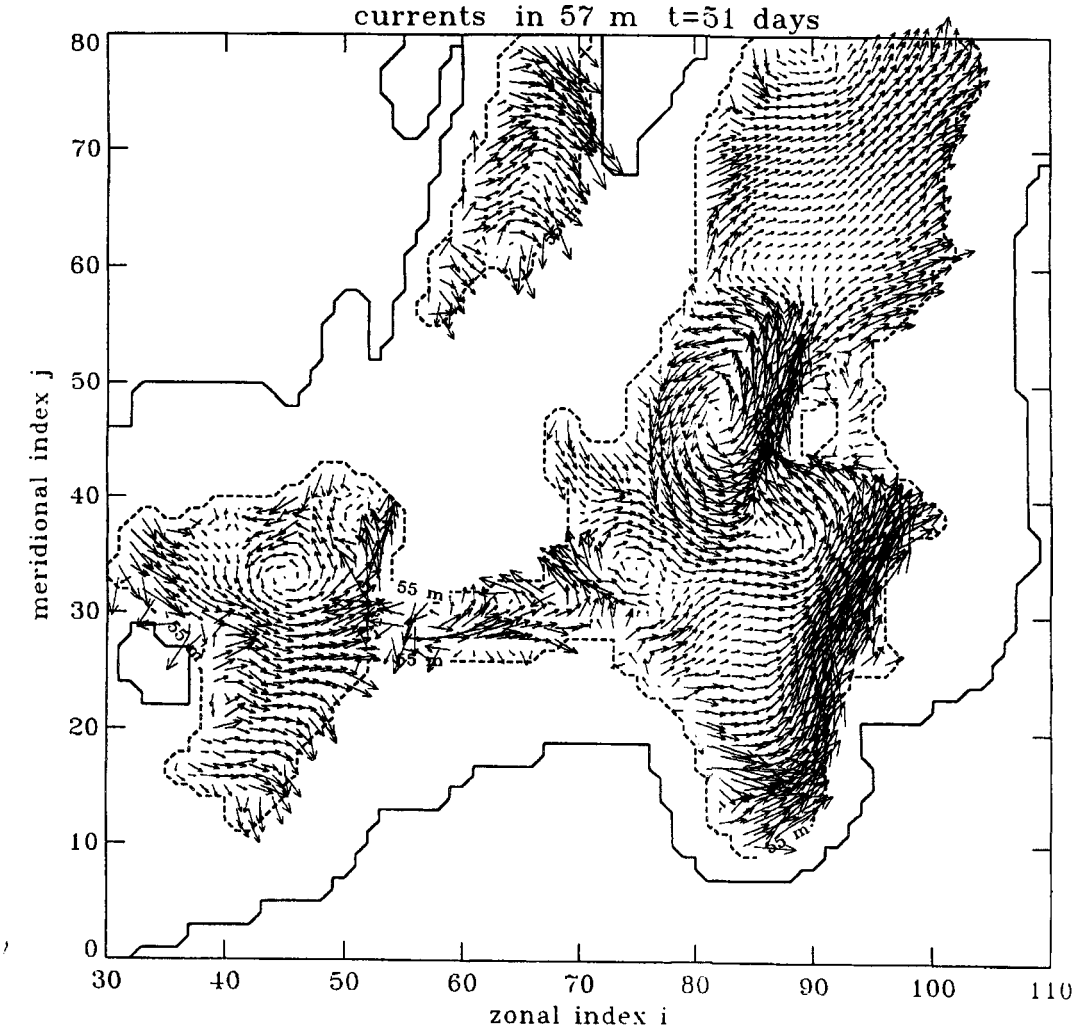


***Fig. 8.4.** Continued. (c) model wind day 21.*

The channel-wide baroclinic eddy produced by the model is similar to the eddy observed in May 1980 (Fig. 5.4.1b). This is also valid for the cross-channel salinity section, compare the model salinity at wind day 20 (Fig. 8.5) with observed salinity (Fig. 5.4.2b). But, reminding that the initial stratification and wind were taken from winter 1985/1986, better agreement with 1986 observations (Fig. 5.4.1c, 5.4.2c) could have been expected. Smaller baroclinic eddies may be misresolved due to the grid step (2.5 miles) being too large. Since the baroclinic eddy has been found to be generated by dense water overflow from the Gdansk Basin, proper simulation of dense water supply from the Stolpe Channel is of critical importance.

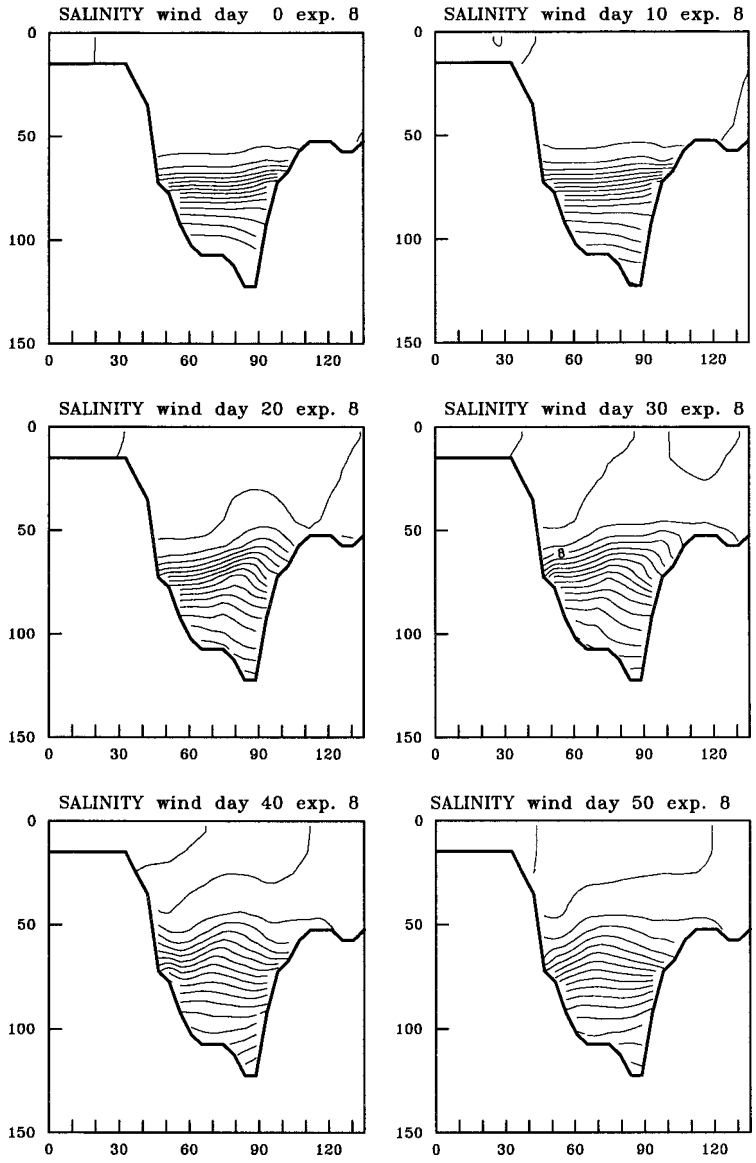


***Fig. 8.5.*** *Sections of modelled salinity across the Hoburg Channel with 10 days interval.*

## 8.3. Spreading of deep water

It is often assumed that major part of the dense water overflowing from the Bornholm Basin spreads directly to the Gotland Basin and only a minor part fills the deep layers of the Gdansk Basin. Traditionally the hydrographic transects of the Baltic Sea are drawn in a way that the Gdansk Basin is not at all displayed (see also Fig. 8.2 and 8.3). However several hydrographic observations made by the Polish oceanographers reveal saline water core on the slope of the Gdansk Basin, with the more saline deep water and the more shallow halocline depth found there as compared with the central parts of the Gdansk Basin. Cyclonic dense water transport along the slope of the Gdansk Basin may be also assumed from the distribution of current vectors, Fig. 8.4.

Spreading of the deep water was studied by a free tracer which was initially inserted in the Bornholm Basin layers below 50 m and was zero elswhere. The subsequent distributions are depicted in Fig. 8.6 as the mean tracer concentrations over the layer 50-75 m. In the given experiment the tracer has turned, after passing the narrow Stolpe Channel, to the right spreading further anti-clockwise along the soutwestern slope of the Gdansk Basin. The spreading pattern had not been influenced very much by the wind forcing. However, signs of the intruding water detachment from the slope could be noted between the wind days 20 and 30, in the period of dominating north-westerly winds which create compensation flow of opposite direction below the Ekman layer of drift currents. Hence it may be assumed that the Gdansk Basin plays a role of the buffer zone for deep water renewal, and that before spreading further to the Gotland Basin the new deep water rich in oxygen *etc.* accumulates in the Gdansk Basin.

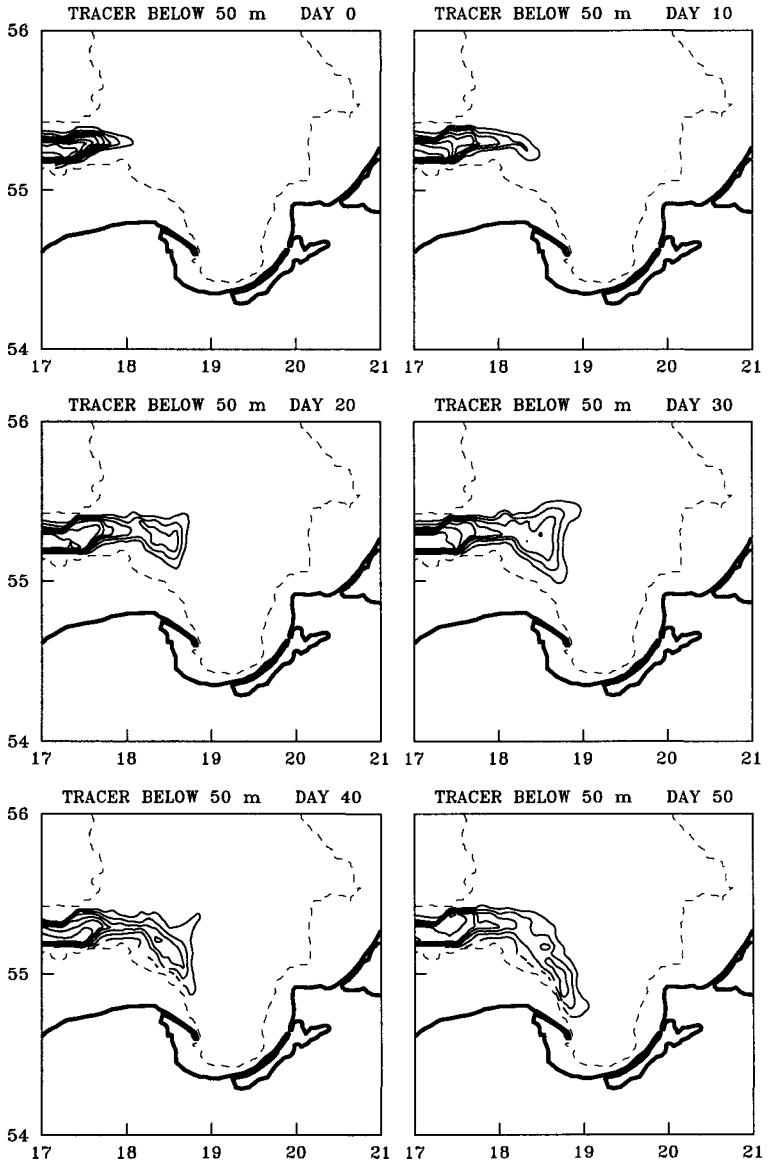


***Fig. 8.6.*** *Maps of the modelled mean tracer of the layer 50-75 m with 10 days time interval. Source of the tracer is located in the halocline of the Bornholm Basin.*

### 8.4. Transports between the sub-basins

Pedersen (1977) has got from the data 1949-1961 that continous flow in the Stolpe Channel takes place between the mean halocline depth 45 m and the sill depth 60 m. The deep water outflow from the Bornholm Basin was estimated to be in a range 23-54 mSv (millisverdrups, 1 Sv = $10^6$ $m^3s^{-1}$). The same values were observed in August 1976 by Lars Rydberg. Kõuts and Omstedt (1993) have estimated the mean flow rate 33 mSv for the period 1970-1990. In the present study, budget calculation of the intermediate layers of the Gotland Basin gave the flow rate only 11 mSv for the period 1979-1994.

Budget-type box models (Stigebrandt, 1983, Omstedt, 1990) use geostrophic formula (4.6) for calculating the baroclinic transport where transports are tuned to follow the observed trends by modifying the sill depths. Gidhagen and Håkansson (1992) have shown importance of bottom friction and channel width.

Krauss and Brügge (1992) have studied the wind-produced water exchange through the Stolpe Channel by a numerical model, with density driven flow component absent. They found that maximum transports from the Bornholm Basin are caused by north-easterly winds. While changing the wind by 180° then the transport with the same magnitude took opposite direction.

Model-produced water exchange through the Stolpe Channel was investigated by integrating the east-west velocity component on a cross-channel transect of the north-south direction, located ≈ 50 km east from the sill.

Density-driven transports during the initialization without wind were in a range 10-14 mSv in the layer 60-80 m for different experiments which is in agreement with our budget calculations. Fluctuating winds applied in the model caused fluctuations also in the volume transport. Least-square fit for the cumulative volume transport ($km^3$) gave good results when the 2-day filtered model volume transport (mSv) was approximated to the 2-day filtered forcing wind stress by a formula

$$Q = Q_o + A_W \tau_\varphi, \tag{8.4}$$

where $\tau_\varphi$ is the forcing wind stress projected to the direction $\varphi$ and $t$ is time. The term $Q_o$ may be interpreted as density-driven transport. The second term $A_W \tau_\varphi$ represents the wind-driven transport.

Fit example by the formula (8.4) is given in Fig. 8.7 for the two selected wind periods. The approximation by (8.4) is rather good what means that coupling between the density- and wind-driven transport is weak and the total transport may be calculated as a sum of components.

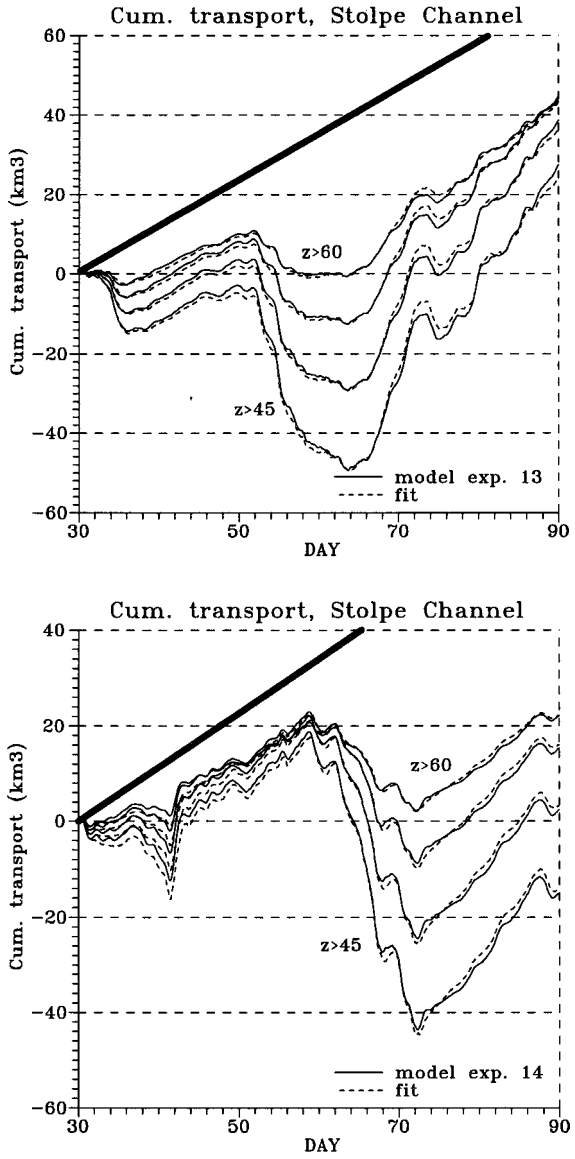


***Fig. 8.7.*** *Cumulative volume transport in the Stolpe Channel below the levels 45, 50, 55 and 60 m calculated by the model (solid line) and by the linear fit formula (8.4) for the wind period W86 (above) and W85 (below). Heavy solid line presents the cumulative transport in the layer 60-80 m without wind forcing. Days are counted from the start of the run, wind was switched on in the day 30.*

Summary of the estimated values of the fit parameters for the two wind periods is given in Table 8.1.

***Table 8.1.*** *Fit parameters of the modelled volume transports by the formula (8.4) for the wind periods W85 (mean wind stress 0.33, 0.11) and W86 (0.02, 0.18). $Q_{ini}$ is the volume transport without wind forcing.*

| Layer (m) | W85 | | | W86 | | | $Q_{ini}$ (mSv) |
|---|---|---|---|---|---|---|---|
| | $Q_o$ (mSv) | $A_w$ (mSv/ dyn/cm$^2$) | $\varphi$ | $Q_o$ (mSv) | $A_w$ (mSv/ dyn/cm$^2$) | $\varphi$ | |
| 45-80 | 14 | 69 | 25 | 16 | 67 | 27 | 20 |
| 50-80 | 14 | 55 | 25 | 16 | 52 | 28 | 18 |
| 55-80 | 13 | 42 | 24 | 14 | 38 | 29 | 16 |
| 60-80 | 11 | 27 | 24 | 13 | 26 | 29 | 14 |

From the fit parameters we may conclude, that the fitted density-driven transport $Q_o$ is close to the transport obtained during initialization $Q_{ini}$ and the wind-driven transport to the Gdansk and Gotland basins is maximal for wind direction of about 30$^o$ which is in agreement with the qualitative results obtained by Krauss and Brügge (1992). For the density-driven component, the calculated flow rate per unit depth is maximal near the bottom (however, just on the bottom friction reduces the flow by about 10%) and vanishes at the depths above 50 m. The wind-driven flow rate is small on the bottom and increases towards the top layers of the halocline.

For the sensitivity analysis we may say that the flow depends only a little on reasonable variations of the channel width, viscosity and diffusion. However, water density variation in the far upstream basins modifies the transport considerably. In the experiments where the Arkona Basin had the same density as in the Bornholm Basin, the density-driven transport component was reduced by more than 20% but the wind-driven component remained unchanged. The influence of the upstream basins is not considered by the geostrophic formalae (4.5) and (4.6). Closed boundaries used in the experiments without fresh and saline water supply did not change the transports considerably, but due to the decay of the density differences between the basins, a slight decrease of the $Q_o$ term over the time was obtained.

Although the mean dense water transport is directed from the Bornholm Basin to the Gdansk and Gotland Basin, strong westerly winds may reverse the flow as can be seen from Fig. 8.4. Dominating westerly winds in the Baltic Sea region work against the dense water overflow in the Stolpe Channel (*cf.* Fig. 8.7). The flow reversal in the middle of the channel, with rising isopycnals at the northern slope, has been recently demonstrated by Paka (1994). Strong north-easterly winds combined with significant Bornholm Basin halocline height may cause dense water pulses which are intense enough to be transported quickly to the Gotland Basin, but also to rise the Gdansk Basin halocline and generate vigorous baroclinic eddies as were observed in spring 1980. In the Hoburg Channel, the baroclinic eddies were found to recirculate the deep water whereas the net leakage to the north (along the eastern slope, the northward flow generally exceeds the opposite flow at the western slope) roughly equals to the dense water supply from the Stolpe Channel.

## 9. DISCUSSION AND CONCLUSIONS

Saline water is supplied from the upstream basins through the connecting channels. The box models traditionally ignore the wind forcing and calculate the transport from the inter-basin density difference. Geostrophic relation with continuous stratification, used in the present diagnostic box model, gave 'effective sill depths' 60 m for the Stolpe Channel and 99 m for the Farö Channel which are closer to the physical sill depths than of the earlier calculations with a two-layer approach. Compared with the earlier results, smaller flow rates have been obtained in the Gotland Basin and the mean volume transport for the period 1979-1994 was estimated about 11 000 $m^3$ $s^{-1}$ for both the Stolpe and Farö Channel. Independent calculations by 3D circulation model provided nearly the same density-driven transport in the Stolpe Channel. In addition to the inter-basin dependence, the 3D model revealed about 20% transport increase due to increased sea level gradients if the far upstream Arkona Basin has been filled with more dense water. Variable wind forcing applies in the channel compensating flows due to the sea level gradients. Dense water transport in the deep channels may be approximated by a sum of the density- and wind-driven components, with the maximum overflow occurring in the Stolpe Channel at north-easterly winds and in the Hoburg and Farö Channel at northerly winds. This parameterisation can be used in the box models in a straightforward way. With the westerly winds dominating in the Baltic Sea region, the wind forcing tends to reduce the Stolpe Channel overflow as compared with the pure density-driven transport.

Data from the monitoring stations, considered in the box models as representative for the basin mean stratification, are affected by the circulation patterns as evident from the polygon observations and long transects. Near the Stolpe Channel, salinity has been higher than at the monitoring station, located in the Bornholm Basin interior, in several cases. Also in the Farö Channel, halocline doming relative to the Gotland Deep was frequently found. This means, that the salinity range of overflowing water may be underestimated by the box model if the circulation effects are not taken into account.

Waters leaving the Bornholm Basin continue in the Gdansk and Gotland Basins at different depth levels. On the average for 1979-1994, the maximum inflow rates as estimated by the box model occurred around 100 m depth in the Gotland Basin. Assuming, as traditional, instantaneous transport with no under-way cross-isopycnal mixing, 12% of the inflow entered the Gotland Deep on the bottom, 17% in the layer from 150 m to the bottom and 71% above 150 m.

On the intra-basin scales, overflowing water is preferably spreading anti-clockwise along the right-hand slopes of the downstream basins as can be seen from the mesoscale observations and the 3D circulation model. Therefore the dense water coming from the Stolpe Channel has a tendency to spread along the south-western slope of the Gdansk Basin. By the model experiments, the spreading pattern had not been influenced very much by the wind forcing. However, signs of the intruding water detachment from the slope could be noted in the period of dominating north-westerly winds which create compensation flow of opposite direction below the Ekman layer of drift currents. Hence it may be assumed that the Gdansk Basin plays a role of the buffer zone for deep water

renewal, and that before spreading further to the Gotland Basin the new deep water rich in oxygen *etc.* accumulates in the Gdansk Basin.

The Hoburg Channel is wide enough to allow development of energetic baroclinic eddies which are persistent to variable wind conditions. By the observations, higher eddy amplitudes are observed during the increased dense water supply from the Bornholm Basin. Hypothesis that baroclinic eddies may be generated by interaction of wind-induced Kelvin waves and instability of wind-generated jets was not confirmed by the model experiments and the large-scale, estuarine potential energy was found to be necessary for the eddy formation. While the eddies recirculate dense water in the channel, the net leakage to the Gotland Deep is roughly equal to the transport in the Stolpe Channel.

Warming-up of the intermediate layers, observed at the end of eighties and culminated in winter 1990/1991, was governed by the enhanced wintertime advection along the eastern slope of the Gotland Basin and subsequent detachment of warm-core deep lenses spreading the warmer slope water over the basin interior. Important role of the Northern Basin as a sink for the intermediate water is pointed out.

By our budget estimates, about 50% of the saline water entering the Bornholm Basin is spreading further through the Stolpe Channel and the remaining part increases the dense water volume and lifts up the halocline. Saline water is entrained into the surface layers and the halocline depth is restored during the winter. Long-term vertical advection was found to be small at the halocline level in the Eastern Gotland Basin. However, considerable downward flow has been estimated for the period 1987-1990. On the shorter time scales, salt is effectively lost during the short storm events in winter. In the Northern Basin, vertical advection is again very important, which together with higher mixing rates explains the highest seasonal changes observed in the deep water.

Turbulence observations have revealed minor vertical salt fluxes in the halocline during the normal conditions. Higher percentage of low Richardson number values and larger turbulent kinetic energy dissipation rates were estimated in the field of developed inertial motions. Therefore, stronger cross-isopycnal mixing is expected to take place during the storms by generation of inertial waves which lead to shear instability. Surface layers are effectively supplied with salt and other deep water tracers during the winter when the storm events and convection re-establish the high vertical gradients in the halocline against the diffusion. Signs of intensified mixing have been found near the slopes. Problems of turbulence modelling are also considered within the RAT theory.

Finally we would like to stress the importance of the saline water terminal areas - the Northern Basin and the entrance to the Gulf of Finland - in the Baltic global salt cycle. Although we have got smaller estimates for the deep water supply and upward advection as compared with some of the earlier works, we still assume much larger vertical supply of the euphotic layer by salt and nutrients than in many other parts of the Baltic. Unfortunately, historical mesoscale and turbulence observations are rather fragmentary in this region, not allowing to draw up the conclusions even on a such level what we have made for the Gotland Basin. Another region what we think is not sufficiently studied as compared to its potential role in deep water transformation, is the Gdansk Basin playing supposedly the role of a buffer basin.

**Acknowledgements**

The study has been made with the financial support by the Estonian Science Foundation, grants No. 907/92/231. In the observational part we have used materials from the HELCOM BMP programme. We note assistance by H.-U.Lass, A.Omstedt, A.Trzosinska and E.Lysiak-Pastuszak. Some of the process-oriented observations outlined in the report have been made jointly with H.-P.Hansen, P.Mälkki and V.Nabatov. Towed CTD measurements within GOBEX have been made from the RV Alexander von Humboldt, with H.-U.Lass as the chief scientist. 3D modelling part of the study started on the basis of EU Contract No ERB-CIPA-CT-92-0466, with IfM Kiel as the Host Institution and Prof. W.Krauss as Scientific officer. Introduction to the model code by A.Lehmann is highly appreciated. Some of the numerical experiments and analysis were made during the editor's stay at IOW, Warnemünde by kind invitation from Prof. W.Fennel. Our gratitude goes to F.Wulff and T.Seifert for providing the Baltic Sea digitised topography and H.Dahlin for providing the wind forcing data.

**Süvavee ülevool, tsirkulatsioon ja vertikaalne vahetus Läänemere avaosas**
**Eesti Mereinstituut, Tallinn, 1996**

Eesti Teadusfondi grantide 907/92/231 lõpparuanne
Grantide hoidjad: 907 - J.Elken, 92 - J.Laanemets, 231 - J.Heinloo

## KOKKUVÕTE

Analüüsitakse Läänemere avaosa süvakihtide vee ülevoolu, tsirkulatsiooni ja vertikaalset vahetust tuginedes aastatel 1979-1995 teostatud hüdrograafilise seire ja protsess-orienteeritud polügoonvaatluste andmetele. Kirjeldatakse Gotlandi basseinis jälgitud stratifikatsiooni muutusi - soolsuse ja vertikaalse stabiilsuse vähenemine stagnatsiooniperioodi kestel, vahekihtide soojenemine kaheksakümnendate aastate lõpul, süvakihtide vee uuenemine soolase vee suure sissevoolu tagajärjel 1993. a. Külg- ja vertikaalset transporti ning vertikaalset diffusiooni hinnatakse diagnostilise kast-mudeli abil. Gotlandi basseinis on hinnatud väiksemad vooluhulgad võrreldes varasemate arvutustega. Mesomastaapseid vaatlusi analüüsitakse basseinidevahelise veevahetuse ja tuule mõju kontekstis. Tsirkulatsiooni mudeli abil saadi, et barokliinsed keerised mis muudavad süvakihtide vee ringkäiku, tekitatakse sügavates kanalites ülevoolava tiheda vee poolt. Mudelarvutused näitasid, et tiheda vee transporti võib süvakanalites lähendada tihedusliku ja tuuletranspordi summana, kusjuures maksimaalne ülevool toimub Stolpe kanalis kirdetuulte korral ning Hoburgi ja Farö kanalis põhjatuulte korral. Ülevoolav vesi liigub eelistatult kellaosutile vastassuunas piki basseinide parempoolseid nõlvasid. Vahekihtide soojenemisel toimis suurenenud sügistalvine lõunarajoonide vee juurdevool piki Gotlandi basseini idanõlva. Nõlvaäärne vesi kanti üle basseini laiali soojade läätsede eraldumise kaudu. Turbulentsi modellerimise küsimusi käsitletakse RAT teooria raames. Turbulentsi vaatlused näitasid, et diffusiooni vood on halokliinis tavaliselt väga väikesed. Suuremad diapüknilise segunamise vood võivad esineda tormide ajal tekitatud inertslainete väljas mis viivad nihkelisele ebastabiilsusele. Ülakihid saavad suurel hulgal soola ning halokliinis sisalduvaid biogeene talvise halokliini erosiooni ajal, nii tormidest tingitud kaasahaarde kui ka konvektsiooni tõttu, mis ühtlasi taastavad diffusiooni mõjul nõrgenenud vertikaalsed gradiendid. Intensiivse segunemise jälgi on leitud Gotlandi basseini nõlvade ääres.

Käesolevas töös on detailselt analüüsitud vahetusprotsesse Gotlandi basseinis ning hinnatud basseinide vahelist vee- ja ainevahetust. Saadud hinnangud näitavad Põhja-Läänemere (Põhja süvik, Soome lahe suue) olulist osakaalu ülakihtide varustamisel soola ja biogeenidega. Kahjuks, fragmentaarse iseloomuga varasem protsess-orienteeritud vaatluste materjal ei võimalda ilma täiendavate mesomastaapsete ning turbulentsi mõõtmisteta teha detailsemat analüüsi selle Läänemere jaoks olulise piirkonna vahetusprotsesside kohta.

Käesolev töö koosneb sissejuhatusest, regiooni (2) ning pikaajalisi vaatlusandmeid (3) kirjeldavast peatükist, suuremastaabilisi vahetusvoogusid hindavast osast (4), mesomastaapsete (5) ja turbulentsi (6) vaatluste analüüsist, vertikaalse struktuuri (7) ja tsirkulatsiooni (8) mudeluuringute tulemustest ning kokkuvõttest (9).

## REFERENCES

Aitsam, A., J.Elken, 1982. Synoptic scale variability of hydrophysical fields in the Baltic Proper on the basis of CTD measurements. - In: *Hydrodynamics of Semi-Enclosed Seas, Amsterdam, Elsevier,* 433-468.

Aitsam, A., J.Elken, 1980. Results of CTD surveys on the BOSEX polygon in the Baltic. - In: *Proceedings of the 1st All-Union Symposium on Finestructure and Synoptic Variability of the Sea, Tallinn,* 19-23 (in Russian).

Aitsam, A., H.-P.Hansen, J.Elken, M.Kahru, J.Laanemets, M.Pajuste, J.Pavelson and L.Talpsepp, 1984. Physical and chemical variability of the Baltic Sea: a joint experiment in the Gotland Basin. - *Continental Shelf Research, 3, 3,* 291-310.

Aitsam, A., L.Talpsepp, 1982. Synoptic variability of currents in the Baltic Proper.- In: *Hydrodynamics of Semi-Enclosed Seas, Amsterdam, Elsevier,* 469-488.

Bergström, S. and W.Matthäus, 1996. Meteorological,hydrological and hydrographical conditions. -In: *HELCOM Third Periodic Assessment of the State of the Baltic Marine Environment* (in press).

Elken, J., 1994. Numerical study of fronts between the Baltic sub-basins. - In: *Proceedings of 19th Conference of the Baltic Oceanographers, Sopot, vol.1,* 438-446.

Elken, J., L.Talpsepp and J.Pavelson, 1987. Dynamics and distribution of water masses in the Southern Gotland Basin (polygon studies). - In: *Proceedings of the 15th Conference of the Baltic Oceanographers, Copenhagen,* 145-166.

Elken, J., 1987. Empirical and theoretical modes of density inhomogeneities in the Baltic. - In: *Proceedings of the 15th Conference of the Baltic Oceanographers, Copenhagen,* 136-144.

Elken, J., 1985. Comparison of some aspects of synoptic variability of the Baltic Sea and the Ocean. - In: *Investigation of Ocean Currents, Moscow, Nauka,* 139-143 (in Russian).

Elken, J., 1984. Density structure of synoptic eddies. - In: *Variability of the Ecosystem Components and Water Dynamics (project "Baltica"), Leningrad, Gidrometeoizdat,* 61-68 (in Russian).

Elken, J., M.Pajuste, T.Kõuts, 1988. On intrusive lenses and their role in mixing in the Baltic deep layers. - In: *Proceedings of the 16th Conference of the Baltic Oceanographers, Kiel,* 367- 376.

Elken, J., L.Talpsepp, T.Kõuts and M.Pajuste, 1994. The role of mesoscale eddies and saline stratification in the generation of spring bloom heterogeneity in the southeastern Gotland Basin: an example from PEX '86. - *ICES Cooperative Research Report, No.201, Patchiness in the Baltic Sea (edited by B.I.Dybern),* 40-48.

Fennel, W., H.-U.Lass, 1989. Analytical theory of forced oceanic waves. - *Akademie-Verlag Berlin,* 312 pp.

Fennel, W., H.-U.Lass and T.Seifert, 1986. Some aspects of horizontal and vertical excursions of phytoplankton. - *Ophelia, Suppl. 4,* 55-62.

Fennel, W. and M.Sturm, 1992. Dynamics of the western Baltic. - *J. Mar. Systems, 3,* 183-205.

Fonselius, S.H., 1969. Hydrography of the Baltic deep basins III. - *Fishery Board Sweden, Ser. Hydrogr. Rep., 23,* 97 pp.

Fonselius, S.H., 1970. On the stagnation and recent turnover of the water in the Baltic. -*Tellus, 22,* 533-544.

Gade, H.G., 1970. Hydrographic investigations in the Oslofjord, a study of water circulation and exchange processes. - *Geophysical Institute, Oceanography, University of Bergen, Report 24,* 193 pp.

Gade, H.G. and A.Edwards, 1995. Topographic influence on determination of one-dimensional vertical diffusivity in sea basins. - *Geophysical Institute, Oceanography, University of Bergen, Report 73,* 20 pp.

Gaspar, P.Y., 1990. A simple eddy kinetic energy model for simulations of oceanic vertical mixing: tests at station Papa and Long-Term Ocean Study site. - *J. Geophys. Res, C95.*

Gerdes, R., C.Köberle, J.Willebrand, 1991. The influence of numerical advection schemes on the results of ocean general circulation models. - *Climate Dynamics, 5,* 211-226.

Gidhagen, L., B.Håkansson, 1992. A model of the deep water flow into the Baltic Sea. - *Tellus, 44A,* 414-424.

Heinloo J., 1984. Phenomenological mechanics of turbulent flows. - *"Valgus", Tallinn,* (in Russian).

Heinloo J., Ü.Võsumaa, 1992. Rotationally anisotrophic turbulence in the sea.- *Ann. Geophysicae, v.10.*

HELCOM, 1988. Guidelines for the Baltic Monitoring Programme for the third stage. - *BSEP No. 27A-27B.*

HELCOM, 1990. Second Periodic Assessment of the State of the Marine Environment of the Baltic Sea, 1984-1988; Background Document. - *BSEP No. 35B.*

HELCOM, 1993. First assessment of the state of the coastal waters of the Baltic Sea. - *BSEP No. 54.*

Holland, W.R., L.B.Lin, 1975. On the generation of mesoscale eddies and their contribution to the oceanic general circulation. I. A preliminary numerical experiment. - *J. Phys. Oceanogr., 5,* 642-657.

Horstmann, U., 1983. Distribution patterns of temperature and water colour in the Baltic Sea as recorded in satellite images: indicators for phytoplankton growth. - *Ber. Inst. f. Meeresk., Kiel, Nr. 106,* 147 pp.

ICES, 1989. The Baltic Sea Patchiness Experiment: General Report (B.I.Dybern and H.P. Hansen, Eds), Vols. 1-2. - *Cooperative Research Report, No. 163,* 100 + 156 pp.

Itsweire, E.C., T.R.Osborn and T.P.Stanton, 1989. Horizontal distribution and characteristics of shear layers in the seasonal thermocline.- *J. Phys. Oceanogr., vol.19, No.3,* 301-320.

Keunecke, K.H., L.Magaard, 1974. Measurements by means of towed thermistor cables and problems of their interpretation with respect to mesoscale processes. - *Memoires Societe Royale des Sciences de Liege, 6, VII,* 147-160.

Kielmann, J., 1981. Grundlagen und Anwendung eines numerischen Modells der geschichteten Ostsee. - *Ber. Inst. f. Meeresk., Kiel, Nr. 87a/87b,* 158/116 pp.

Killworth, P., D.D.Stainforth, D.J.Webbs, S.M.Paterson, 1989. A free surface Bryan-Cox-Semtner model. - *Inst. of Oceanogr. Sciences, Deacon Laboratory, Report No. 270,* 184 pp.

Knudsen, M., 1900. Ein hydrographischer Lehrsats. - *Ann. der Hydr. usw., 28,* 316-320.

Koshlyakov, M.N., Y.M.Grachev, 1973. Meso-scale currents at a hydrophysical polygon in the tropical Atlantic. - *Deep-Sea Res., 20, 6,* 507-526.

Krauss, W. and B.Brügge, 1992. Wind-produced water exchange between the deep basins of the Baltic Sea. - *J. Phys. Oceanogr., 21,* 373-384.

Kõuts, T., J.Elken, U.Lips, 1990. Late autumn intensification of deep thermohaline anomalies and formation of lenses in the Gotland Deep. - In: *Proceedings of the 17th Conference of the Baltic Oceanographers, Norrköping 1990,* 280-293.

Kõuts, T. and A.Omstedt, 1993. Deep water exchange in the Baltic Proper. - *Tellus, 45A,* 311-324.

Laanemets, J., 1984. Characteristics of the intrusive finestructure in the southern Baltic. - In: *Proceedings of the 2nd All-Union Symposium on Finestructure and Synoptic Variability of the Sea, Tallinn,* 56-58 (in Russian).

Launiainen, J. and T.Vihma, 1990. Meteorological, ice and water exchange conditions. - In: *Second periodic assesment of the state of the marine environment of the Baltic Sea, 1984-1988; Background document. Baltic Sea Environment Proc., 35B,* 23-33.

Lehmann, A., 1992. Ein dreidimensionales wirbelauflösendes Modell der Ostsee. - *Ber. Inst. f. Meeresk., Kiel, Nr. 231,* 104 pp.

Lehmann, A., 1994. A model study of major Baltic inflows. - In: *Proceedings of the 19th Conference of the Baltic Oceanographers, Sopot 1994,* 410-421.

Liljebladh, B. and A.Stigebrandt 1995. Observations of deep water flow into the Baltic Sea. - *J. Geophysical Res.* (in press).

Lilover, M.-J., 1987. On the possibility of shear instability in the inertial wave field of the Baltic Sea. - In: *Abstracts of III Conference of Soviet Oceanographers, Leningrad,* 69- 70 (in Russian).

Lilover, M.-J., I.D.Lozovatsky, C.H.Gibson and V.Nabatov, 1993. Turbulence exchange through the equatorial undercurrent core of the central Pacific. - *Journal of Marine Systems, 4,* 183-195.

Lilover, M.-J. and V.N.Nabatov, 1990. On the turbulence mixing in the frontal zone of the Baltic Sea. - In: *Proceedings of the 3rd All-Union Symposium on Finestructure and Synoptic Variability of the Sea, Tallinn,* 96-97 (in Russian).

Lilover, M.-J., M.Otsmann and R.Tamsalu, 1989. Near-inertial waves and shear instability. - In: *Proceedings of the 16-th Conference of Baltic Oceanographers, Kiel, 2,* 648-652.

Lips, U. and J.Laanemets, 1994. On the evolution of thermohaline structure and mixing in the Baltic halocline during the stagnation period. - In: *Proceedings of the 18th Conference of the Baltic Oceanographers, St.Petersburg,* 277-285.

Lips, U., M.-J.Lilover, U.Raudsepp and L.Talpsepp, 1995. Water renewal processes and related hydrographic structures in the Gulf of Riga. - In: *Hydrographic studies within the Gulf of Riga Project 1993-1994, Estonian Marine Institute, Report Series, No. 1,* 1-34.

Lundberg, P., 1983. On the mechanics of the deep-water flow in the Bornholm Channel. - *Tellus, 35A,* 149-158.

Matthäus, W., 1990. Langzeittrends und Veränderungen ozeanologischer Parameter während der gegenwärtigen Stagnatsionsperiode im Tiefenwasser der zentralen Ostsee. - *Fischerei-Forsch. Rostock, 28, 3,* 25-34.

Matthäus, W., 1990. Mixing across the primary Baltic halocline. - *Beitr. Meeresk., Berlin 61,* 21-31.

Matthäus, W., 1984. Climatic and seasonal variability of oceanological parameters in the Baltic Sea. - *Beitrge zur Meereskunde, 51,* 29-49.

Matthäus, W., 1979. Long-term variations of the primary halocline in the Gotland Basin. - *ICES C.M. 1979/C:22 Hydrography Committee,* 1-14.

Matthäus, W. and H.Franck, 1992. Characteristics of major Baltic inflows, a statistical analysis. - *Continental Shelf Research, 12,* 1375-1400.

Matthäus, W. and H.-U.Lass, 1995. The recent salt inflow into the Baltic Sea. - *J. Phys. Oceanogr., 25,* 280-286.

Meier, M. and W.Krauss, 1994. Data assimilation into a numerical model of the Baltic Sea using the adjoint method. - In: *Proceedings of the 19th Conference of the Baltic Oceanographers, Sopot 1994,* 447-458.

Mälkki, P. and J.Elken, 1990. Hydrophysical processes on a polygon in the northern Baltic near the entrance to the Gulf of Finland. *(Manuscript).*

Nemirovsky, Y.Y. and J.Heinloo, 1982. The local vortex theory of turbulent flows. - In: *Novosibirsk Univ.Press, Novosibirsk* (in Russian).

Omstedt, A., 1990. Modelling the Baltic Sea as thirteen sub-basins with vertical resolution. - *Tellus, 42A,* 286-301.

Padman, L. and T.M.Dillon, 1989. Thermal microstructure and internal waves in the Canada Basin diffusive staircase. - *Deep- Sea Research, v.36.*

Paka, V.T., 1994. Thermohaline structure in the Stolpe Channel of the Baltic Sea in spring 1993. - *Russian Journal of Oceanology* (in press).

Pavelson, J., 1988. Nature and some characteristics of thermohaline fronts in the Baltic Proper. - In: *Proceedings of the 16th Conference of the Baltic Oceanographers, Kiel,* 796-805.

Pedersen, Bo F., 1977. On dense bottom currents in the Baltic deep water. - *Nordic Hydrology,* 297-316.

Peters, H., M.C.Gregg, J.M.Toole, 1988. On the parameterization of equatorial turbulence.- - *J. of Geophys. Res. vol.93, No. C2,* 1199- 1218.

Pratt, L.J., 1986. Hydraulic control of sill flow with bottom friction. - *J. Phys. Oceanogr., 16,* 1970-1980.

Price, J.F., R.A.Weller and R.Pinkel, 1986. Diurnal cycling: observations and models of the upper ocean response to diurnal heating, cooling and wind mixing. - *J. Geophys. Res., v.91.*

Raudsepp, U. and J.Elken, 1995. Application of the GFDL circulation model for the Gulf of Riga. - In: *Hydrographic studies within the Gulf of Riga Project 1993-1994, Estonian Marine Institute, Report Series, No. 1,* 143-176.

Seifert, T. and W.Fennel, 1994. Numerical experiments in the transition area between Baltic Sea and North Sea. - In: *Proceedings of the 19th Conference of the Baltic Oceanographers, Sopot 1994,* 422-437.

Seifert, T. and B.Kayser, 1995. A high resolution grid topography of the Baltic Sea. *Technical Report, IOW, Warnemünde.*

Shaffer, G., 1979. Conservation calculations in natural coordinates (with an example from Baltic Sea).- *J. Phys. Oceanogr.,97,* 847-855.

Siedler, G., 1968. Schichtungs- und Bewegungsverhältnisse am Südausgang des Roten Meeres. - *"Meteor" Forschungsergebnisse A, Helft 4.*

Stigebrandt, A., 1995. The large-scale vertical circulation of the Baltic Sea. - In: *Proceedings of the First Study Conference on BALTEX, BALTEX Secretariat Publication No. 3, Geesthacht,* 28-47.

Stigebrandt, A., 1987. Computations of the flow of dense water into the Baltic Sea from hydrographical measurements in the Arkona Basin. - *Tellus, 39A,* 170-177.

Stigebrandt, A., 1987. A model for the vertical circulation of the Baltic deep water. - *J. Phys. Oceanogr., 17,* 1772-1785.

Stigebrandt, A, 1983. A model for the exchange of water and salt between the Baltic and the Skagerrak. - *J. Phys. Oceanogr., 13,* 411-427.

Swallow, J.C. and J.Crease, 1965. Hot salty water at the bottom of the Read Sea. - *Nature, v.205.*

Talpsepp, L., 1982. On topographically trapped waves in the Baltic Sea. - In: *Proceedings of the 13th Conference of the Baltic Oceanographers, Helsinki,* 705-712.

Turner, J.S., 1986. Turbulent entrainment: the development of entrainment assumption, and application to geophysical flows. - *J. Fluid Mech. v.173.*

Rahm, L., 1985. On the diffusive salt flux of the Baltic proper. - *Tellus, 37A,* 87-96.

Roden, G.I., 1994. Effects of the Fieberling seamount group upon flow and thermohaline structure in the spring of 1991. - *Journal of Geophysical Research, 99,* 9941-9961.

Roden, G.I., 1991. Mesoscale flow and thermohaline structure aroubd Fieberling seamount. - *Journal of Geophysical Research, 96,* 16653-16672.

Roden, G.I. and B.A.Taft, 1985. Effect of the Emperor seamounts on the mesoscale thermohaline structure during the summer of 1982. - *Journal of Geophysical Research, 90,* 839-855.

UNESCO, 1988. The acquisition, calibration and analysis of CTD data.- *A Report of SCOR Working Group 51, Unesco technical papers in marine science, Unesco 1988,* 94 p.

Whitehead, J.A., A.Leetmaa and R.A.Know, 1974. Rotating hydraulics of strait and sill flows. - *Geophys. Fluid Dyn., 6,* 101-125.